

ABSTRACT

Title of Thesis: MITIGATION OF FRAME ACCELERATION
INDUCED BY A BURIED CHARGE

Thomas James Brodrick, Master of Science 2010

Thesis Directed By: Professor William Fourney
Department of Mechanical Engineering

In this thesis, methods to mitigate acceleration delivered to the frame of a vehicle with an attached v-shaped hull are investigated. The frame of a vehicle represents an alternative location for crew seating, as opposed to seats being secured to the floorboard. Mitigation techniques were investigated for three test setups: aluminum frame with a downwardly convex aluminum hull, steel frame with a downwardly convex steel hull, and a steel frame with a downwardly concave steel hull. Accelerations of the frame were measured using piezoelectric accelerometers placed at three different locations on the frame. These acceleration measurements were verified against video recorded by high speed cameras. Each test was intended to reduce peak accelerations experienced by the frame, and to reduce the width of the acceleration envelope at large g levels. Mitigation techniques focused on reducing the initial hull-frame interactions, while damping subsequent responses of the system. Mitigation systems and hull orientation were compared for their ability to reduce blast effects experienced by the frame.

Mitigation of Frame Acceleration Induced by a Buried Charge

By

Thomas James Brodrick

Thesis submitted to the Faculty of the Graduate School of the
University of Maryland, College Park in partial fulfillment
of the requirements for the degree of
Master of Science
2010

Advisory Committee:

Professor William Fourney (Chair)

Professor Balakumar Balachandran

Professor Teng Li

© Copyright by
Thomas James Brodrick
2010

Dedication

This thesis is dedicated to everyone in my acknowledgements, who made this thesis a reality, and the people who serve in the armed forces, who this research will hopefully help in the future.

Acknowledgements

First, I would like to thank Dr. William Fourney for allowing me to be a graduate student under his advisory, while performing research in the Dynamic effects lab.

I also want to thank The Dynamic Effects lab manager Uli Leiste, who was always available to help and give advice. Uli always had answers regarding any issue in the lab.

I would like to thank Les Taylor for his ability to describe blast effects in great detail, helping me with my research.

I would also like to thank Ryan Hurley, an undergraduate student who assisted me in my research, namely the pocket plate series of tests.

I would like to thank the German students who worked in the lab: Thomas Mehlich, Sven Baumgartner, and David Hofman for assisting with tests and machining.

The developers of UERD Tools: Paul Mantz, Jamie Howell III, David Ingler, Benjamin Stow, Frederick A Costanzo, Eric Luft, and Jonathan Wood. This program was instrumental in providing the post processing tools necessary for this paper.

I would like to thank Scott Yamada, for his assistance during my undergraduate and graduate years on homework, tests, and research.

I would like to thank Dana Colegrove for showing me the Dynamic Effects lab, and teaching me how to perform tests.

I also would like to thank Howie Grossenbacher, who taught me everything I know about machining.

I would like to thank Dr. Bob Bonenberger, who helped me conduct tensile tests needed for stiffness value calculation.

I would like to thank Amarildo Damata and Fitzgerald Walker for helping me with all the required paperwork during my graduate years.

I would like to thank Professor Balakumar Balachandran and Professor Teng Li for being a part of my thesis defense committee.

Finally, thanks to my family and friends for their support and constant encouragement throughout my years at the university.

Table of Contents

Chapter 1 - Introduction and Background	1
1.1 Overview	1
1.2 Improvised Explosive Devices.....	3
1.3 Scaling.....	6
Chapter 2 - Research Equipment	10
2.1 The Explosive Charge	10
2.2 Firing System	15
2.3 The Dummy Charge.....	16
2.4 Sand Pit	17
2.5 Aluminum Frame – Navy Test Series.....	18
2.6 Steel Frame – Army Test Series.....	19
2.7 The Angled Hull.....	20
2.7.1 The Pocket Plate	21
2.8 Lighting Specifications and Preparation	22
2.9 High Speed Camera Equipment and Setup	23
2.10 PCB Accelerometers.....	25
2.11 Oscilloscope.....	27
2.12 UERDTools Software.....	28
Chapter 3 - General Experimental Procedures.....	29
3.1 Test Procedure.....	29
3.2 Phantom Software Analysis Procedure	33
3.3 UERDTools Data Analysis Procedure	34
Chapter 4 - Test Series Overview	37
4.1 Aluminum Test Series.....	37
4.1.1 Aluminum 1: Control Frame.....	38
4.1.2 Aluminum 2: Spider Frame	39
4.1.3 Aluminum 3: Sliding Hull	41
4.1.4 Aluminum 4: Spring Spider Frame.....	42
4.1.5 Aluminum 5: Pink Foam.....	43

4.1.6	Aluminum 6: White Foam	44
4.2	Steel Test Series	45
4.2.1	Steel 1: Steel Control Frame	46
4.2.2	Steel 2: Pink Foam	47
4.2.3	Steel 3: 3/16" Single Coil Spring	48
	Tensile Testing	49
4.2.4	Steel 4: Single Coil Spring + Foam Coating	50
4.2.5	Steel 5: Polyurethane-Polyurea Coated Hull	52
4.2.6	Steel 6: Steel Cable Vibration Isolators	53
4.3	Pocket Plate Series	54
4.3.1	Pocket Plate 1: Pocket Plate Control	55
4.3.2	Pocket Plate 2: 3/16" Single Coil Spring Pocket Plate	56
4.3.3	Pocket Plate 3: 1/8" Single Coil Spring Pocket Plate	57
Chapter 5 - Post-Processing and Data Verification		58
5.1	Frame Fundamental Frequencies	58
5.2	Data Filtering	61
5.3	Verification of Data: Filtered Data vs. Camera Data	62
Chapter 6 - Results		64
6.1	Aluminum Test Series	65
6.1.1	Aluminum 1: Control Frame	65
6.1.2	Aluminum 2: Spider Frame	66
6.1.3	Aluminum 3: Sliding Hull	67
6.1.4	Aluminum 4: Spring Spider Frame	68
6.1.5	Aluminum 5: Pink Foam	69
6.1.6	Aluminum 6: White Foam	70
6.1.7	Aluminum Series Peak Acceleration Overview	71
6.1.8	Aluminum Series Acceleration Envelope Overview	72
6.2	Steel Test Series	74
6.2.1	Steel 1: Control Frame	74
6.2.2	Steel 2: Pink Foam	75
6.2.3	Steel 3: 3/16" Single Coil Springs	76

6.2.4	Steel 4: 3/16'' Single Coil Springs + Foam Coating	78
6.2.5	Steel 5: Polyurethane-Polyurea Coated Hull	80
6.2.6	Steel 6: Steel Cable Isolators	81
6.2.8	Steel Series Acceleration Envelope Overview	83
6.3	Pocket Plate Series	85
6.3.1	Pocket Plate 1: Pocket Plate Control	85
6.3.2	Pocket Plate 2: 3/16'' Single Coil Spring Pocket Plate	86
6.3.3	Pocket Plate 3: 1/8'' Single Coil Spring Pocket Plate	87
6.3.4	Pocket Plate Series Peak Acceleration Overview	88
6.3.5	Pocket Plate Series Acceleration Envelope Overview.....	89
Chapter 7 - Conclusions.....		91
7.1	Aluminum Test Series	91
7.2	Steel Test Series	92
7.3	Pocket Plate Series	93
7.4	Combined Conclusions	94
Appendix A: FS-17 Specifications [14].....		96
Appendix B: Aluminum Frame		97
Appendix C: Steel Frame.....		98
Appendix D: Sliding Hull		99
Appendix E: 3/16'' Single Coil Aluminum Springs.....		100
Appendix F: 1/8'' Single Coil Aluminum Springs.....		101
Appendix G: Steel/Aluminum Hull		102
Appendix H: Accelerometer Specifications [25].....		103
Appendix I: Compression Spring Information [20].....		105
Appendix J: Foam - Load v. Deflection Curves		106
Appendix K: Aluminum 6061-T6 Material Properties [26]		107
Appendix L: 1018 Steel Material Properties [27].....		107
Appendix M: Steel Cable Isolators [22]		108
Appendix N: Tensile Tests for Spring Specimens		110
Appendix O: Data Verification (Accelerometer vs. Camera).....		113
Bibliography		153

Table of Tables

Table 1.1: Test Parameters.....	8
Table 2.1: RP-87 Firing Parameters [12].....	11
Table 2.2: Recording Specifications	24
Table 2.3: Calibration Factors.....	26
Table 4.1: Aluminum Test Series Specimen Weights/Masses	37
Table 4.2: Steel Test Series Specimen Weights/Masses.....	45
Table 4.3: Spring Stiffness Measurements	49
Table 4.4: Pocket Plate Series Specimen Weights/Masses.....	54
Table 6.1: Aluminum Test Series Peak Accelerations.....	71
Table 6.2: Aluminum Series Acceleration Envelope Data	73
Table 6.3: Steel Test Series Peak Acceleration Data.....	82
Table 6.4: Steel Series Acceleration Envelope Data	84
Table 6.5: Pocket Plate Series Peak Acceleration Data	88
Table 6.6: Pocket Plate Series Acceleration Envelope Data.....	90
Table O.1: Accelerometer Verification.....	113

Table of Figures

Figure 1.1: MRAP Field Testing [3].....	2
Figure 1.2: IED Attacks an Increasing Trend [5]	3
Figure 1.3: IED Related Casualties [5].....	3
Figure 1.4: Acceleration v. Exposure Time [7]	5
Figure 1.5: Penetrated Hull.....	6
Figure 2.1: RP-87 Explosive Train [12]	10
Figure 2.2: RP-87 Dimensions [12].....	10
Figure 2.3: Sample Charge Preparation	12
Figure 2.4: Finished Charge.....	12
Figure 2.5: 1 Gram Charge	13
Figure 2.6: 4.4 Gram Charge	13
Figure 2.7: 1 Gram Charge Casing Cross Section	14
Figure 2.8: 4.4 Gram Charge Casing Cross Section	14
Figure 2.9: FS-17 Firing System [6].....	15
Figure 2.10: Dummy Charge [1].....	16
Figure 2.11: Sand Pit.....	17
Figure 2.12: Aluminum Frame	18
Figure 2.13: Steel Frame.....	19
Figure 2.14: Angled Hull Diagram	20
Figure 2.15: North Star Flexible Light [17].....	22
Figure 2.16: Phantom v12.1 High Speed Camera [17].....	23
Figure 2.17: Accelerometer	25
Figure 2.18: Accelerometer Placement (Top View).....	26
Figure 2.19: Oscilloscope Setup	27
Figure 2.20: Amplifier	27
Figure 2.21: UERDTools Software.....	28
Figure 3.1: Test Setup (Not to Scale).....	29
Figure 3.2: Before (Left) and After (Right) Leveling.....	30
Figure 3.3: Imaginary Floorboard.....	31
Figure 3.4: Test Diagram	31
Figure 3.5: Final Step before Testing	32
Figure 3.6: Tracking Points with Phantom Software.....	33
Figure 3.7: FFT Plot.....	36
Figure 4.1: Aluminum Control Frame	38
Figure 4.2: Spider Frame	39
Figure 4.3: Deformed Sliding Hull	41
Figure 4.4: Side View of Spring Spider Frame.....	42
Figure 4.5: Failure of White Foam during Testing.....	44

Figure 4.6: Steel Control 6mS after Detonation	46
Figure 4.7: Steel Series Pink Foam Test.....	47
Figure 4.8: 3/16" Single Coil Spring Deformation	48
Figure 4.9: Tensile Testing of Spring Specimens.....	49
Figure 4.10: Cardboard Molding Setup	50
Figure 4.11: Spring Covered in Foam.....	51
Figure 4.12: Steel 4 before Testing.....	51
Figure 4.13: Polyurethane-Polyurea Hull Deformation at 6mS after Detonation	52
Figure 4.14: Steel 6 (Steel Cable Isolators)	53
Figure 4.15: Pocket Plate Control.....	55
Figure 4.16: 3/16" Single Coil Spring Pocket Plate.....	56
Figure 4.17: 1/8" Single Coil Spring Pocket Plate.....	57
Figure 5.1: Fourier Analysis (Aluminum Frame).....	59
Figure 5.2: Fourier Analysis (Steel Frame)	59
Figure 5.3: Steel Frame First Two Mode Shapes	60
Figure 5.4: Filtered Data (600Hz Low Pass Filter) vs. Unfiltered Data.....	61
Figure 5.5: Verified Accelerometer Data.....	62
Figure 5.6: Incorrect Accelerometer Data	63
Figure 6.1: Sample Acceleration Envelope	64
Figure 6.2: Aluminum 1 Filtered Acceleration Data	65
Figure 6.3: Aluminum 2 Filtered Acceleration Data	66
Figure 6.4: Aluminum 3 Filtered Acceleration Data	67
Figure 6.5: Aluminum 4 Filtered Acceleration Data	68
Figure 6.6: Aluminum 5 Filtered Accelerometer Data	69
Figure 6.7: Aluminum 6 Filtered Accelerometer Data	70
Figure 6.8: Aluminum Test Series Peak Accelerations vs. Accelerometer Position	71
Figure 6.9: Steel 1 Filtered Acceleration Data.....	74
Figure 6.10: Steel 2 Filtered Acceleration Data.....	75
Figure 6.11: Steel 3 Filtered Acceleration Data.....	77
Figure 6.12: Steel 4 Filtered Acceleration Data.....	78
Figure 6.13: Steel 5 Filtered Acceleration Data.....	80
Figure 6.14: Steel 6 Filtered Acceleration Data.....	81
Figure 6.15: Steel Test Series Peak Acceleration v. Accelerometer Position	82
Figure 6.16: Pocket Plate 1 Filtered Acceleration Data.....	85
Figure 6.17: Pocket Plate 2 Filtered Acceleration Data.....	86
Figure 6.18: Pocket Plate 3 Filtered Acceleration Data.....	87
Figure 6.19: Pocket Plate Series Peak Acceleration v. Accelerometer Position	89

Chapter 1 - Introduction and Background

1.1 Overview

This thesis research was conducted at the University of Maryland, College Park within the Mechanical Engineering Department in the A. James Clark School of Engineering. Tests were performed in the sand pit of the Dynamic Effects Laboratory located in the basement of the Engineering Lab Building. The purpose of this research was to investigate techniques for mitigating frame acceleration of a hulled specimen, after a charge buried in water saturated sand was detonated beneath the specimen.

In previous research conducted in the Dynamics Effects Lab, mitigation techniques associated with accelerations of the floorboard of vehicles have been investigated [1]. This thesis will discuss accelerations of the frame of vehicles along with methods for acceleration mitigation. This research follows up on the idea that the frame of a vehicle will have a much less volatile response to an Improvised Explosive Device (IED) explosion when compared against the floorboard. This idea was formulated through testing; accelerations calculated at the frame were consistently lower throughout testing when compared against accelerations at the floorboard of the same specimen. Deformations of the floorboard are significantly more probable than deformations of the frame, indicating a greater likelihood for harm to an individual in contact with that particular medium.

The idea of sacrificial armor also focuses on the idea of separating the crew from the hull/floorboard, designing towards a calculated loss of that component in the event of an IED detonation [2]. By making an expendable addition to the vehicle's underbody, the

force from the explosion is diverted away from the crew compartment and the energy from the blast is absorbed through the loss of the expendable addition. Crumple zones on a car act in this fashion during an impact, absorbing energy from the impact through plastic deformation of the material. This concept will be the focus of this paper; what additions can be made to the hull of a vehicle to absorb blast energy and act as a deterrent to forces that would normally act on the frame of a vehicle. Figure 1.1 shows field testing of a Mine Resistant Ambush Protected vehicle (MRAP). MRAP's are designed so the occupants, but not necessarily the vehicle, survive an IED attack [3].



Figure 1.1: MRAP Field Testing [3]

The setup of each experiment allows for three accelerometers to be mounted to the frame of the specimen. The data recorded by these accelerometers will then be analyzed and filtered using Underwater Explosives and Research Division software (UERDTools) and compared against high speed video data to ensure its accuracy. Phantom high speed camera software was used to track points on the specimen for comparison against accelerometer data.

1.2 Improvised Explosive Devices

The ideology of warfare is changing; open warfare is no longer agreed upon or expected. IEDs can be buried and left by the enemy, without ever having to witness the destruction. According to the Pentagon, IEDs are “the single most effective weapon against our deployed forces” [4]. IED related attacks have been steadily increasing since 2003, as seen in Figure 1.2 [5].

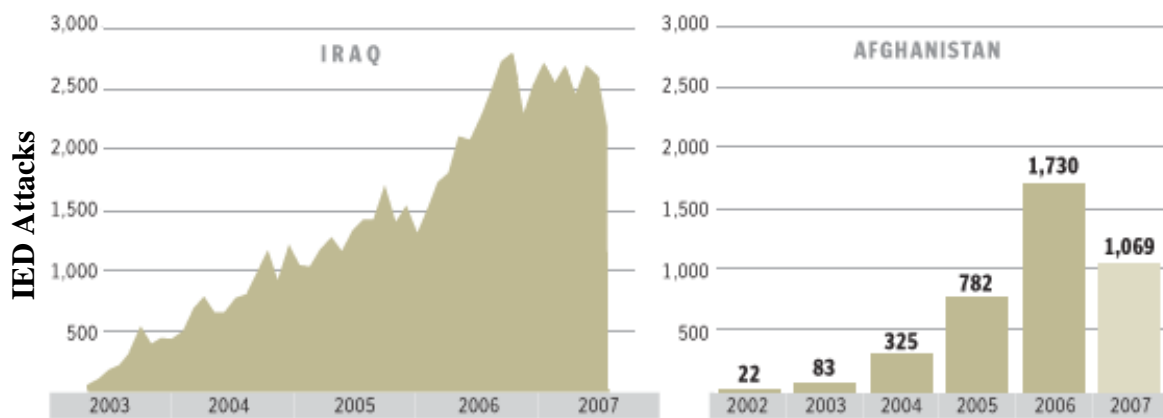


Figure 1.2: IED Attacks an Increasing Trend [5]

Casualties due to IED attacks have also been increasing according to the Iraq Coalition Casualty Count [6]. From Figure 1.3, shown below, it can be seen that IED casualties currently make up roughly two thirds of casualties overseas [5].

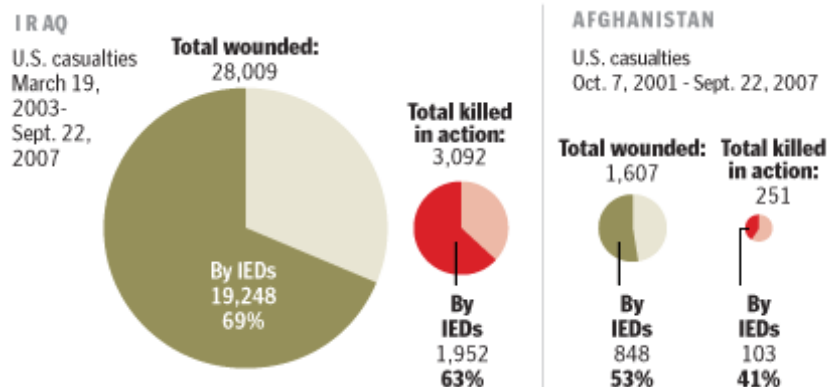


Figure 1.3: IED Related Casualties [5]

Though forms of landmines have been in use for centuries, the extent of their current involvement requires an immediate response. Vehicles, such as the MRAP are being pushed into combat by an enormous demand for a means to transport troops safely. Originally, shrapnel being projected into the crew compartment was thought to be the most vicious outcome of an IED, but high accelerations of the crew compartment are also likely to cause injury and death. Traumatic brain injury (TBI) due to an IED explosion can occur even if the vehicle remains intact after a blast. Accelerations of the crew compartment can reach hundreds of g's during a blast, severe enough to cause brain injury. The exact number of g's needed to cause brain injury is unknown; it's dependent on the individual and the acceleration loading curve on the brain. Accelerations cause the brain to smash into the interior skull wall (the skull and the brain do not move as one system) [7]. Forces due to this contact can be large enough to cause hemorrhaging of the brain and stretching of the axons, both of which are severe injuries. Screenings performed between 2006 and 2009 showed that ~18% of all troops have TBI [7].

In this thesis, accelerations of the frame of specimens will be studied in order to produce the least volatile response for a crew member encountering a blast. Brain damage from IEDs and accelerations in general do not always result in death. However, due to the complexity of brain injury, treatment for these individuals has not been set in stone. Brain scans and other tests may not depict the severity of the individual's damage. It is not unusual for someone who has survived many IED incidents to be labeled unfit for service, due to the uncertainty involved with diagnosing their injuries. It is therefore just as important to understand the risk of experiencing large accelerations, as it is keeping individuals from experiencing those accelerations in the first place.

Metrics have been laid in place by the military for analyzing acceleration effects on humans. Such metrics study the acceleration loading for specific periods of time. An exposure time of 5.5ms at 23g's has been used by the military for determining whether aircraft ejections are harmful to pilots [8]. This was later relaxed to 23g's over a period of 25ms, created for helicopter crash simulations [9]. These two exposure criteria will be used in this thesis to analyze acceleration curves and their possible effects to human occupants. Though the area under the acceleration curve, not just whether it reaches a threshold value, is more determinant of the acceleration effects received the two criteria listed give a baseline for evaluations. In reality, there isn't one set measure for determining what level of acceleration (over a time period) will cause injuries. This discrepancy can be seen below in Figure 1.4 [7].

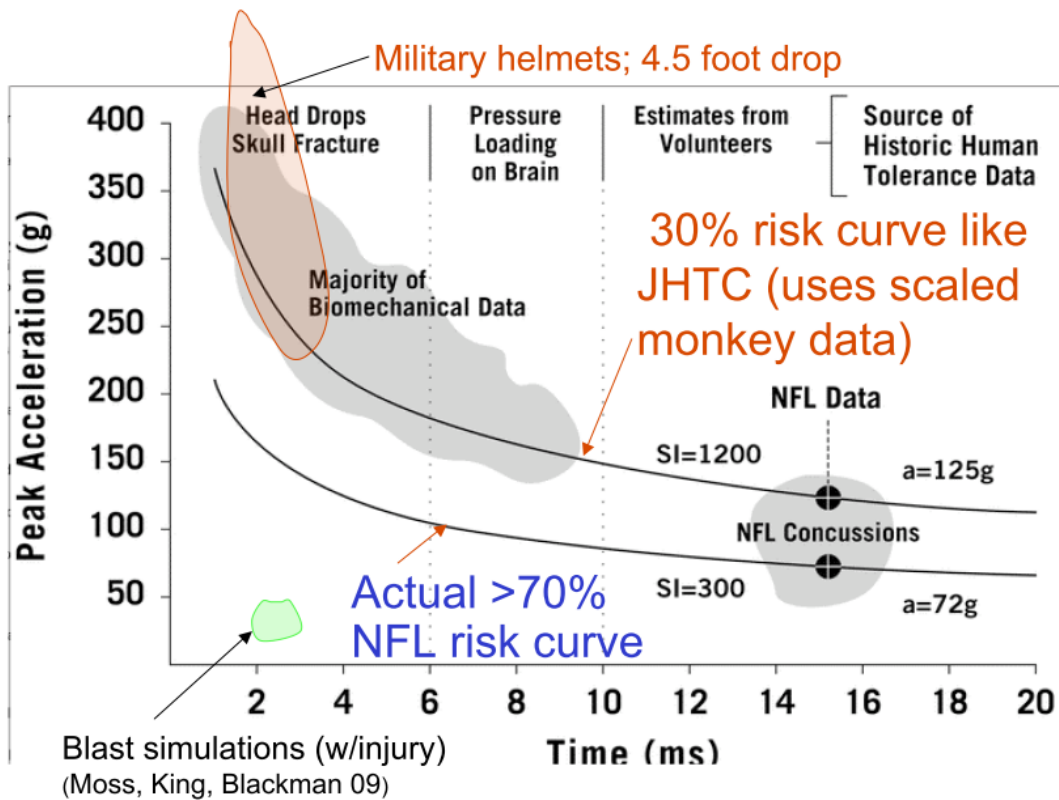


Figure 1.4: Acceleration v. Exposure Time [7]

1.3 Scaling

Scaled testing was necessary due to the enormous amount of resources involved in full scale tests, “full scale tests are very expensive, and each damage test by land mine detonation expends not only the vehicle but also many man-hours of skilled engineering and support labor” [10]. Scaling tests made tests cheaper, quicker, and more repeatable due to the increased monetary and physical feasibility. Tests in this paper were scaled based on 5 and 10 pound full scale tests. It was important in these scaled tests that there was deformation to the hull the specimen, but that the hull of the specimen was not penetrated by the blast, as seen in Figure 1.5. Tests for frame acceleration are useless in the event of hull penetration; non-penetrated hulls resemble the case where brain damage is the only cause for concern (shrapnel doesn’t enter the crew compartment in this case). All scaling factors are calculated by dividing the full scale charge mass by the scaled charge mass and then raising that quantity to the $1/3$ power.

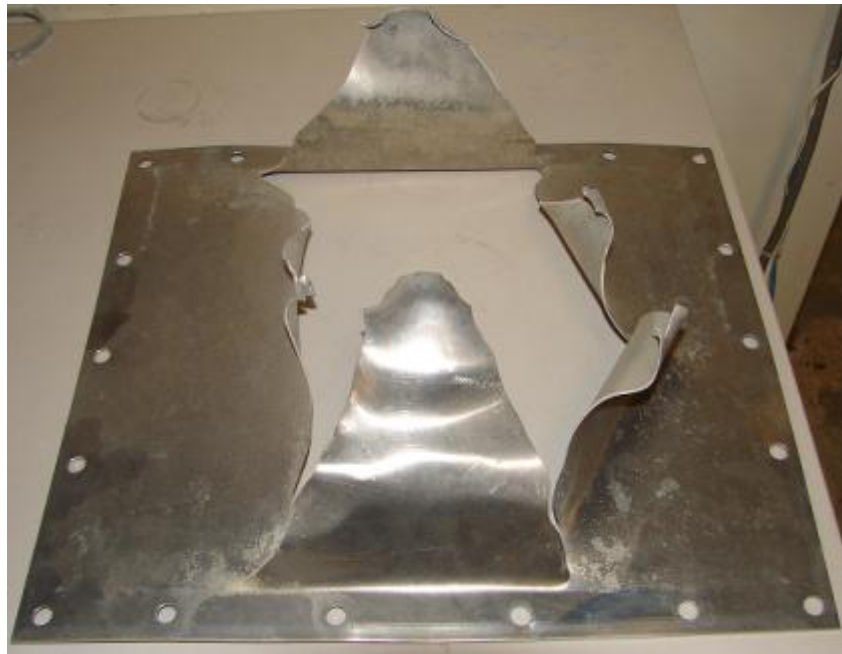


Figure 1.5: Penetrated Hull

The 5 pound charge was investigated using a scaling factor of 13.14. This scaling factor (SF) results in a charge size of 1 gram, a depth of burial (DOB) of 0.3 inches, and a standoff distance (SOD) of 3.19 inches. For these tests, an Aluminum specimen was used in order for proper deformations to occur to the hull. Aluminum was chosen due to its low stiffness and weight. Calculations for determining the scaling factor for this test series can be seen below.

$$\text{SF} = \left(\frac{\text{Mass}_{\text{Full-Scale}}}{\text{Mass}_{\text{Small-Scale}}} \right)^{1/3} = \left(\frac{2268 \text{ grams}}{1 \text{ grams}} \right)^{1/3} = 13.14$$

The 10 pound charge was investigated using a scaling factor of 10.1. This scaling factor results in a charge size of 4.4 grams, a DOB of 0.39 inches, and a SOD of 3.17 inches. A steel specimen was used for this test set; an increased material stiffness was required to withstand the increased blast energy due to the transition from a 1 gram charge to a 4.4 gram charge. Calculations for determining the scaling factor for this test series can be seen below.

$$\text{SF} = \left(\frac{\text{Mass}_{\text{Full-Scale}}}{\text{Mass}_{\text{Small-Scale}}} \right)^{1/3} = \left(\frac{4536 \text{ grams}}{4.4 \text{ grams}} \right)^{1/3} = 10.1$$

Length scaling was introduced in order to scale a full sized test down to a feasible size for testing. The scaling factor used was the same factor used to scale charges; the calculation can be seen below. Table 1.1 on the following page overviews charge size,

SOD, DOB, and scaling factor for each test. Note that standoff distances are measured to the floorboard of the specimen.

$$\mathbf{SF} = \left(\frac{\mathbf{Mass}_{\mathbf{Full-Scale}}}{\mathbf{Mass}_{\mathbf{Small-Scale}}} \right)^{1/3} = \frac{\mathbf{Length}_{\mathbf{Full-Scale}}}{\mathbf{Length}_{\mathbf{Small-Scale}}}$$

The scaling factor for accelerations must also be considered if small scale accelerations are to be viewed as full scale accelerations. The equation below shows how the acceleration scaling factor (ASF) is determined [11]. Since the scaled time follows the same procedure as the length scaling, the outcome is simply 1 divided by the scaling factor.

$$\mathbf{ASF} = \frac{\mathbf{Length\ Scaled}}{\mathbf{Time\ Scaled}^2} = \frac{\mathbf{Scaling\ Factor}}{\mathbf{Scaling\ Factor}^2} = \frac{\mathbf{1}}{\mathbf{Scaling\ Factor}}$$

Table 1.1: Test Parameters

	5 Pound Charge	10 Pound Charge
Scaling Factor	13.14	10.1
Full Scale Charge Size	5 Pounds	10 Pounds
Scaled Charge Size	1 Gram	4.4 Grams
Full Scale SOD	41.92 Inches	32.02 Inches
Scaled SOD	3.19 Inches	3.17 Inches
Full Scale DOB	3.94 Inches	3.94 Inches
Scaled DOB	.3 Inches	.39 Inches

Scaling problems between the aluminum (5pound charge) and steel series (10 pound charge) rendered direct comparisons between the two sets impossible. In order to compare the two tests directly, all dimensions of the steel series would have to be 1.64 times the dimensions of the aluminum series. This would change the hull dimensions, frame dimensions, specimen weight, etc. These changes could not be made because a 3/32'' steel sheet was the thickest sheet able to be bent to specifications.

Length scales used for the series were correct, in terms of the standoff distance and depth to burial, based on 10 pound charge full scale tests. This makes the steel series a valid tests series, based on 10 pound full scale tests, but changes the acceleration response compared to the aluminum series. Therefore the aluminum and steel series acceleration data cannot be compared directly. However, inferences to what kind of mitigation was best could be derived from both test sets.

$$\text{Aluminum Series to Steel Series} = \left(\frac{4.4 \text{ grams}}{1 \text{ gram}} \right)^{1/3} = 1.64$$

Chapter 2 - Research Equipment

2.1 The Explosive Charge

Explosive charges used for experimentation incorporate an explosive detonator with soft plastic explosive. The detonator is an RP-87 Exploding Bridge Wire (EBW) detonator manufactured by Teledyne Technologies Incorporated. An EBW contains a bridge wire that is vaporized by electricity igniting the initiating explosive, followed by an output explosive located in the head of the device. Figure 2.1 shows a cross section view of an RP-87 EBW detonator. Figure 2.2 shows the dimensions of an RP-87 detonator, used for all tests series in this thesis.

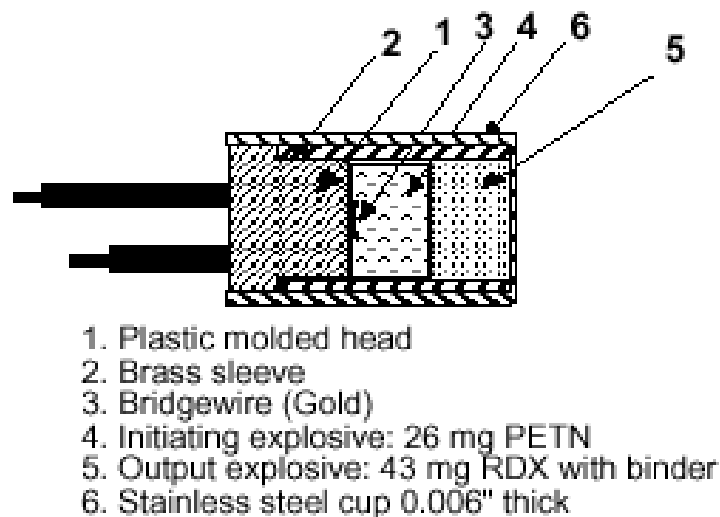


Figure 2.1: RP-87 Explosive Train [12]



Figure 2.2: RP-87 Dimensions [12]

Inside of the detonator, the two explosives are Pentaerythritol Tetranitrate (PETN) and Cyclotrimethylenetrinitramine or Cyclonite (RDX). One RP-87 detonator contains .069 grams of explosive, important for calculating the amount of plastic explosive needed to complete the total charge. Below, Table 2.1 shows the firing parameters for an RP-87 detonator.

Table 2.1: RP-87 Firing Parameters [12]

Threshold Burst Current	210 Amps
Threshold Voltage	~ 500 Volts
Threshold Voltage Std. Deviation	75 Volts Max
Functional Time	1.95 μ sec. Typical
Function Time Simultaneity Std. Deviation	.125 μ sec Max

Plastic sheet explosive known as Deta Sheet makes up the remainder of the charge. Deta Sheet is comprised of 63% PETN by weight, and was purchased from Omni Explosives [13]. Below, calculations are shown for the amount of Deta Sheet in each charge used. The five pound charge test series utilized a one gram charge, while the 10 pound charge test series utilized a 4.4 gram charge.

$$1 \text{ gram} = .069 \text{ grams (Detonator)} + .63 \times 1.48 \text{ grams (Deta Sheet)}$$

$$4.4 \text{ grams} = .069 \text{ grams (Detonator)} + .63 \times 6.875 \text{ grams (Deta Sheet)}$$

A sample preparation of an explosive charge can be seen in Figure 2.3 below. From left to right, a charge casing was packed with Deta Sheet, and then an RP-87 detonator was placed in one side. The Deta Sheet was rolled into tight balls for charge preparation, to eliminate air pockets and increase the malleability of the explosive.

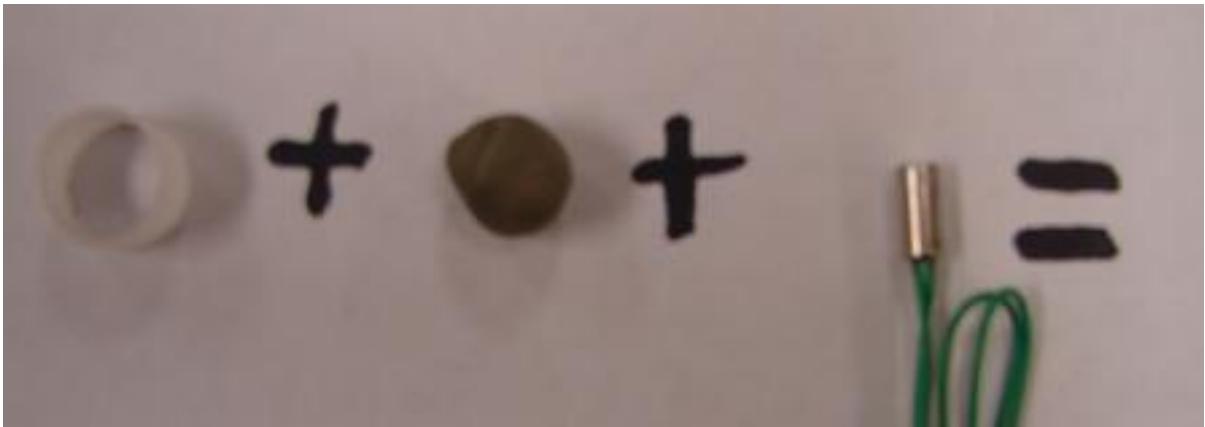


Figure 2.3: Sample Charge Preparation

It was essential that once the Deta Sheet is inside the charge casing, the ends of the charge are as flat as possible (one end of the charge must have Deta Sheet flush with the end of the casing). At this time, the RP-87 detonator is stuck roughly 1mm into the end opposite the flat side of the charge. Figure 2.4, below, shows a finished charge.

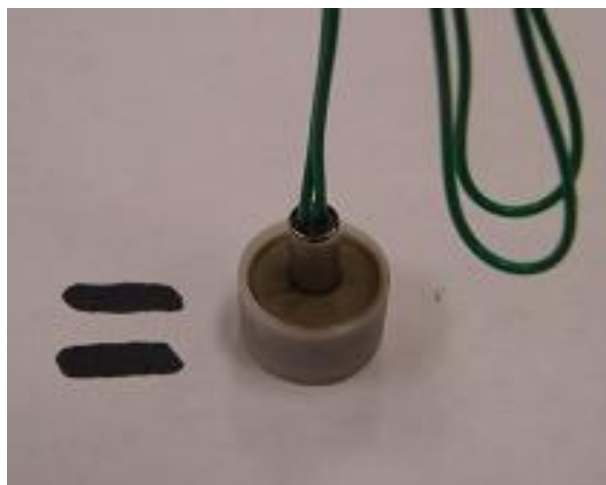


Figure 2.4: Finished Charge

For the two test series in this paper, 1 gram and 4.4 gram charges were used. Figure 2.5 and Figure 2.6 below show these charges respectively.

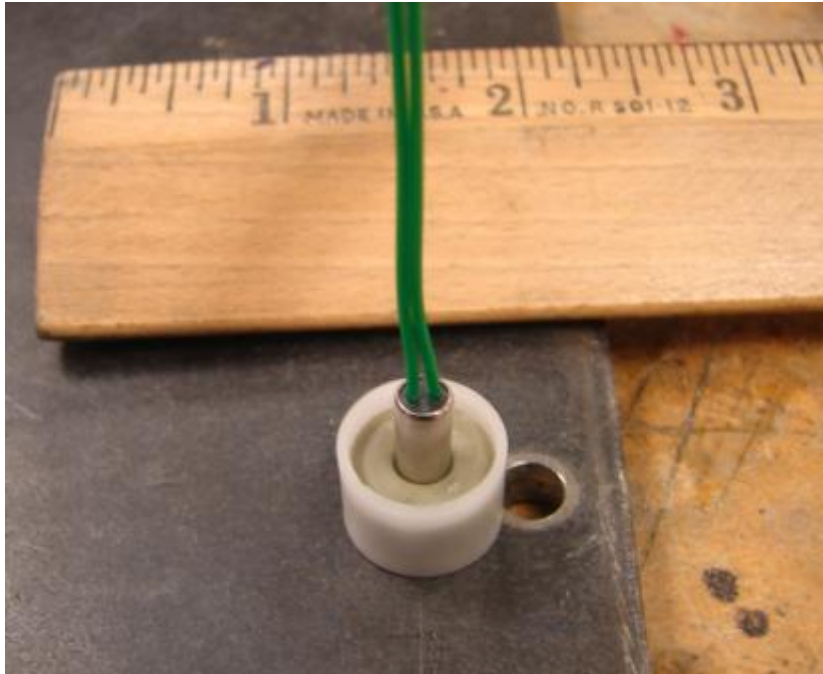


Figure 2.5: 1 Gram Charge

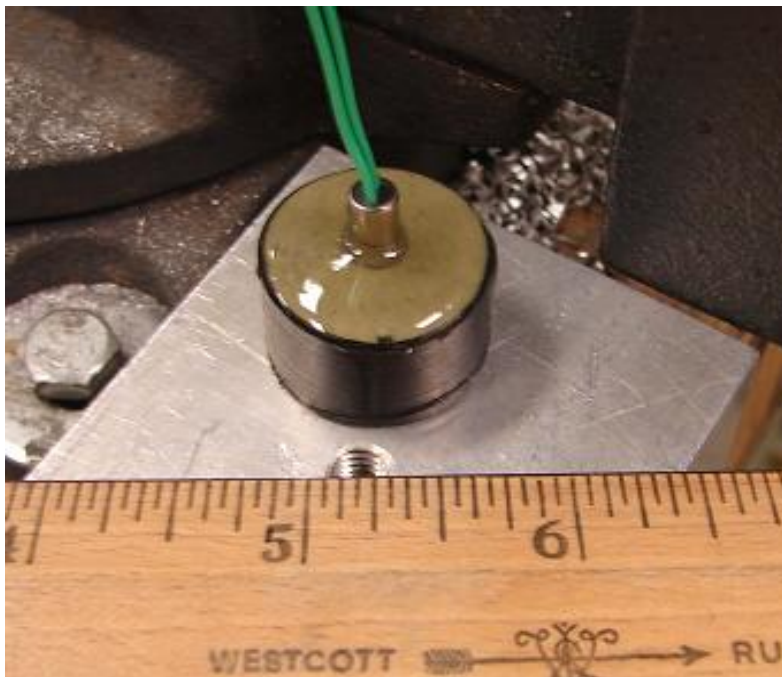


Figure 2.6: 4.4 Gram Charge

Charge casing were made out of Delrin rod, machined on a lathe. The outer diameter of the Delrin rod was shaved down, and then the inner diameter bored out via drill bit until specifications were met. Cross sections of the two charge casings used can be seen below in Figure 2.7 and Figure 2.8 (Note: Drawings not to scale).

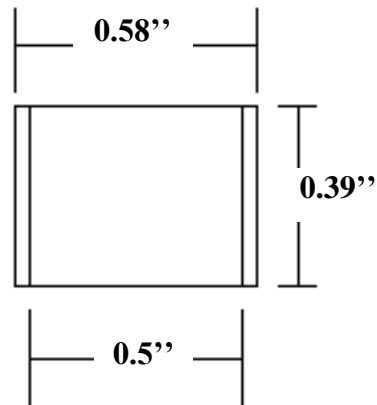


Figure 2.7: 1 Gram Charge Casing Cross Section

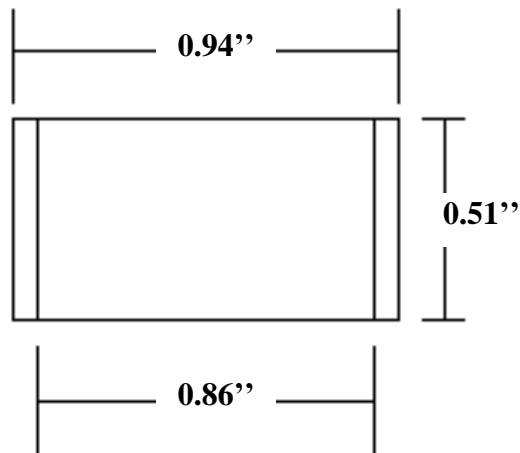


Figure 2.8: 4.4 Gram Charge Casing Cross Section

2.2 Firing System

The FS-17 firing system, seen in Figure 2.9 below, was used to trigger explosive charges for all experiments in this paper. The system consists of a control unit, a firing module, and a connected triggering mechanism. When the safety is removed from the position “Short to Discharge” and placed into the position “Safety Interlock”, the box is ready to be armed. The key in the bottom left of the control unit is then turned and held, until a voltage of 3500 volts or more is achieved by the unit [14]. At this time, the charge is ready to be fired by the firing switch in the lower right of the box. It is important to notify lab personnel before detonation, when the safety is removed, when arming the unit, and through a countdown previous to firing the charge with the firing switch. These steps are crucial because aside from bodily injury, auditory injury can occur if lab mates do not protect their ears during a blast. All firing specifications can be found in Appendix A.

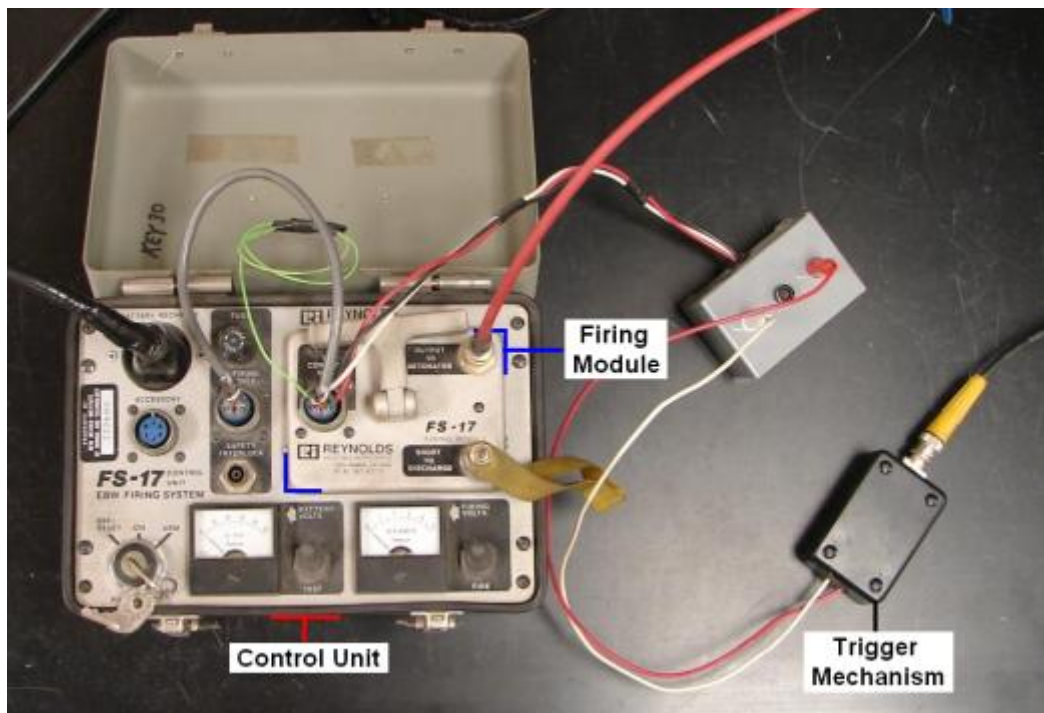


Figure 2.9: FS-17 Firing System [6]

2.3 The Dummy Charge

Before testing, it is imperative that the setup triggers and the firing box works correctly. To ensure this, a dummy charge is connected to the firing box. At this time, the charge is fired, and the user can check that all connected instruments have triggered. The dummy charge consists of two exposed wires, 1/8 in apart, housed in an aluminum cylinder. When the box is fired, electricity jumps across the gap between the wires creating a flash of light and an audible noise. This flash of light can be seen using high speed cameras, further verifying the triggering of the setup and the efficiency of the firing box. A picture of a dummy charge can be seen in Figure 2.10 below.

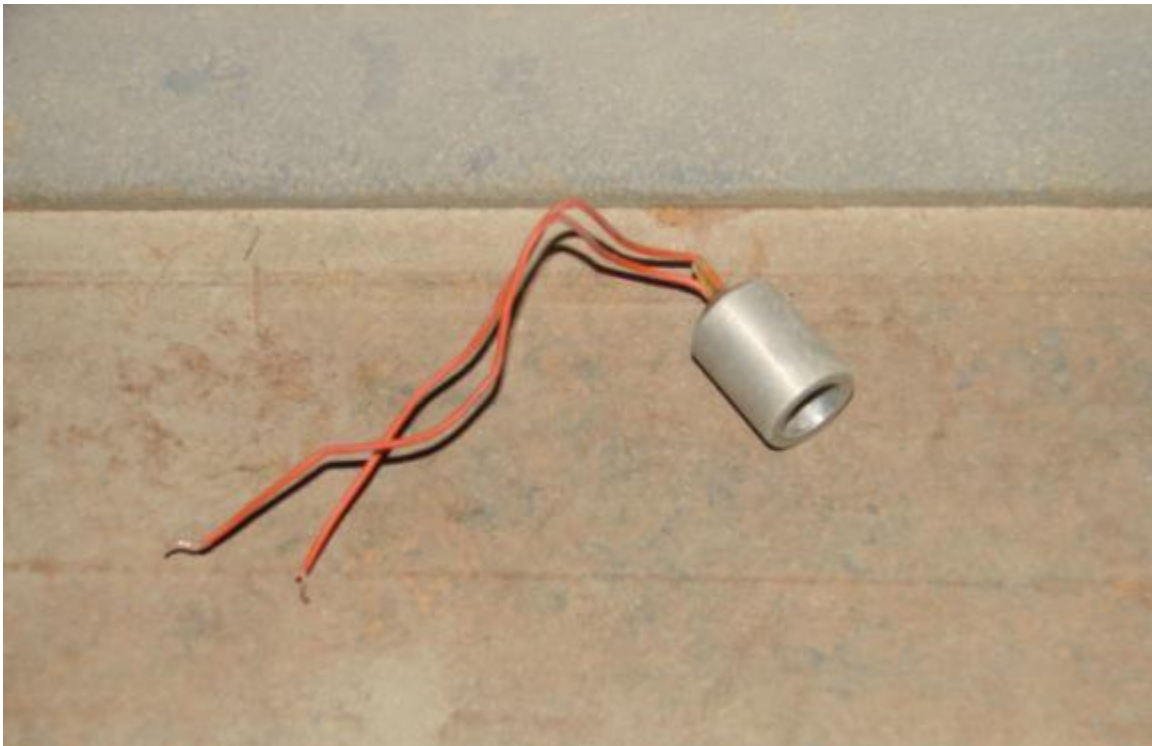


Figure 2.10: Dummy Charge [1]

2.4 Sand Pit

All discussed tests were conducted in the sand pit shown in Figure 2.11 below. The sand pit, also referred to as the test bed, is a 5x5x2 foot steel box filled with Home Depot HD-2 sand [1]. The box is filled with water to create saturated sand for testing via the water piping system seen in Figure 2.11. Beneath the sand, there is a mesh net, followed by a layer of gravel which keeps the water inlet free of sand.



Figure 2.11: Sand Pit

2.5 Aluminum Frame – Navy Test Series

A 5.47 pound (2.48kg) aluminum frame, shown below in Figure 2.12, was used for all tests in this series. A schematic of this frame can be found in Appendix B. In this schematic, black dots represent the approximate accelerometer tap locations. These positions were centered as best as possible between bolt holes and the frame width. First holes were drilled 0.3 inches into the frame with a 0.202” diameter drill bit. Then the holes were tapped with a ¼” – 28 male tap. All tap specifications were based on schematics for PCB accelerometers, found in Appendix H. The frame is made of 6061 aluminum, and consists of two identical 0.5” thick pieces which are bolted together.

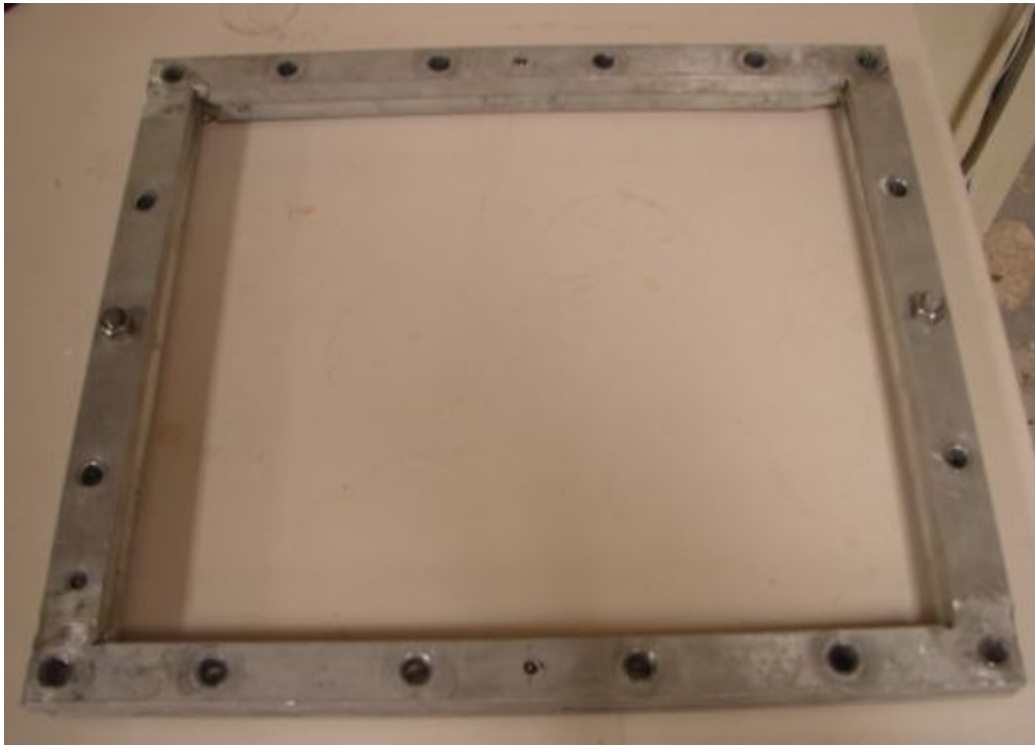


Figure 2.12: Aluminum Frame

2.6 Steel Frame – Army Test Series

A 7.58 pound (3.44 kg) steel frame, shown below in Figure 2.13, was used for all tests in this series. A schematic of this frame can be found in Appendix C. In this schematic, black dots represent the approximate accelerometer tap locations. These positions were centered as best as possible between bolt holes and the frame width. First, holes were drilled 0.3 inches into the frame with a 0.2188” diameter drill bit. Then the holes were tapped with a ¼” – 28 male tap. All tap specifications were based on schematics for PCB accelerometers, found in Appendix H. This frame is made of 1018 steel and, unlike the aluminum frame, only consists of one piece. This was to reduce weight, while maintaining a rigid frame that can endure many blasts.

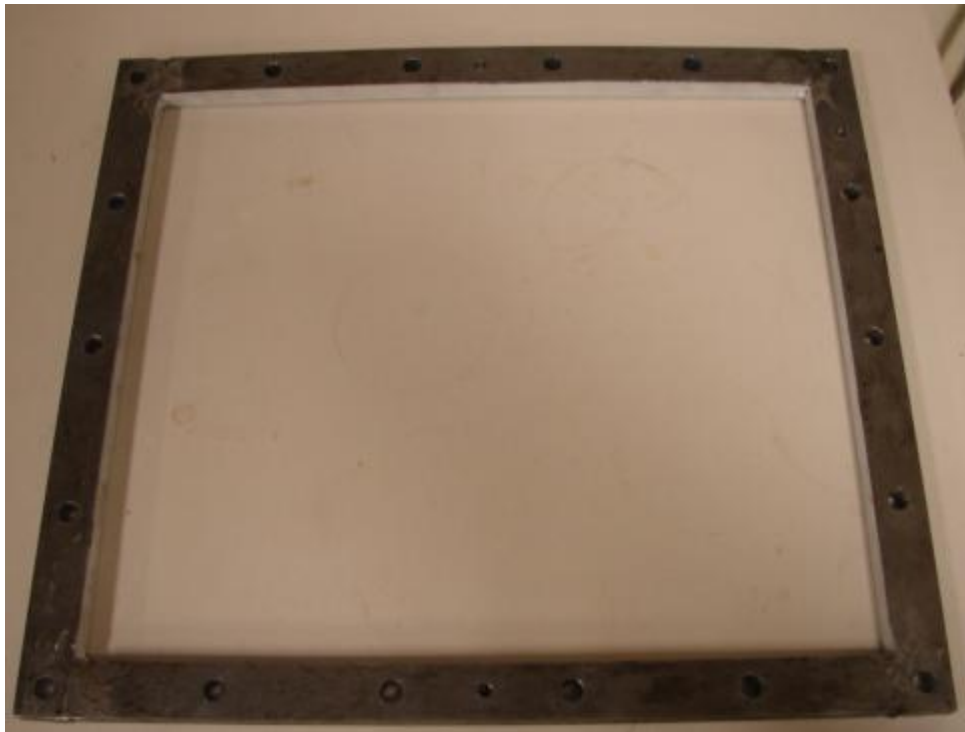


Figure 2.13: Steel Frame

2.7 The Angled Hull

For all tests conducted in this paper, an angled hull was utilized to reduce blast damage. In previous testing, it has been found that a hull with a 13 degree angle measured against the horizontal is the most efficient design for blast effect reduction [15]. Larger angles were also studied, and it was found that increasing the angle past 13 degrees minimally improved the overall design in reducing blast damage. A diagram of the angled hull can be seen below in Figure 2.14, where θ represents where 13 degrees is measured.

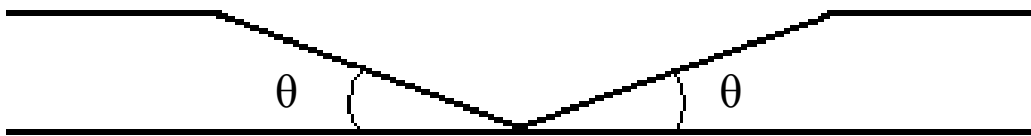


Figure 2.14: Angled Hull Diagram

The angled hull is constructed out of a 16''x18''x3/32'' aluminum or steel plate. Each plate was measured in the 18'' direction and the centerline marked with a ruler on each side of the plate. On one side of the plate, 6.1875'' was measured in either direction from the centerline and marked. The plate is then taken to a bending press and bent along these lines (Starting from one end, bend along each line, flipping the plate between bends). A diagram of the plate dimensions used for all tests in this paper can be found in Appendix G. For the sliding hull test, slightly different dimensions were used, giving the plate more freedom to slide. A diagram of the sliding hull can be found in Appendix D.

2.7.1 The Pocket Plate

A series of pocket plate tests were performed to investigate hull orientation effects on acceleration mitigation. Figure 2.14 depicts a downwardly convex hull shape; a pocket plate would be the reversal of this, or a downwardly concave hull shape. In this series, the spine of the hull was the farthest away from the charge. By placing the spine of the hull farther from the center of the blast, an attempt was made to slow down the fastest portion of the blast before it could contact the specimen. It has been proven theoretically and analytically that a downward concave hull is able to reduce blast damage, "...hulls with bottom geometries that were both downwardly concave and downwardly convex reduced the amount of kinetic energy imparted to the target..." [16]. Impulse testing has been performed comparing downwardly convex and concave hull geometries, but accelerations were not investigated. This paper will compare pocket plate (downwardly concave) results to downwardly convex results, but also look at mitigating accelerations for pocket plate designs specifically. Due to the geometric differences, pocket plate tests had a propensity for ill-advised hull-frame interactions; the increased spacing between the sand and the spine of the hull caused a decreased distance between the spine of the hull and the frame. This decreased distance resulted in the spine of the hull contacting the frame during testing, resulting in increased frame acceleration. This situation was a point of emphasis during design recalculation for the pocket plate series. Future pocket plate tests will involve a redesigned frame, hopefully stopping hull-frame interactions entirely.

2.8 Lighting Specifications and Preparation

All tests utilized 250W halogen photography lights from North Star, seen in Figure 2.15. This allowed high speed footage to be visible when exposure times were in the single micro seconds. The flexible neck and clamp base allowed for easy implementation for all tests. During testing, it was important that the light not reflect off the specimen and over saturate the image. It is recommended that the lights aim in the same direction as the camera, as to not have the chance of shining a light directly into the lens, over saturating the video.



Figure 2.15: North Star Flexible Light [17]

2.9 High Speed Camera Equipment and Setup

Phantom high speed cameras were used to record video of each test. Figure 2.16 shows the Phantom v12.1 high speed camera, capable of 1 million pictures per second [17]. The camera has a 1200x800 pixel monochrome sensor, but because higher frame rates were needed 512x512 pixels were used for all tests. All camera settings can be found in Table 2.2 on the following page. Cameras were fitted with a 28-75mm variable focus zoom lens (Not pictured).



Figure 2.16: Phantom v12.1 High Speed Camera [17]

The camera was mounted on a tripod for the most flexibility between camera height, angle, and placement. Cameras were run using Phantom camera software via laptop computer. Here, camera settings were chosen such as, how the camera was

triggered before the blast. Phantom software also allows for displacement vs. time calculations by tracking points in the video frame by frame. This data can then be compared against other experimental data for verification purposes.

Table 2.2: Recording Specifications

Resolution	512 x 512
Exposure Rate	49 μ s
Frames per Second	20000
Total Frames	21397

2.10 PCB Accelerometers

Accelerometers from PCB Piezotronics (Model 350C02) were used for acceleration measurements. These accelerometers were chosen because of their ability to withstand a large g level, long cable, and tap dimensions. Accelerometer specifications can be found in Appendix H. Three accelerometer holes were tapped in each frame, recording accelerations of the left, right, and corner of the frame. Figure 2.17 below shows one of the three accelerometers used for each test.

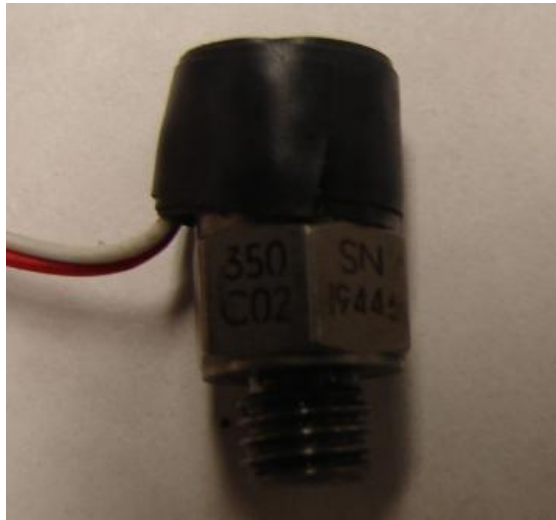


Figure 2.17: Accelerometer

Kenlube grease was used to further the bond between accelerometers and the metal frame. A thin layer of grease was applied to the thread of the accelerometer, around holes on the frame where accelerometers were screwed in.

Accelerometers were calibrated up to 10000Hz, and required calibration factors to convert their output in voltage, to acceleration in g's. Table 2.3 shows the calibration factors for each accelerometer used in testing. An acceleration in g's was easily translated

into either $\frac{ft}{s^2}$ (data was multiplied by 32.2) or $\frac{m}{s^2}$ (data was multiplied by 9.81).

Accelerometer placement can be seen in Figure 2.18, shown from overtop the test specimen. Left, right, and corner accelerometers are labeled as viewed by the camera.

Table 2.3: Calibration Factors

Serial Number	Calibration Factor (g's/mV)
19445	8.84956
19446	10.7527
30279	9.7087

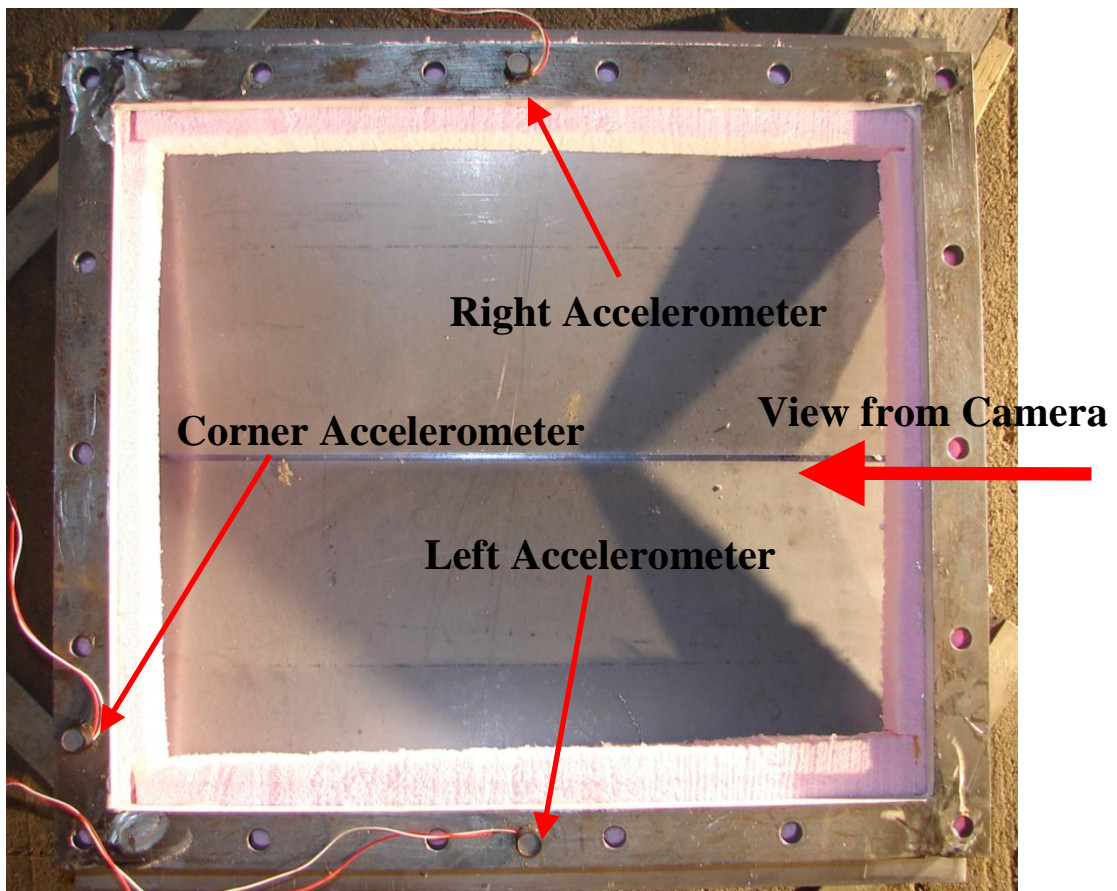


Figure 2.18: Accelerometer Placement (Top View)

2.11 Oscilloscope

Accelerometer signals were sent to two LeCroy oscilloscopes (9314AM and 9315AM). Signals were split between the two scopes, so that different scope settings could be chosen, as seen in Figure 2.19. Time per division and voltage per division were differed to focus in on the data while avoiding clipping.



Figure 2.19: Oscilloscope Setup

Before accelerometer signals were received by the oscilloscopes, they were pre-processed by a PCB Piezotronics model 483A amplifier. The amplifier can be seen in Figure 2.20 below, where the dial on the right of the image showed whether the connected accelerometers were functioning properly.



Figure 2.20: Amplifier

2.12 UERDTools Software

Post processing of acceleration data was performed solely with UERDTools software (version 4.4). Here data can be multiplied and divided by scaling factors, viewed in its frequency spectrum, and filtered a variety of ways. UERDTools software was also used to verify camera data versus accelerometer data. Camera data was uploaded into the program as displacement vs. time plots, and compared against acceleration data that was integrated twice. UERDTools software was developed at NAVSEA at Carderock's Underwater Explosives and Research Division [18]. A screenshot of the UERDTools software interface can be seen in Figure 2.21 below.

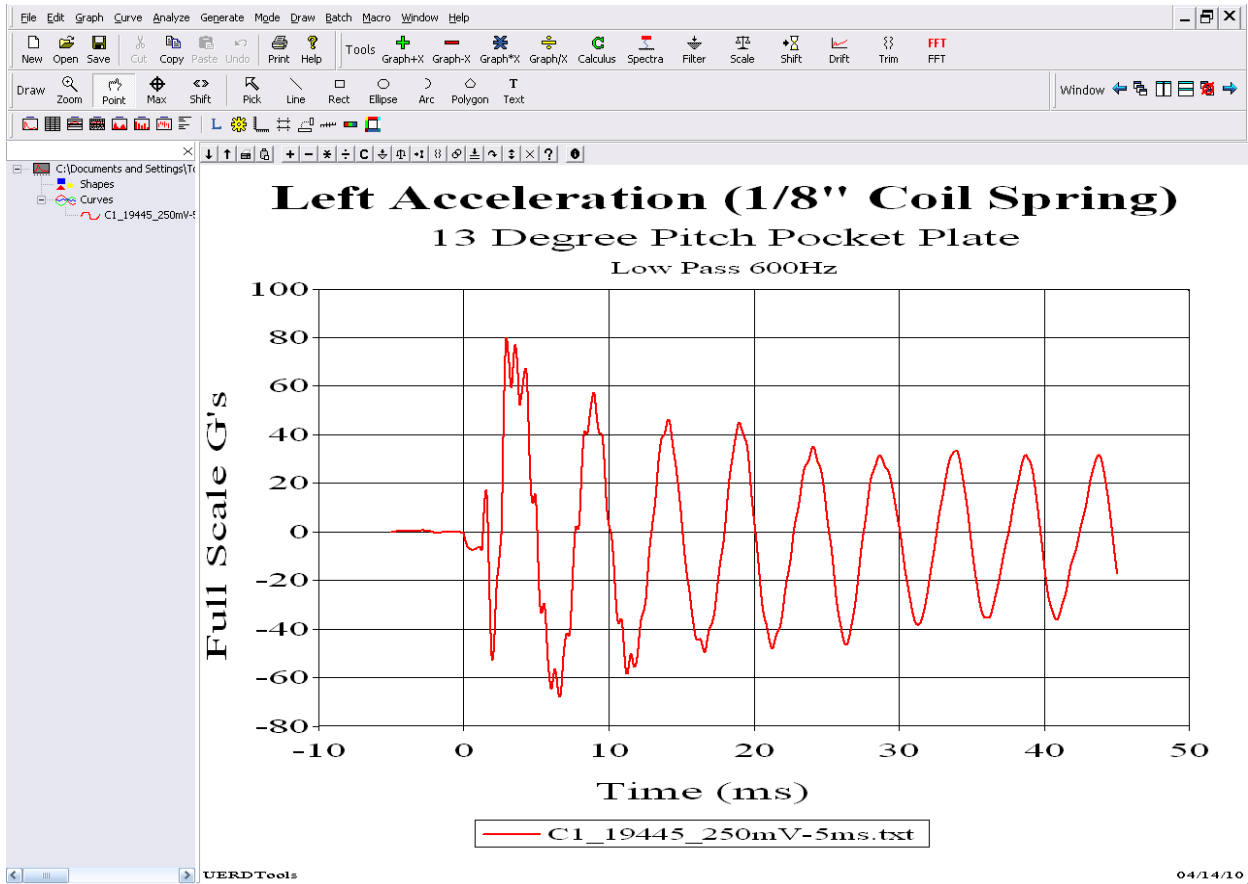


Figure 2.21: UERDTools Software

Chapter 3 - General Experimental Procedures

3.1 Test Procedure

All tests were performed in the sand pit located in the basement of the Dynamic Effects Lab. A diagram of the test setup can be seen below in Figure 3.1. Here, accelerometers were run to an amplifier, and then split between two oscilloscopes. The firing box trigger was connected to the camera and the oscilloscopes, while the firing wire was connected to the charge. When triggered, the oscilloscopes and camera recorded data (camera data was sent to a laptop for viewing purposes).

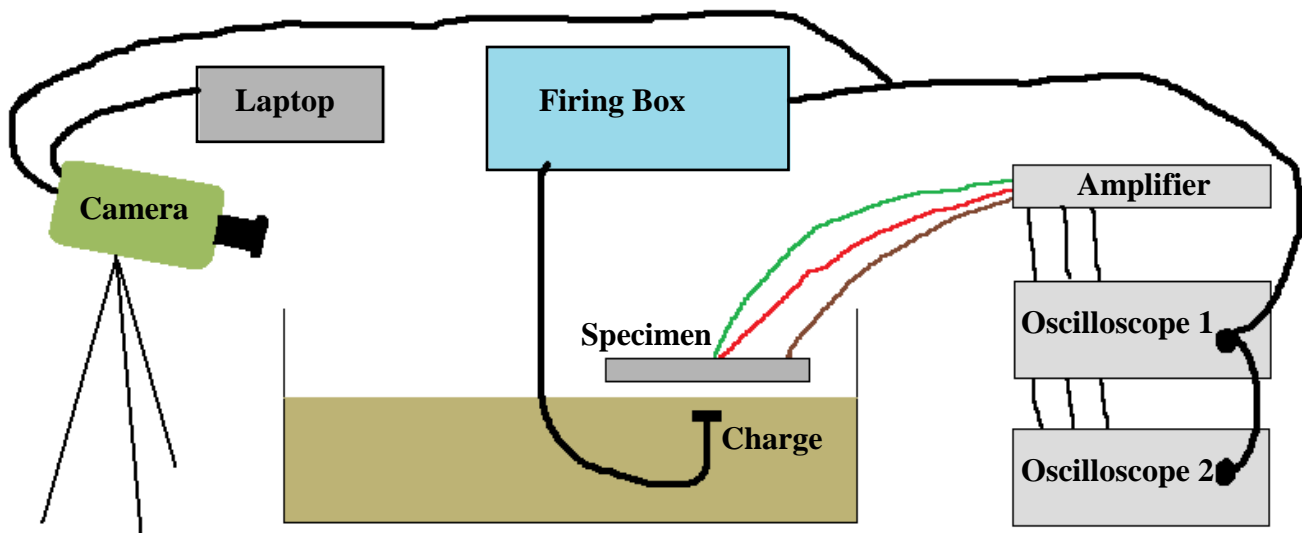


Figure 3.1: Test Setup (Not to Scale)

First, the sand pit was prepared; sand was piled up over the test location, compacted, and then leveled. The left picture in Figure 3.2 shows the sand pit after loose sand had been piled up on the test location. The pictured cinder block was then used to compact the test bed, to get a uniform density of the sand in the bed. The right picture in

Figure 3.2 shows the sand pit after a leveling tool had been drug across the top surface. The test bed would now be ready for the next step: charge burial.



Figure 3.2: Before (Left) and After (Right) Leveling

Before the charge was buried in the test bed, the specimen was placed in the test location, and the perimeter traced into the sand. Lines are then traced, diagonally, from corner to corner making an 'X' where the center of the specimen would lie. The charge was then placed at the center of the 'X' at the correct depth of burial. Sand was then placed over the charge, leaving the pit level and smooth.

In Figure 3.4, on the following page, a sample diagram shows how, where measurements were taken for both test series. The standoff distance (SOD) was measured from the top of the sand to an imaginary floorboard. Figure 3.3 shows where the imaginary floorboard was located for the aluminum and steel test series (the pocket plate series was similar to the steel series). For the steel series, the imaginary floorboard was at the bottom of the single frame piece. For the aluminum series, the imaginary floorboard was located between the two frame pieces. In both cases, the floorboard was 0.5 inches from the top of the specimen, or 0.5 inches from the base of the accelerometers. There was a 1.4 inch gap between the imaginary floorboard and the top of

the hull for all test series'. This gap was kept constant, so that the distance between the top of the sand and the spine of the hull was the same for each test. The depth of burial was measured as the distance between the top of the sand and the top of the buried charge.

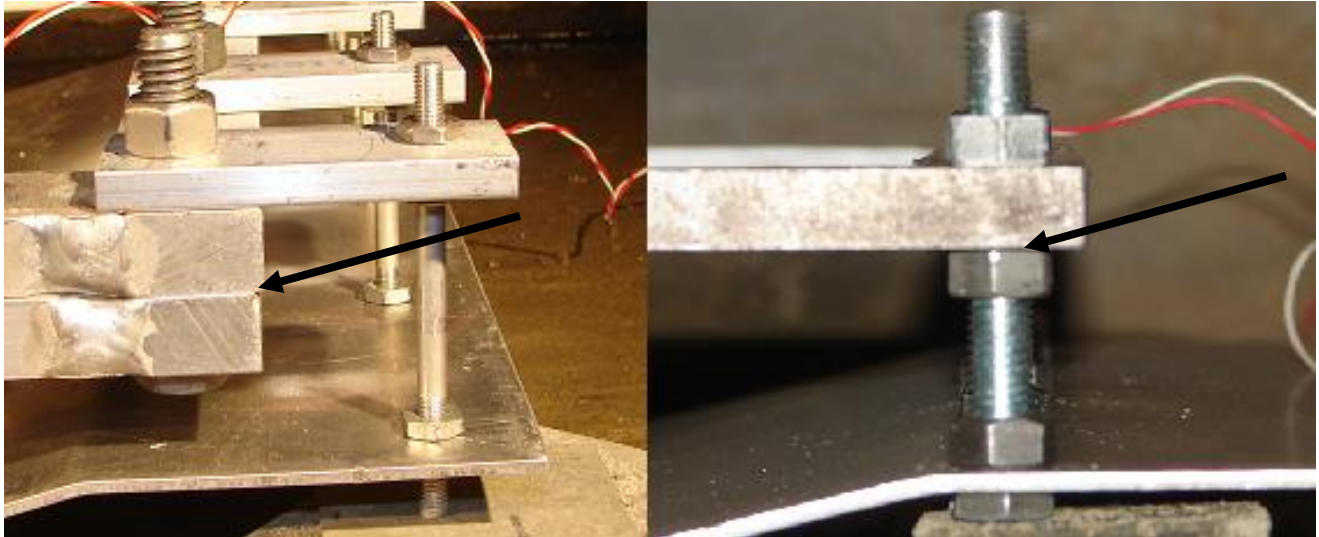


Figure 3.3: Imaginary Floorboard

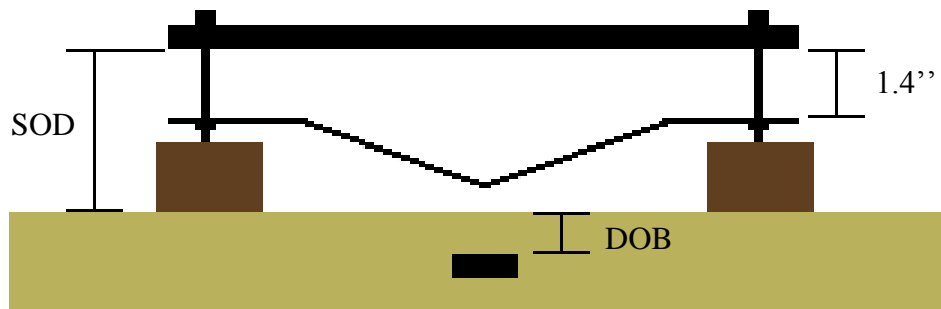


Figure 3.4: Test Diagram

When all the measurements were correct, the camera was setup to the desired viewing specifications. Accelerometers were placed on the frame in three locations, and secured with a wrench. Accelerometers were connected to oscilloscopes, which were then set to desired specifications. The test bed was then filled with water, saturating the sand.

A dummy charge was connected, fired to ensure the setup functions properly. The charge was then connected to the firing wires, and the test was run. Data was then collected from the camera and oscilloscopes for post processing. Figure 3.5 shows the test setup just before testing, when the dummy charge was tested.

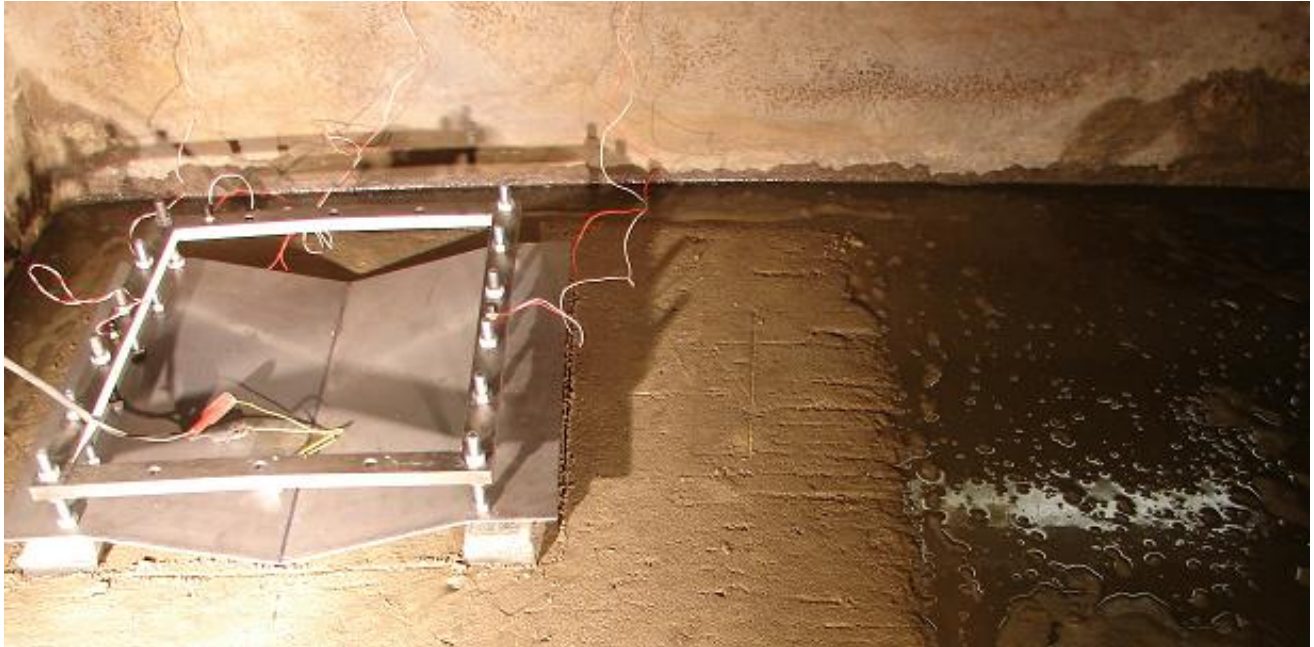


Figure 3.5: Final Step before Testing

3.2 Phantom Software Analysis Procedure

Video recordings were analyzed using Phantom camera software to get displacement vs. time results. These results were then compared against accelerometer data (integrated twice) for verification purposes. To collect points for displacement plots, units (English or metric) were first selected. Once an origin had been set, a file was created to collect space, time data for each click in a particular frame. These points were imported into UERDTools software and plotted against accelerometer data that had been integrated twice. This allowed for the comparison of displacement based on video data and displacement based on accelerometer data. In Figure 3.6, a screenshot of the Phantom program shows how points were tracked. The blue crosshairs indicate the origin, while the white dot indicates a point that was tracked, in this case the accelerometer on the left of the frame. Tracking the displacement of the accelerometers, allows for the direct comparison to twice integrated acceleration data in UERDTools.

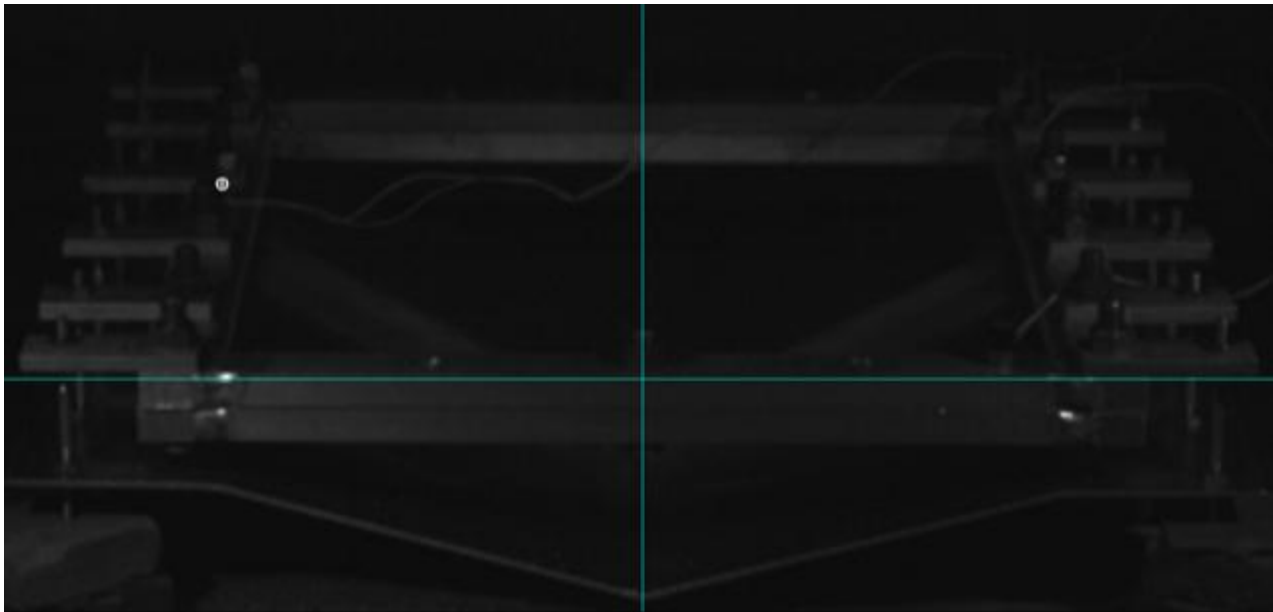


Figure 3.6: Tracking Points with Phantom Software

3.3 UERDTools Data Analysis Procedure

Data from accelerometers was post processed using UERDTools software. When importing data into the program, it was important to first correct the data. Data correction involved correcting offsets in the data, converting time into milliseconds, drift compensation, shifting the data, and trimming the data. Correcting the offset ensured that the data starts at zero when time is zero. Compensating for drift ensured that the data does not drift as time increases (drift can be identified when the data does not return to zero at an appropriate time). The other corrections were aesthetic type corrections, though converting from seconds to milliseconds must be done before filtering.

Once corrections have been made to the data, the data was converted into the appropriate units and filtered. To convert into the appropriate units, the following equations must be considered.

$$\text{Raw Data (Volts)} * 1000 \left(\frac{\text{mV}}{\text{V}} \right) = \text{Raw Data (mV)}$$

$$\text{Raw Data(mV)} * \text{Calibration Factor} \left(\frac{\text{G's}}{\text{mV}} \right) = \text{Small Scale G's}$$

$$\text{Small Scale G's} * (\text{ASF}) = \text{Full Scale G's}$$

When the raw data is uploaded, it was first multiplied by 1000 to convert to millivolts. The data was then multiplied by the accelerometer specific calibration factor. The data was then multiplied by the acceleration scaling factor, which was equivalent to dividing by the scaling factor for that particular test series. The data was now in the

appropriate units (g's vs. millivolts). The next step in post processing was filtering the data to remove noise. Accelerometers were only calibrated to 10000Hz, so it was essential to remove pieces of the data above this level. Initial accelerations peaks were also found to be unrealistically high, further stressing the need to filter the data. High frequency data was due to internal resonance of the structure [19].

To choose a filtering frequency a fast Fourier transform (FFT) of the data was created, shown in Figure 3.7 on the following page. A Fourier transform broke the data up into sine and cosine functions of different amplitude and frequency. This allowed for the identification of the fundamental frequency and overtones. The fundamental frequency describes the lowest frequency at which the system resonates; resonance describes a frequency at which the system exhibits larger amplitudes of oscillation than other frequencies. Overtones are frequencies, higher than the fundamental frequency, where the system also exhibits resonance. Once these frequencies were identified, the data was appropriately filtered to avoid aliasing. Aliasing occurred when the data was filtered too aggressively, or not enough samples were available to describe the data set. It was important to find the first few frequencies of resonance, and filter above that point (data was exclusively filtered using low pass filters).

The FFT plot shows the frequency spectrum of a test in the steel series. Here, a filtering frequency of 600Hz was chosen, still keeping the largest resonant frequencies of the system. This filtering point was checked, however, against camera data to ensure aliasing did not occur. Filtering points for each test series were chosen based on the frame used. This was done so that tests within a series were not biased based on the use of

different filtering methods. Therefore it was assumed that the frequency response of tests within a series were relatively equivalent.

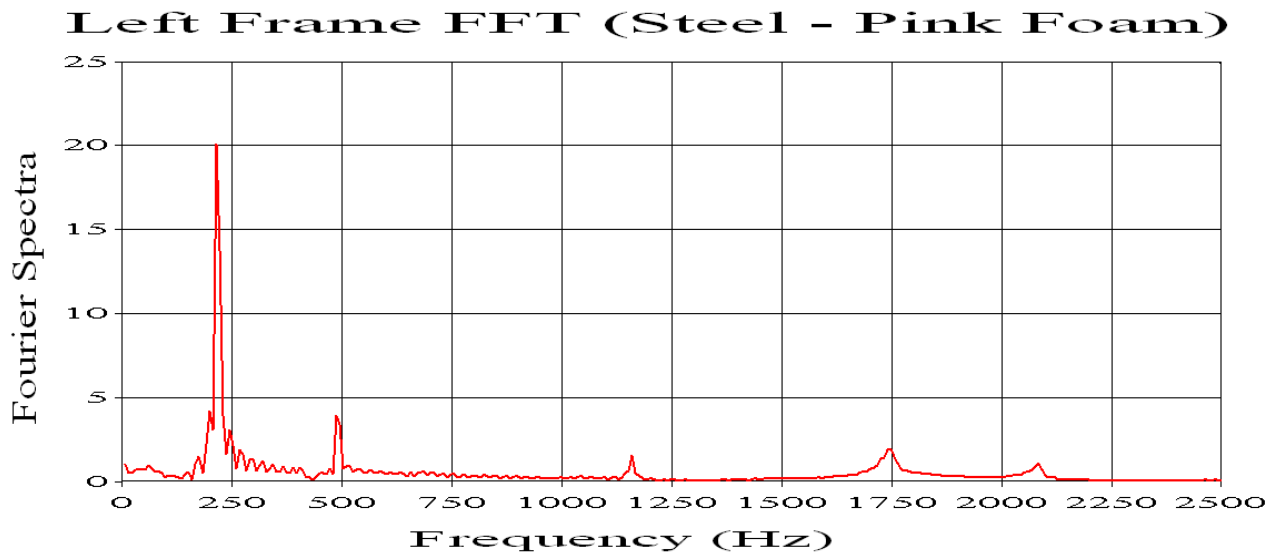


Figure 3.7: FFT Plot

Chapter 4 - Test Series Overview

4.1 Aluminum Test Series

The aluminum test series was based on 5 pound charge (full scale) tests. This scaled down to a 1 gram charge used for testing. Masses, weights for each test specimen in this series can be seen in Table 4.1 below.

Table 4.1: Aluminum Test Series Specimen Weights/Masses

Test	Weight	Mass
	Pounds	Grams
Aluminum 1	8.74	3965.2
Aluminum 2	8.24	3737.6
Aluminum 3	8.71	3950.1
Aluminum 4	8.34	3783.6
Aluminum 5	8.27	3752.1
Aluminum 6	8.23	3731.4

4.1.1 Aluminum 1: Control Frame

A control test was performed for the aluminum (5 pound) test series, as seen in Figure 4.1. Here an angled hull was directly bolted to the frame, with no mitigation techniques involved. The frame assembly was a rigid target, while the hull deformed during testing.



Figure 4.1: Aluminum Control Frame

4.1.2 Aluminum 2: Spider Frame

In this test, 3/16" aluminum threaded rod (10-32 die) was used to connect an angled hull to a rigid aluminum frame, as seen in Figure 4.2. This mitigating system was intended to absorb blast energy through plastic deformation of the aluminum rods. The aluminum rods also allowed the hull to move more freely as it deformed, reducing energy, forces delivered to the frame.

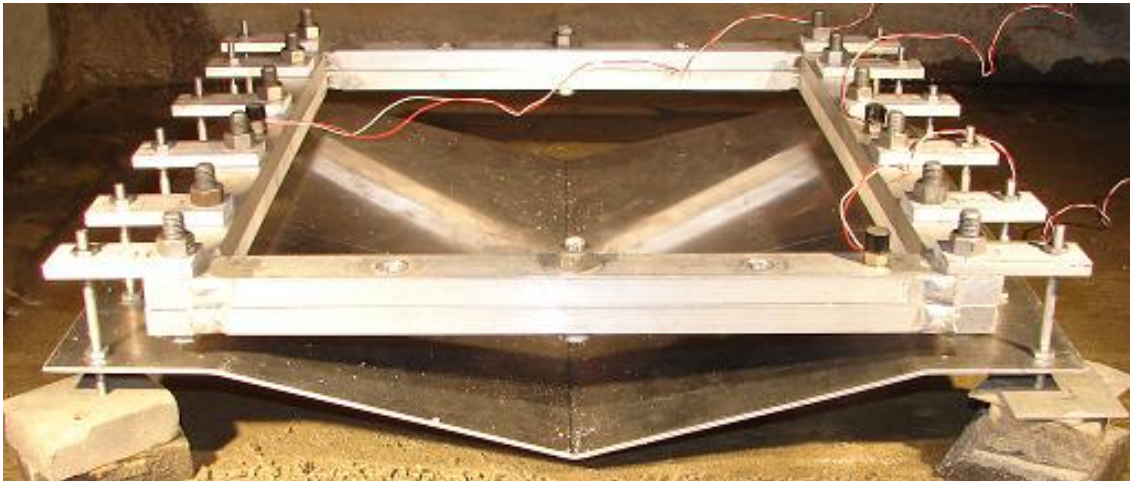


Figure 4.2: Spider Frame

Each aluminum rod was roughly modeled as a cantilever beam; with the deforming hull acting as a point load on the end. Based on this loading definition, the maximum load before plasticity was approximately 15 pounds or 66.7 Newtons (equation show on the following page). There were twelve rods, so the total load was 180 pounds or 800 Newtons. This calculation assumed that yielding was caused solely by bending, when it actually was a combination of axial and bending forces. However, rods showed deformations based on bending, so these calculations were performed. It was also not

presumed that axial forces aided plastic deformation; in some cases axial forces strengthen a material during bending. In conclusion, the fact that the axial forces in a mixed loading condition could not be assumed, they were left out. Material properties for aluminum 6061-T6 can be found in Appendix K.

$$\sigma_{\text{yield}} = \frac{My}{I} = 276\text{MPa} = 40000\text{psi}$$

$$M = Px \rightarrow P = \left(\frac{I\sigma_{\text{yield}}}{yx} \right)$$

4.1.3 Aluminum 3: Sliding Hull

The sliding hull test furthered the idea that deformations to the hull are not necessarily a detriment, as long as penetrations and hull-frame contact do not occur. Here, the hull was allowed to slide in a single direction, in an attempt to dissociate the movement of the hull and the frame. By allowing the hull to slide as freely as possible while deforming, impulse from the blast was absorbed by the hull, not directly transmitted to the frame. A picture of the sliding hull can be seen in Figure 4.3, and a diagram in Appendix D.

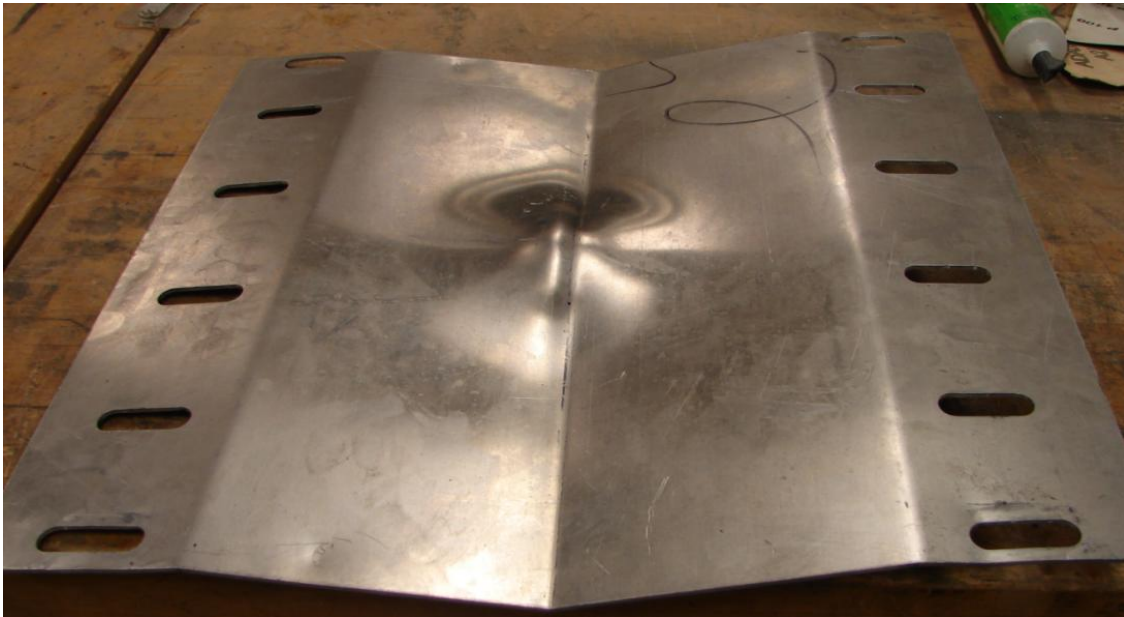


Figure 4.3: Deformed Sliding Hull

4.1.4 Aluminum 4: Spring Spider Frame

Incorporating springs between the frame and the hull allowed less restricted movement of the hull with respect to the frame, but also removed some energy from the system through the compression of the springs (In this case tension was not possible because the springs were not bound to the specimen). The stiffness of each spring was 47.44 lbs/inch and there were eight springs total [20]. Therefore the total stiffness of the mitigation system between the hull and frame was 379.52 lbs/inch. More information on the springs used in this test can be found in Appendix I.

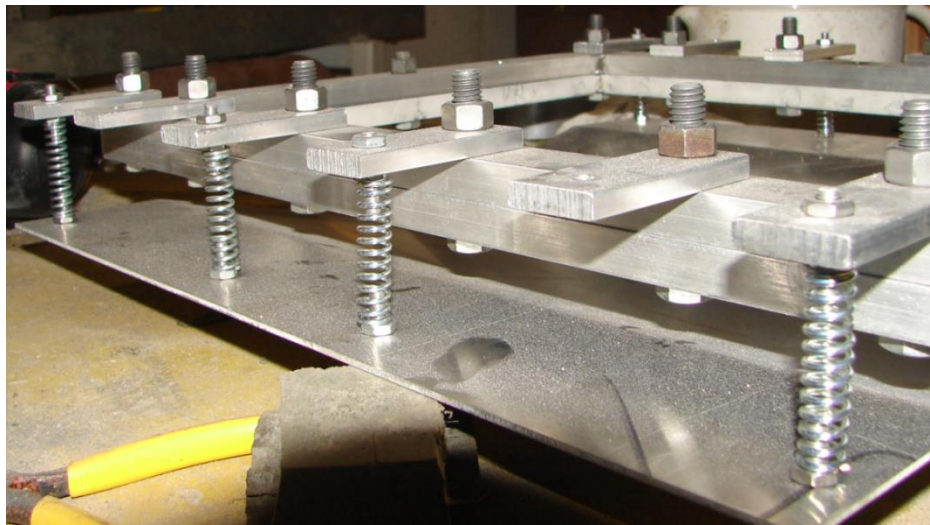


Figure 4.4: Side View of Spring Spider Frame

During the blast, there was dissociation of the frame and the hull, because the springs did not bind the two. This can be seen in Figure 4.4. The springs compressed completely, and as they extended, the frame accelerated away from the hull. This dissociation would leave the vehicle disabled after almost any blast, something that was remedied in later tests (steel isolators that act like springs were bound to the frame and the hull, negating the chance of dissociation during a blast).

4.1.5 Aluminum 5: Pink Foam

Pink foam has been utilized previously in the Dynamic Effects lab to normalize accelerations of steel plates used in air pressure testing. Pink foam was utilized in pressure tests to lower acceleration peaks, and elicited a more repeatable response. A stiffness of 3722 lbs/inch was calculated by fitting a curve to the linear portion of data found in Appendix J. Foam was bonded to the hull and frame directly using fast setting epoxy (This was the bonding technique for all foam tests in this paper). Triggering problems caused video data to be unavailable for this test, though accelerometer data was preserved. For reference, Figure 4.7 shows the same test setup, but for the steel series. In this test, a 0.9 inch thick piece of pink foam was placed between the hull and frame of the specimen and set with epoxy.

4.1.6 Aluminum 6: White Foam

The high stiffness of the pink foam resulted in little energy absorption through deformation; therefore less stiff white foam was utilized in this test. For white foam, a stiffness of 278 lbs/inch was calculated by fitting a curve to the linear portion of data found in Appendix J. Non-linear regions of the curve indicate areas where foam cells compressed freely at specific loads, until the next cell group of the foam was reached. This explains why the load increases in a step like fashion. White foam failed during testing, shown in Figure 4.5, which was not intended. White foam was discontinued as a main mitigation device due to its propensity to shear during testing. In this test, a 0.9 inch thick piece of white foam was placed between the frame and hull of the specimen and set with epoxy.

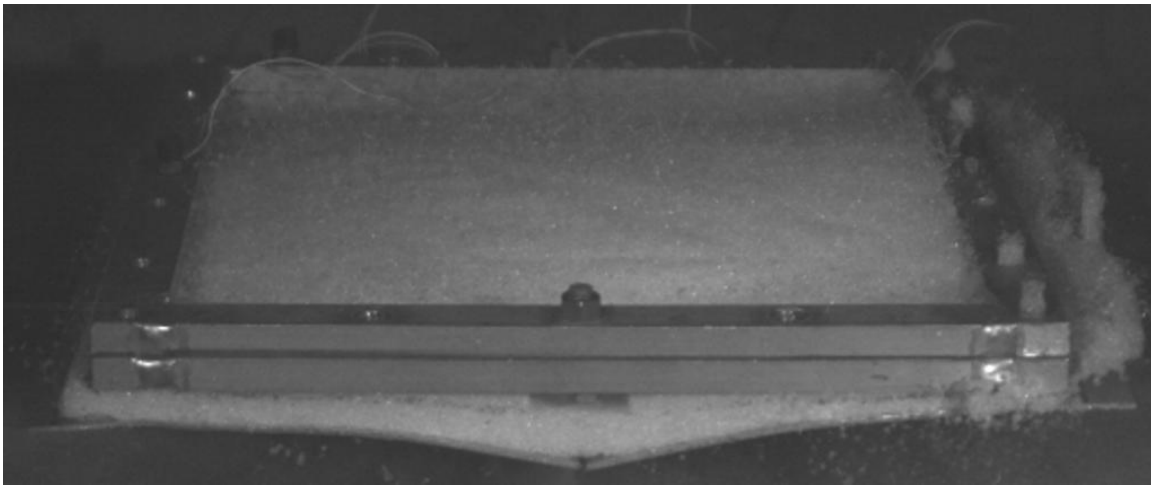


Figure 4.5: Failure of White Foam during Testing

4.2 Steel Test Series

The Steel test series was based on 10 pound charge (full scale) tests. This scaled down to a 4.4 gram charge used for testing. Masses, weights for each test specimen in this series can be seen in Table 4.2 below.

Table 4.2: Steel Test Series Specimen Weights/Masses

Test	Weight	Mass
	Pounds	Grams
Steel 1	17.25	7825.2
Steel 2	16.92	7674.4
Steel 3	16.90	7663.6
Steel 4	16.96	7694.8
Steel 5	17.57	7972.3
Steel 6	17.66	8011.7

4.2.1 Steel 1: Steel Control Frame

A steel control test was performed to provide insight into accelerations experienced during 4.4 gram charge test conditions with no mitigation. This test gives baseline acceleration vs. time data for other tests in this series to be compared against. In Figure 4.6, large deformations to the hull of the specimen can be seen. Deformations seen in this picture are similar to those seen in other tests, except where a polyurethane-polyurea blend was used to coat the hull.

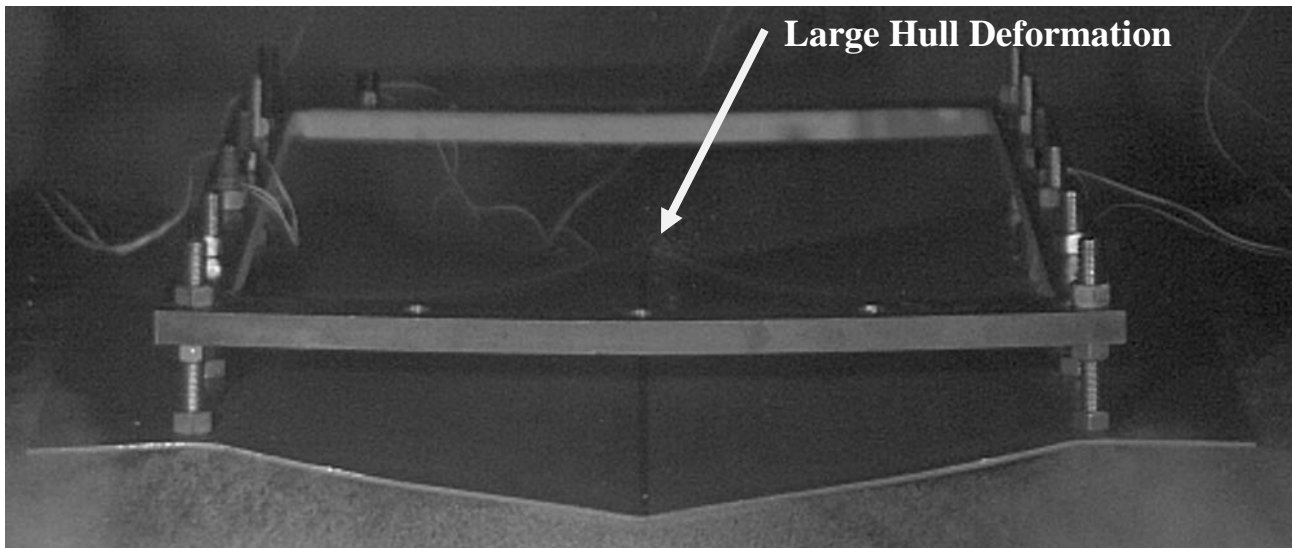


Figure 4.6: Steel Control 6mS after Detonation

4.2.2 Steel 2: Pink Foam

Pink foam tests were conducted to further investigate mitigation properties of foam. This foam was chosen because it was the stiffer of the two foams used in the aluminum test series. It was assumed that white foam would be unable to endure a 4.4 gram blast, if it was unable to resist shear during a one gram blast. A stiffness of 2743 lbs/inch was calculated by fitting a curve to the linear portion of data located in Appendix J. For this test, 1.4 inch thick pieces of pink foam were placed between the frame and hull of the specimen and set with epoxy, as seen in Figure 4.7 below.

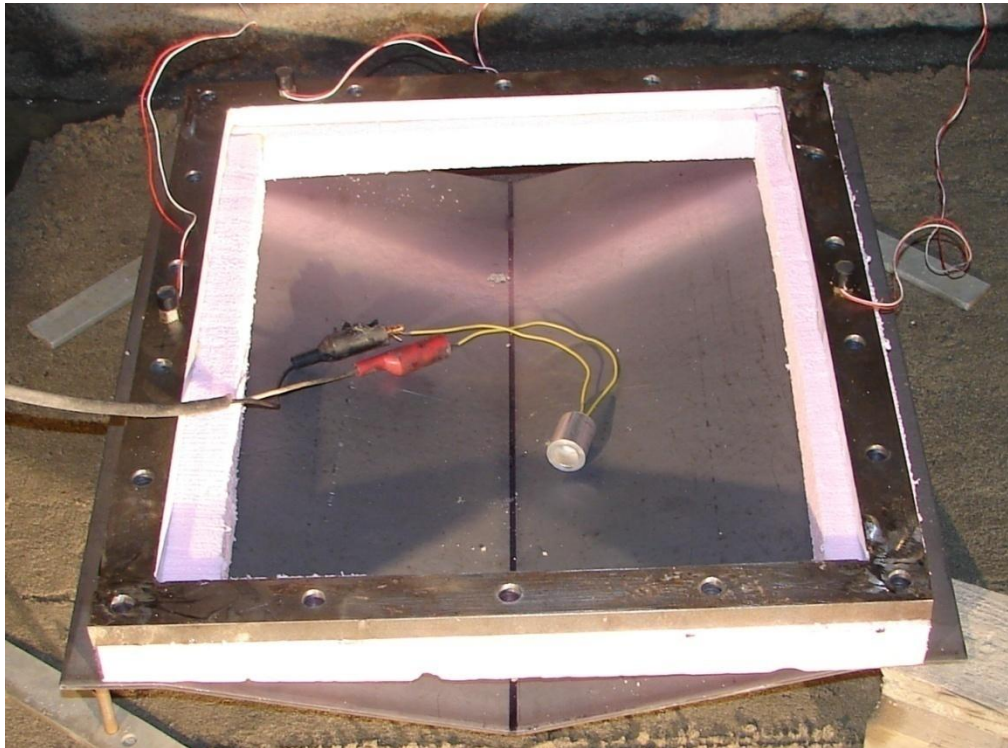


Figure 4.7: Steel Series Pink Foam Test

4.2.3 Steel 3: 3/16" Single Coil Spring

Single coil springs, made of 3/16" 6061-T6 aluminum, were tested for their mitigation properties. Springs were made by hand wrapping aluminum rod with threaded ends around a 0.75 inch bar. Springs were threaded 1.25 inches on each side with a 10-32 die. Springs were worked until pitch and inner diameter were as close as possible to dimensions found in Appendix E. For this test, twelve springs were bound between the hull and frame for mitigation purposes. Unlike the spring test in the aluminum series, these springs held the frame and hull together during testing. A stiffness value of 599 lbs/in was calculated through tensile testing. This translated to a total test stiffness of 7188 lbs/in, when all twelve springs were incorporated. Raw data from these tests can be found in Appendix N, while an overview can be found in Table 4.3. A picture of the specimen during testing can be seen in Figure 4.8 below.

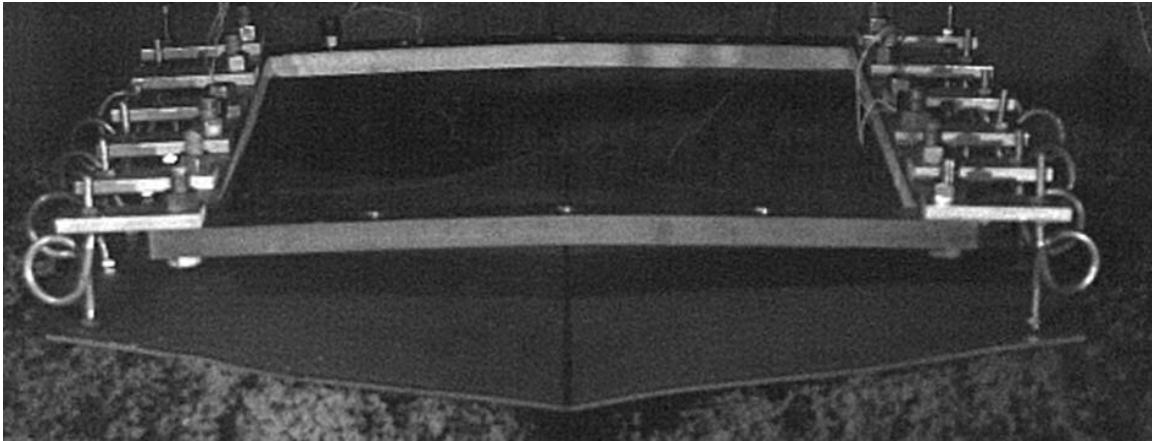


Figure 4.8: 3/16" Single Coil Spring Deformation

Tensile Testing

Tensile testing was performed on all spring specimens used in this paper by the method seen in Figure 4.9. Tensile tests were performed using a 25 kN load cell on a Tinius Olsen tensile testing machine. All tensile testing data can be found in Appendix N, where force in pounds is graphed vs. crosshead displacement in inches. Stiffness values were calculated by finding the slope of the linear region of each graph and averaging between the tests. These values can be seen below in Table 4.3.

Table 4.3: Spring Stiffness Measurements

Spring Type	Stiffness (lbs/in)
3/16" Aluminum Spring	599
1/8" Aluminum Spring	156.2
3/16" Aluminum Spring + Foam	644.4

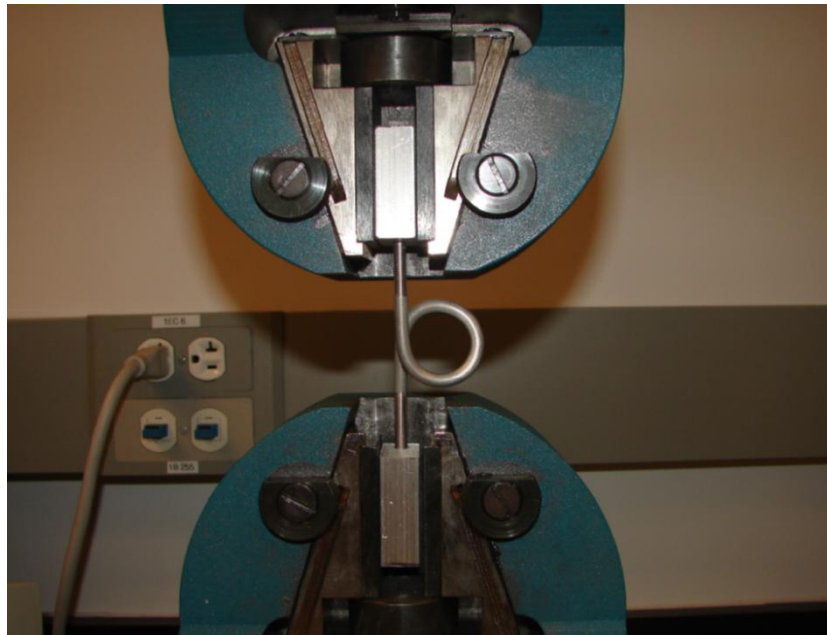


Figure 4.9: Tensile Testing of Spring Specimens

4.2.4 Steel 4: Single Coil Spring + Foam Coating

This test was performed in response to the severe deformations exhibited during the 3/16" single coil spring test. To increase the stiffness of the spring, foam was used to amplify the force needed to open and close the hoop of the spring. Great Stuff insulating foam was injected by gloved hand into cardboard molds seen in Figure 4.10 below. Molds used had an internal diameter of 1.5 inches and a length of approximately 2 inches. Springs rested 0.75 inches deep within the mold, and were held in place during foam injection. Great Stuff polyurethane foam sealant was utilized for expansion properties, cure time, and high durability. Great Stuff was able to expand in the molds, leaving no air pockets and thereby limiting inconsistencies between pieces. Springs used in this test were identical to those used in the 3/16" single coil spring test. Stiffness values for aluminum springs encased in foam can be found in Table 4.3. Tensile testing raw data can be found in Appendix N. A stiffness of 644.4 lbs/in was calculated for one spring, which translated to a test stiffness of 7732.8 lbs/in (12 springs).

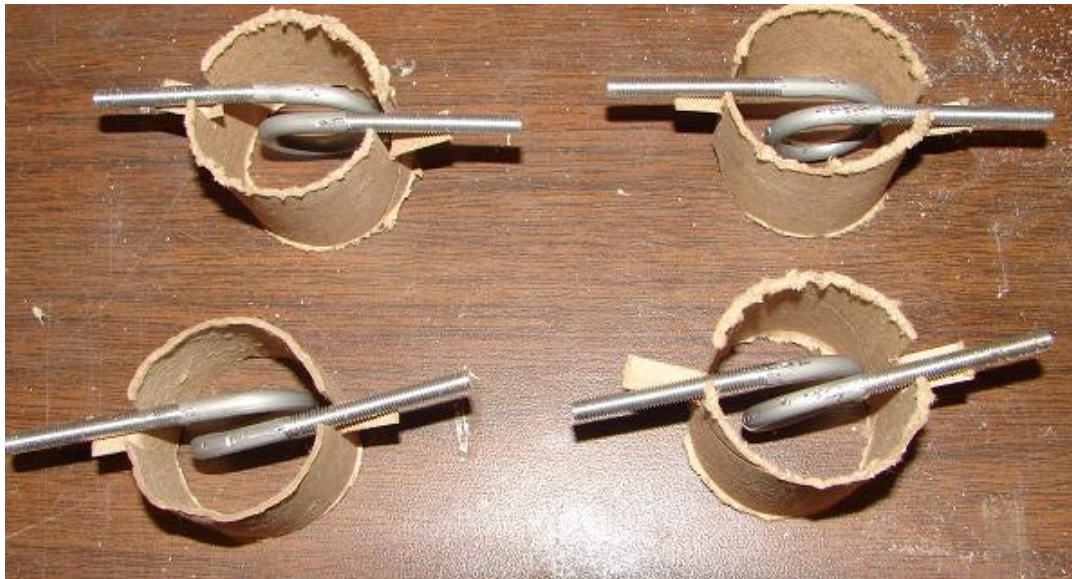


Figure 4.10: Cardboard Molding Setup

After molding, cardboard was cut, and removed from the foam-spring system.

Figure 4.11 shows the system removed from the cardboard mold, after curing overnight.



Figure 4.11: Spring Covered in Foam

The specimen prior to testing can be seen in Figure 4.12 below. The test was intended to provide further stiffness between the hull and frame, while aiding in damping of any system oscillations during the blast.

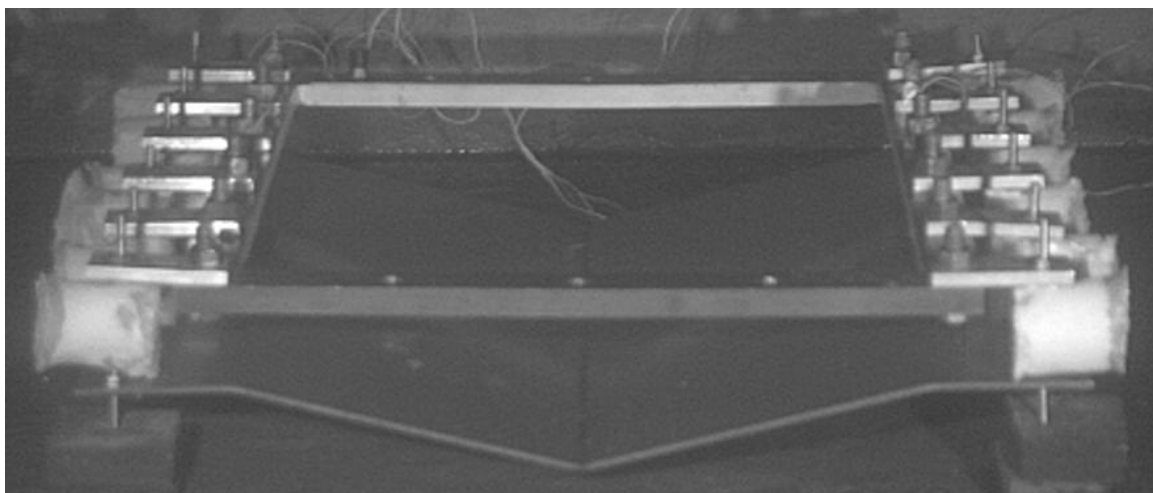


Figure 4.12: Steel 4 before Testing

4.2.5 Steel 5: Polyurethane-Polyurea Coated Hull

A steel hull was coated on both sides with 1/8th inch of a polyurethane-polyurea blend provided by Line-X. Recent blast testing performed by the military, in cooperation with Line-X has shown mitigation properties of a polyurethane-polyurea mixture, previous used for truck bed lining. This elastic material allowed the material to flex during impact, but return to its original arrangement [21]. For blast testing, this allowed for a more elastic deformation of the hull. Thinning of the hull at the center of the impact was retarded, due to the polymer coating's ability to uniformly distribute deformations. This distribution of deformations reduced localized effects such as material thinning. Lower deformations result in a more functional vehicle after it has been exposed to an IED blast, while reducing material thinning makes hull penetration less likely. Deformations seen in Figure 4.13 are distinctively lower than those seen in Figure 4.6. These figures capture the time during a test where maximum deformations are usually recorded.

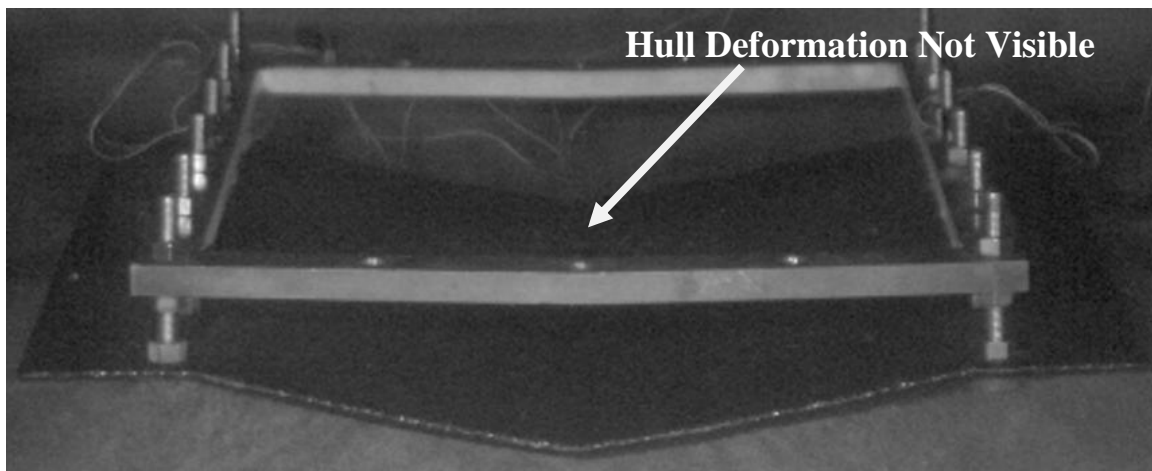


Figure 4.13: Polyurethane-Polyurea Hull Deformation at 6mS after Detonation

4.2.6 Steel 6: Steel Cable Vibration Isolators

Vibration isolators are systems that allow motion of connected objects, while mitigating the transfer of vibration from piece to piece. They can be in the form of rods separated by rubber, or in this case steel cable housed in aluminum retainers. In this application, energy transfer is mitigated through the frictional damping associated with strand rubbing between cables [22]. This mitigation system can be modeled as a spring, damper. Steel cable isolator specifications can be found in Appendix M. The test specimen before testing can be seen in Figure 4.14 below.

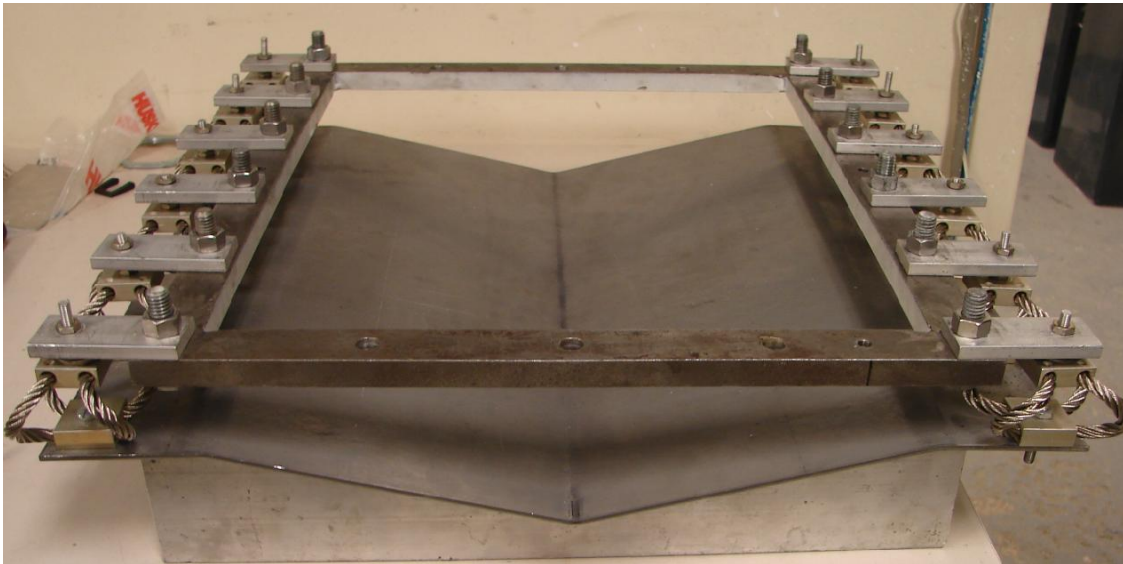


Figure 4.14: Steel 6 (Steel Cable Isolators)

4.3 Pocket Plate Series

The pocket plate test series was based on 10 pound charge (full scale) tests. This scaled down to a 4.4 gram charge used for testing. Specimen frames, hulls were made of steel in this series. The only difference in test setup for this series compared to the steel series was hull orientation. The steel series utilized a downwardly convex hull orientation, while this series utilized a downwardly concave orientation. Masses, weights for each test specimen in this series can be seen in Table 4.4 below.

Table 4.4: Pocket Plate Series Specimen Weights/Masses

Test	Weight	Mass
	Pounds	Grams
Pocket Plate 1	17.25	7825.2
Pocket Plate 2	16.90	7663.6
Pocket Plate 3	16.40	7441.1

4.3.1 Pocket Plate 1: Pocket Plate Control

This test began the pocket plate series, where previously downwardly convex hulls were replaced by downwardly concave hulls, in an attempt to study acceleration mitigation properties of a hull orientation change. Measurements for this test series, because a 4.4 gram charge is used, were identical to those of the steel series (SOD and DOB). This also implied that there is a 1.4 inch gap for all tests measured from the bottom of the single piece steel frame (invisible floorboard) to the top of the hull directly below it. The test specimen before testing can be seen in Figure 4.15 below.

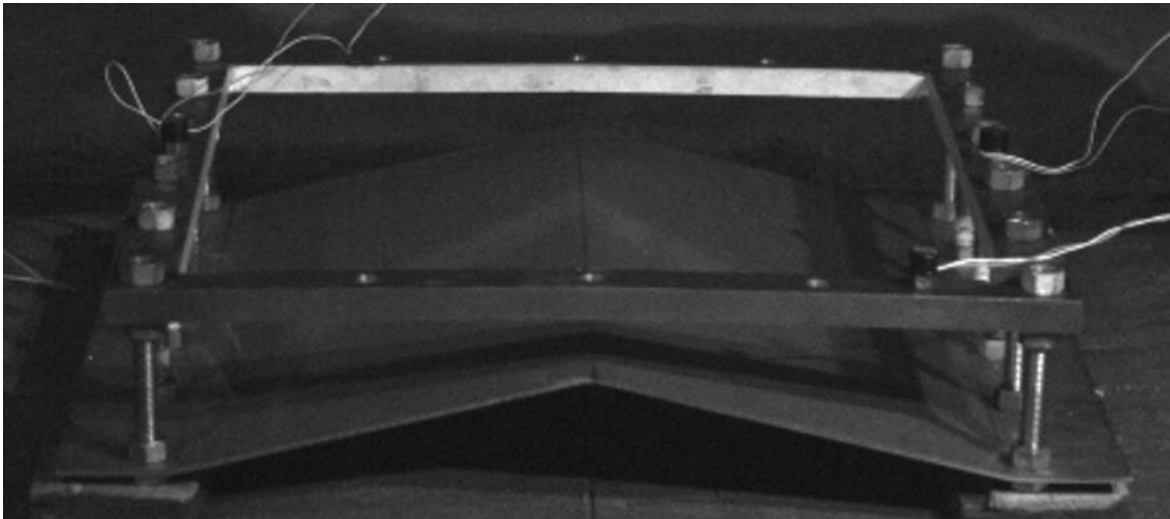


Figure 4.15: Pocket Plate Control

4.3.2 Pocket Plate 2: 3/16" Single Coil Spring Pocket Plate

This test was identical to the 3/16" single coil spring test in the steel series, except the hull orientation was changed to be downwardly concave. This test was not compared to the similar test in the steel series; differing geometries between the tests caused uncertainty in comparing mitigation between the two tests, because of a possible change in the load state. This change of load state made it impossible to distinguish whether differences between the tests were caused by the pocket plate design, or the new reaction of the spring mechanisms. Therefore this test will be considered independent of the test in the steel series. Below, Figure 4.16 shows the pocket plate specimen before testing. A stiffness value of 599 lbs/in was calculated through tensile testing. This translated to a total test stiffness of 7188 lbs/in, when all twelve springs were incorporated. Raw data from these tests can be found in Appendix N, while an overview can be found in Table 4.3.

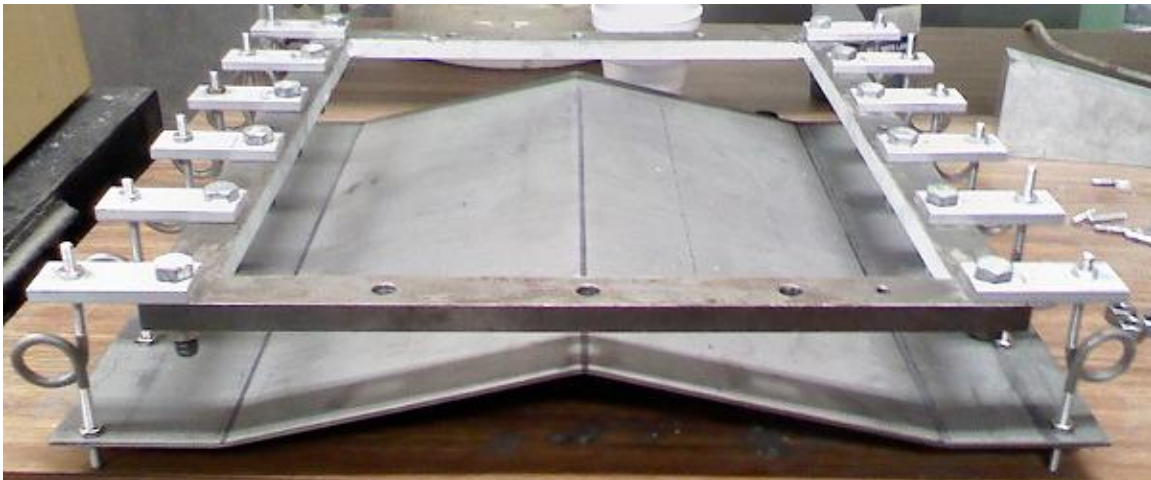


Figure 4.16: 3/16" Single Coil Spring Pocket Plate

4.3.3 Pocket Plate 3: 1/8" Single Coil Spring Pocket Plate

Eighth inch aluminum rod was bent in the shape of springs for mitigation purposes. Springs were threaded using a 5-40 die; a diagram of the spring used for this test can be found in Appendix F. Foam was also utilized in this tests to reduce contact effects between the hull and the frame during testing, seen in Figure 4.17 below. A stiffness value of 156.2 lbs/in was calculated through tensile testing. This translated to a total stiffness of 1874.4 lbs/in, when all twelve springs were incorporated. Raw data from these tests can be found in Appendix N, while an overview can be found in Table 4.3.

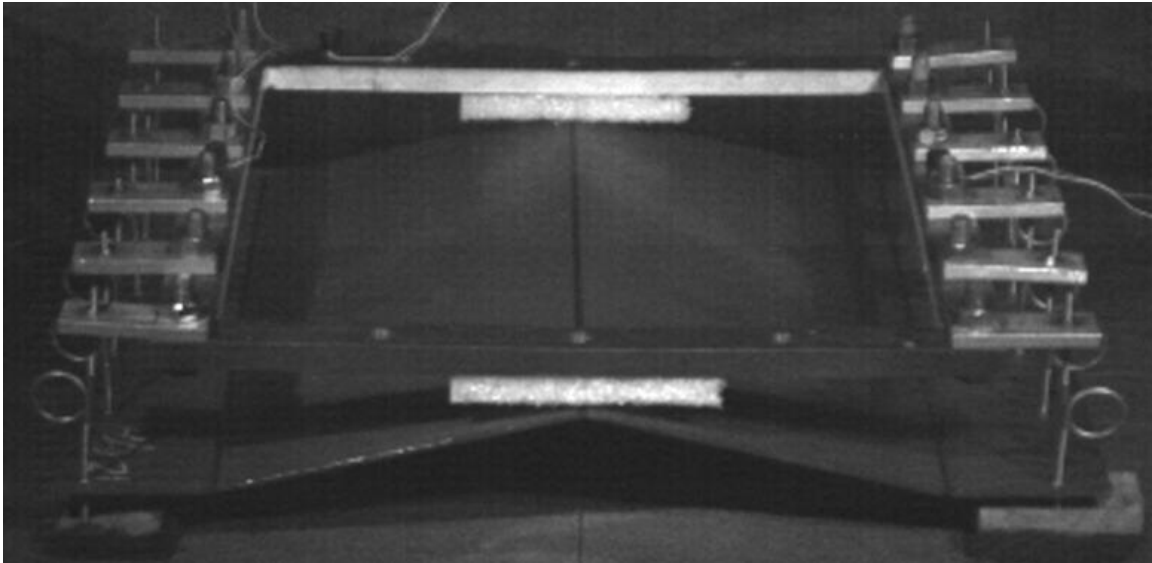


Figure 4.17: 1/8" Single Coil Spring Pocket Plate

Chapter 5 - Post-Processing and Data Verification

5.1 Frame Fundamental Frequencies

Fundamental frequencies of each frame were calculated both theoretically and experimentally. Values for the first few resonance frequencies of each frame were considered during the filtering process. The goal was to remove high frequency portions of the data, without changing the nature of the original data curve. To avoid aliasing, filtered data was verified against unfiltered accelerometer data (integrated twice to become displacement data) and camera data. Appendix O shows all data verification curves for this paper, including a table documenting which accelerometer signals were considered for each test based on their ability to be verified.

The first method used to find fundamental frequencies involved hitting each frame with a hammer and analyzing the response of the attached accelerometers. Data from this experiment can be seen in Figure 5.1 and Figure 5.2. Five separate tests were compared for each frame; frames were hit in different locations for each test to avoid biasing based on impact location. Accelerometer data was imported to UERDTools, where fast Fourier transforms were conducted to identify resonant frequencies. Resonant frequencies were identified when two or more data sets exhibited large amplitudes at the same frequency.

Resonant frequencies for the aluminum frame were recorded at 175Hz, 225Hz, 420Hz, ~1100Hz, and 1675Hz (there appears to be a resonant frequency around 1100Hz, but not all data sets agree on its location). The most heavily populated frequencies were

at 225Hz, 400Hz, and 1675Hz (though the amplitudes at 1675Hz were significantly lower than those at 225Hz and 400Hz).

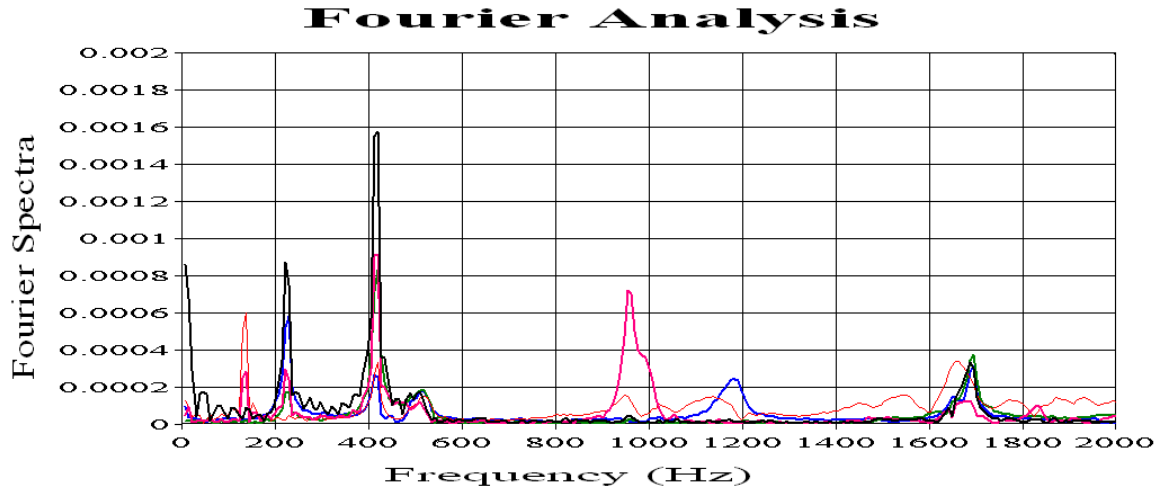


Figure 5.1: Fourier Analysis (Aluminum Frame)

Resonant frequencies for the steel frame were found at 230Hz, 410Hz, 500Hz, 1180Hz, and 1775Hz. For this frame, all five data sets had the same resonant frequencies. The existence of large amplitudes at high resonant frequencies was investigated further, through modal analysis on the following page.

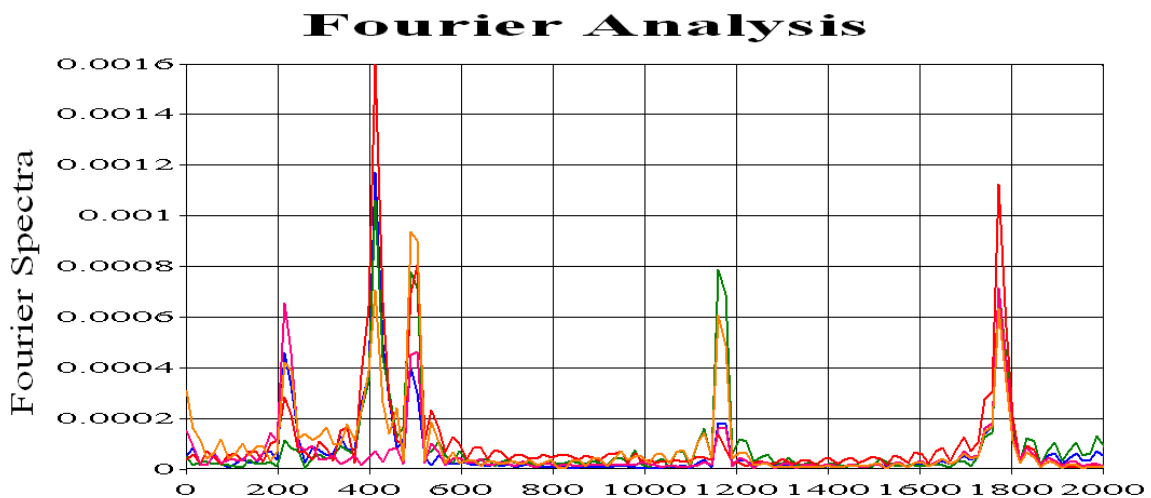


Figure 5.2: Fourier Analysis (Steel Frame)

Resonant frequencies and mode shapes were calculated using Pro-Mechanica, a finite element analysis program inside the Pro-Engineering software package [23]. Materials and restraint locations were chosen for each test (input of a loading condition is not necessary for a modal analysis in Pro-Mechanica). A restraint condition where the edges of the four corner of the frame have zero displacement was chosen. This restraint condition imposes the least movement constraints on the system, preserving the motion seen in real life testing. Figure 5.3 shows the first two mode shapes for the steel frame, with associated frequencies. The first two frequencies found were 282Hz and 315Hz, which correspond relatively well to the first two frequencies found in Figure 5.2 (230Hz and 410Hz). Though these numbers are not identical, they provide enough insight to assume a general location of the first two frequencies of the steel frame. Pro Mechanica testing was not performed for the aluminum frame, because there was less confusion about the location of the resonant frequencies for this test specimen.

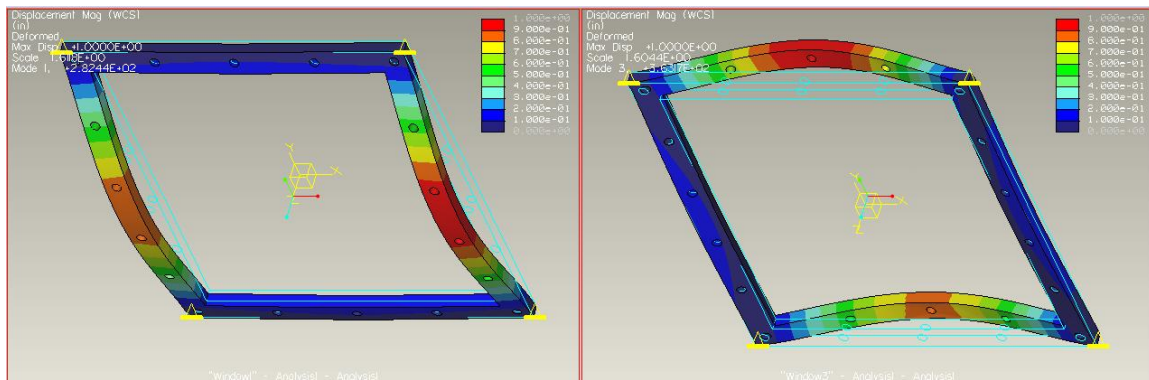


Figure 5.3: Steel Frame First Two Mode Shapes

5.2 Data Filtering

Filtering was applied at multiple frequencies and compared against unfiltered data, camera data. It was found that utilizing a low pass filter at 600Hz was the best filtering method in terms of reducing high frequency noise, keeping the original signal characteristics in tack (for both test sets). This filtering method was utilized for both test sets because of the large gap in each frame's frequency profile at this location. Filtering at this point ensured that the first few resonant frequencies of each frame would remain in the data. In Figure 5.4, a comparison of unfiltered, filtered data can be seen. It is evident that the filtering process did not alter the main characteristics of the data.

The difference between filtered, unfiltered data in this paper was the amplitude of the data sets. Filtering the data removes large, high frequency accelerations that are not possible based on the test setup. These portions of the data are high frequency resonance exhibited by the structure, and were filtered out based on previous research [19].

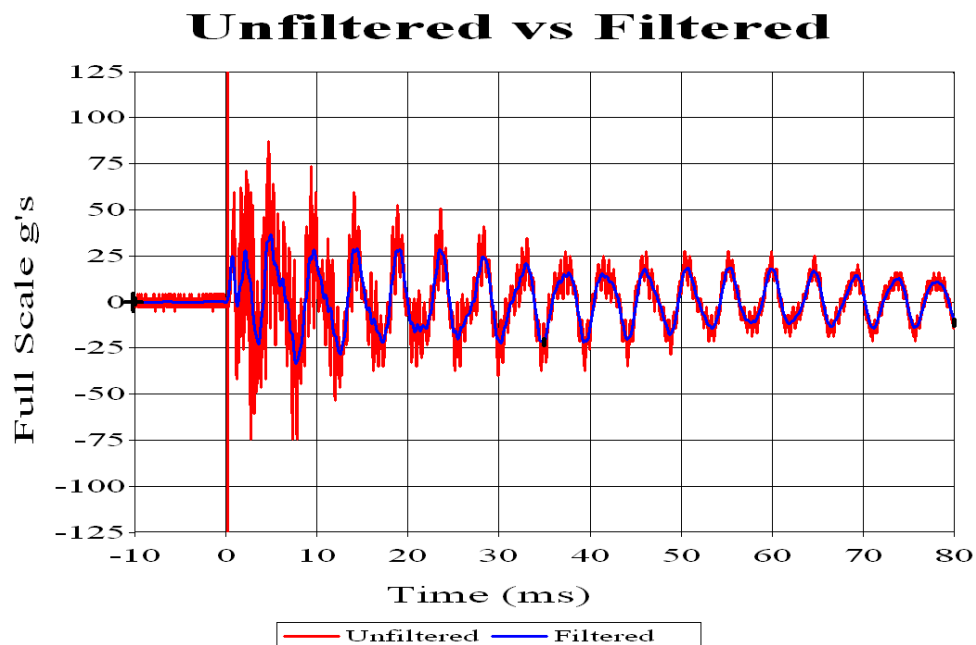


Figure 5.4: Filtered Data (600Hz Low Pass Filter) vs. Unfiltered Data

5.3 Verification of Data: Filtered Data vs. Camera Data

Filtered data was compared to camera data to verify the correctness of the filtering approach. Accelerometer data was integrated twice, resulting in displacement vs. time plots. First, the data was multiplied by either 9.81 or 32.2 in order to translate from g's to m/s^2 or ft/s^2 respectively. Upon integrating acceleration values, the data was multiplied by 1×10^{-6} . This fixed the units of time, which were translated from seconds squared to milliseconds squared. The next integrating factor, when going from velocity to displacement, was 1 since scaling has already been preserved. Now the accelerometer data (unfiltered or filtered) was compared to camera data. In Figure 5.5 below, accelerometer data (filtered and unfiltered) was verified against camera data. The three data sets agreed, and were used for further analysis in this paper.

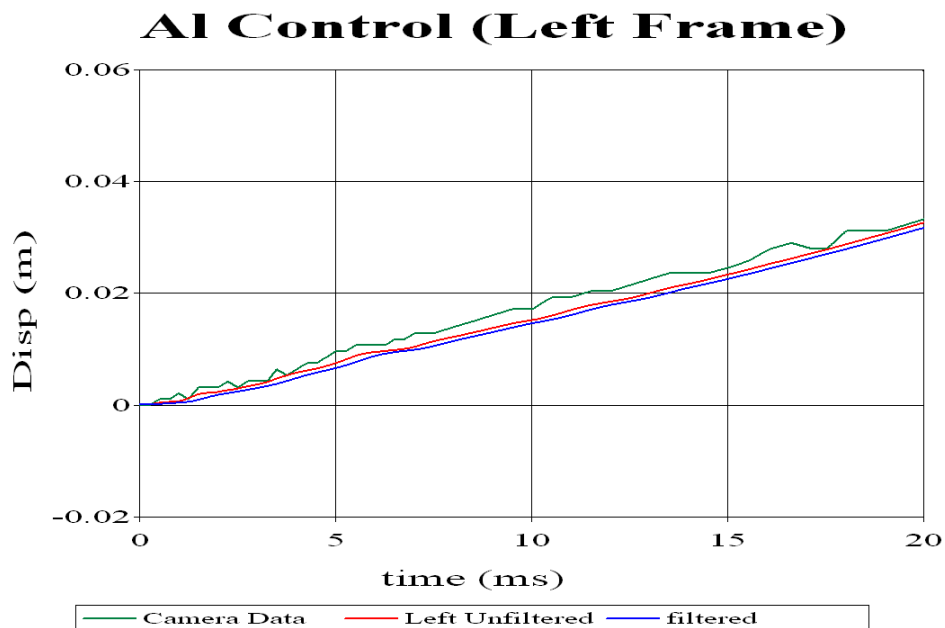


Figure 5.5: Verified Accelerometer Data

Upon integrating the data sets, it was found that certain accelerometer outputs (filtered or unfiltered) did not match camera data. This was due to the drift of accelerometer output over time, causing the displacement values to become corrupted with error. Figure 5.6 shows accelerometer data that could not be used for analysis due to drift in the data. In some cases, data was validated until drift compensation became irrelevant and corrections could not fix the data. These data sets were labeled with the specific time where the validity of the data comes into question. All verified accelerometer data can be found in table and graph format, found in Appendix O.

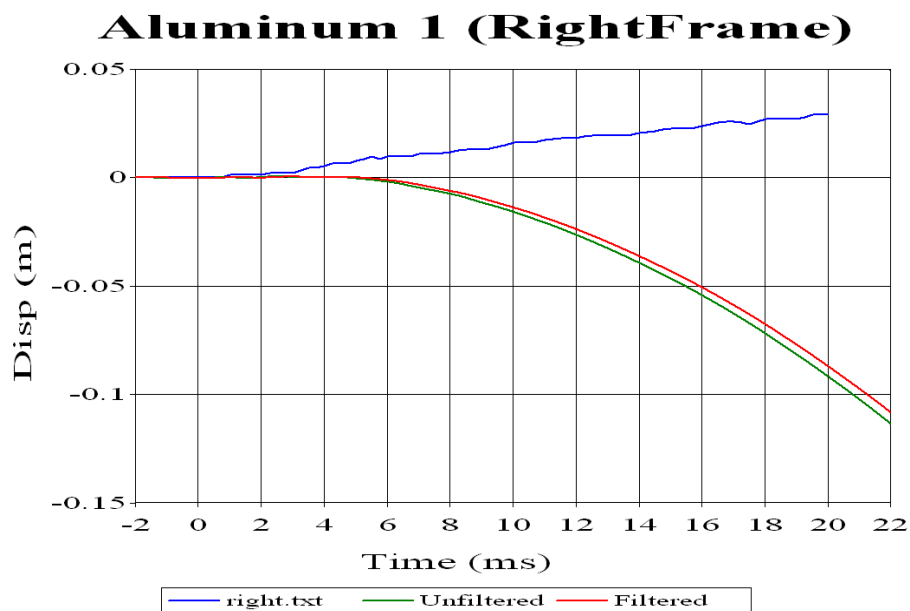


Figure 5.6: Incorrect Accelerometer Data

Chapter 6 - Results

Test results for all specimens will be overviewed in this section. Filtered accelerometer data was used exclusively for analysis because these are the accelerations that better represent the response of the system. Only verified accelerometer output was used in this section, to avoid possibly corrupted, biased accelerometer data. Peak accelerations, and the duration where accelerometer data is above 23g's will be compared between tests. Exposure times to 23g's or more will be compared to criteria used for military aircraft ejections and crashes [8] [24]. In order to calculate the duration where a test undergoes accelerations over 23g's, the absolute value of the data was analyzed, as seen in Figure 57. The time span where the envelope is above or equal to 23g's was recorded in milliseconds.

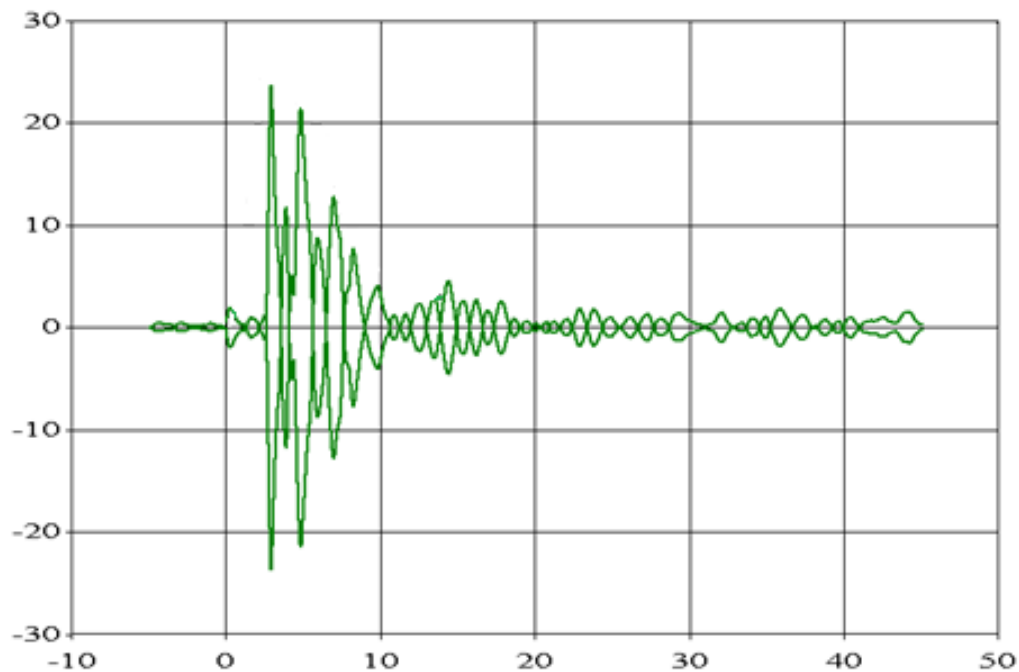


Figure 6.1: Sample Acceleration Envelope

6.1 Aluminum Test Series

6.1.1 Aluminum 1: Control Frame

Accelerometer data for the first aluminum test series can be seen in Figure 6.2 below. Only the left accelerometer output could be verified, so it was the only signal considered for analysis. The peak acceleration for this curve was 39.7g's. There were no mitigating system involved in this test; this test serves as a baseline for other tests in this series to be compared against. Left and right accelerometer data will be compared against the single accelerometer output from this test, while corner data will not be compared for obvious reasons.

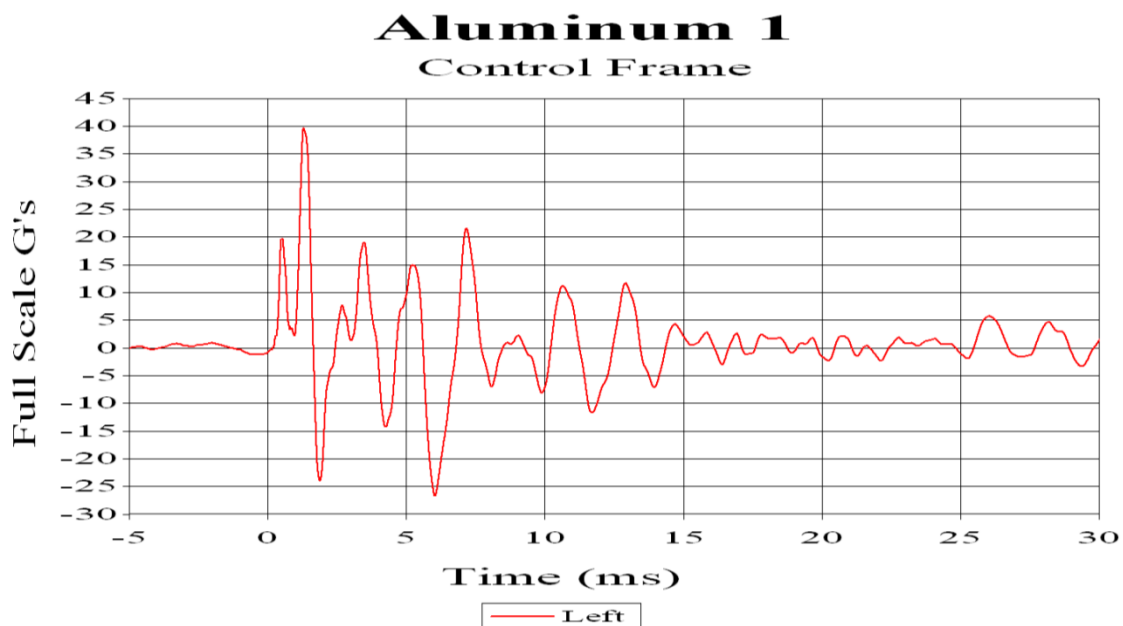


Figure 6.2: Aluminum 1 Filtered Acceleration Data

6.1.2 Aluminum 2: Spider Frame

Acceleration data for the second test of the aluminum series can be seen in Figure 6.3 below. Acceleration data that could not be verified was either not included (corner accelerometer data), or trimmed to the point where verification was unsuccessful (left accelerometer data was ended at 6.4mS). Peak accelerations were found to be 24.1g's (Right) and 22.8g's (Left). Peak accelerations were reduced by 39.3% (Right) and 42.57% (Left) compared to the aluminum control test. This shows that a significant portion of the peak acceleration has been mitigated compared to the control test for this series. Peak accelerations were reduced by the accommodation for outward hull expansion provided by the aluminum rods connecting the hull and the frame. This case is different than the aluminum spring case, where deformations were in the vertical direction, resulting in frame oscillations.

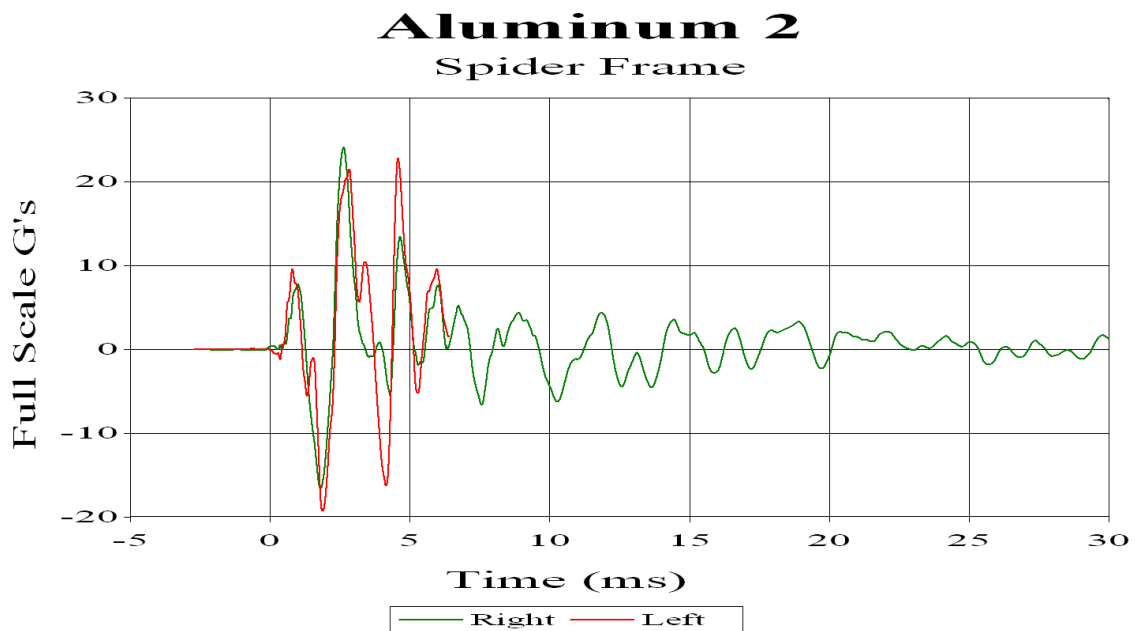


Figure 6.3: Aluminum 2 Filtered Acceleration Data

6.1.3 Aluminum 3: Sliding Hull

Acceleration data for the third test of the aluminum series can be seen in Figure 6.4 below. Acceleration data from all three accelerometers was considered, but the left accelerometer was cut at 5mS and the corner accelerometer at 4.5mS due to verification problems. Peak accelerations of 23.45g's (Left), 24.3g's (Right), and 18.5g's (Corner) were identified. There was almost a 5mS gap between the peak accelerations for the right and left frame. This was due to hull-frame contact caused by the sliding motion of the hull; the hull contacted the connecting bolts upon being pushed out initially by the blast and upon being sucked in by hull deformation. Peak accelerations were reduced by 40.9% (Left) and 38.8% (Right) when compared against the aluminum control frame. Peak acceleration values could have been even lower had there not been hull-frame contact in this test, and avoidable occurrence for future tests.

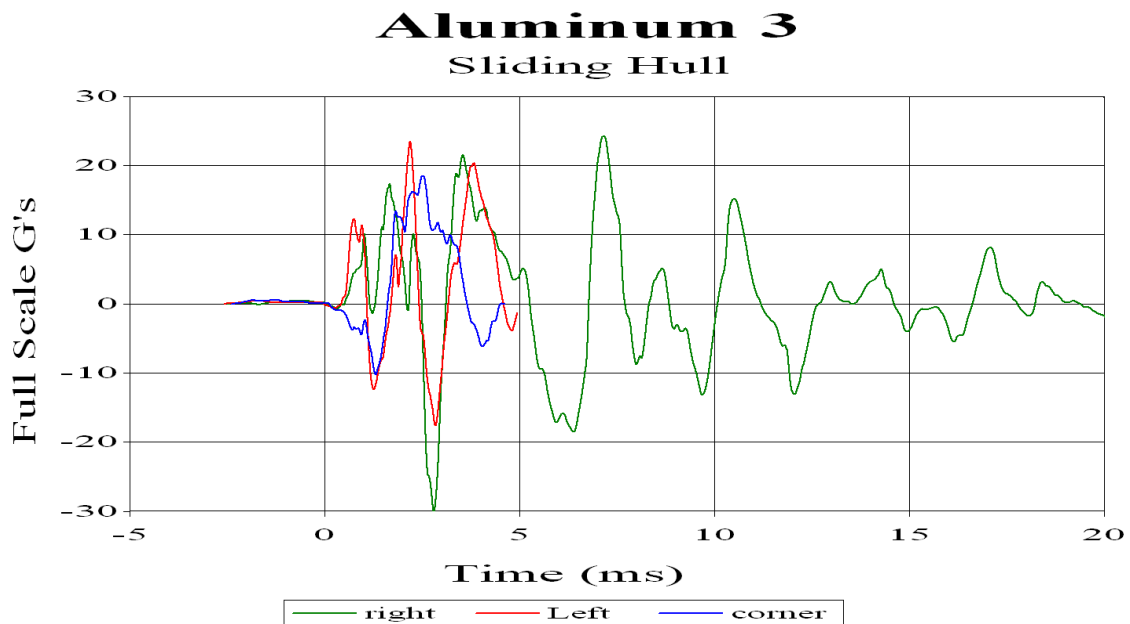


Figure 6.4: Aluminum 3 Filtered Acceleration Data

6.1.4 Aluminum 4: Spring Spider Frame

Acceleration data for the fourth test of the aluminum series can be seen in Figure 6.5 below. Peak accelerations of 23.7g's (Right), 22.5g's (Left), and 13.5g's (Corner) were identified. Peak acceleration reductions of 43.3% (Left) and 40.3% (Right) were found when compared to the aluminum control test. Compression of the springs found when compared to the aluminum control test. Compression of the springs elongated the acceleration response of this system, causing a wider acceleration envelope than previously discussed tests. There was dissociation of the hull and the frame at approximately 7mS due to springs not being bound to either the hull or frame.

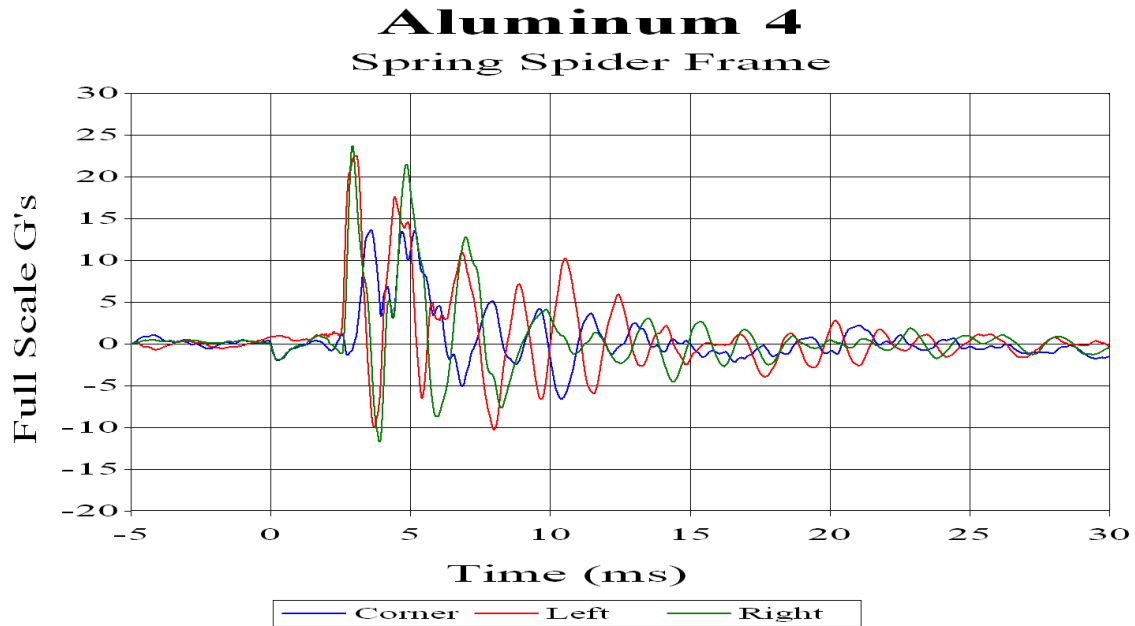


Figure 6.5: Aluminum 4 Filtered Acceleration Data

6.1.5 Aluminum 5: Pink Foam

Acceleration data for the fifth test of the aluminum series can be seen in Figure 6.6 below. Acceleration data from the corner and right accelerometers was verified and considered for analysis. Peak accelerations were found to be 35.7 g's for the right accelerometer, and 25 g's for the corner accelerometer. There was a 10.1% decrease in peak acceleration for the right accelerometer compared to the aluminum control test. The data shows that the peak accelerations were lowered relatively well by the pink foam, but there was a continuation of large acceleration oscillations in the system. As a mitigating device, the pink foam was too rigid for this test setup; a one gram charge did not exert enough energy to deform foam with stiffness of 3782.6lbs/in. Therefore peak accelerations were only slightly mitigated, because the test was too rigid.

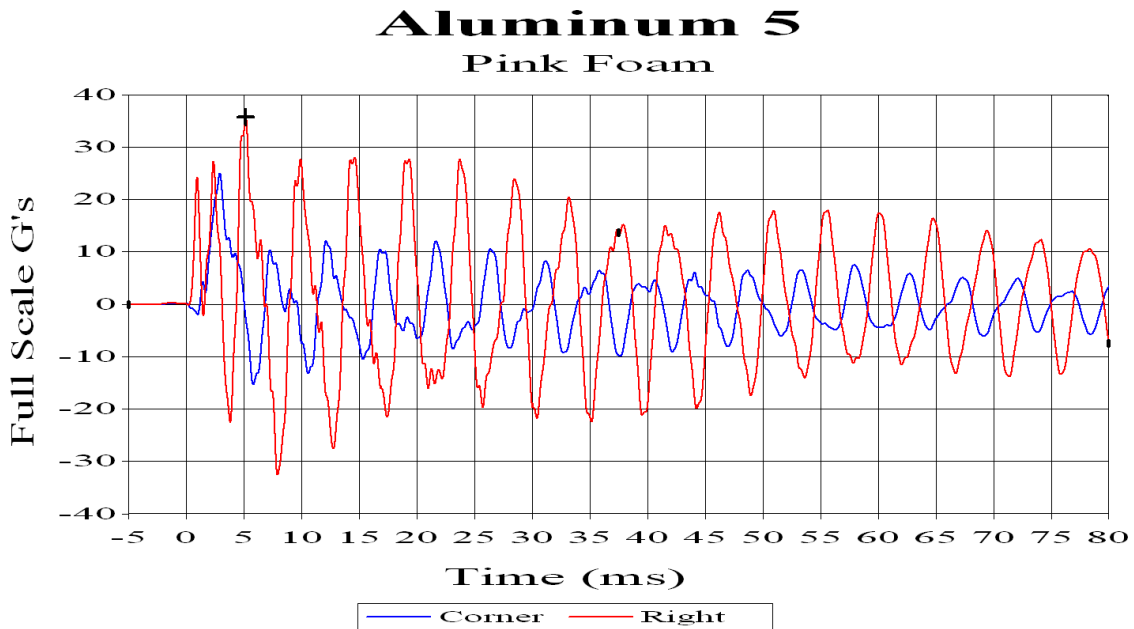


Figure 6.6: Aluminum 5 Filtered Accelerometer Data

6.1.6 Aluminum 6: White Foam

Acceleration data for the sixth test of the aluminum series can be seen in Figure 6.7 below. Acceleration data from all three accelerometers was verified and considered for analysis. Peak accelerations were found to be 23 g's (left), 24.8 g's (right) and 18.17 g's (corner). Acceleration peaks were reduced by 42% (Left), 37.5% (Right) when compared against the aluminum control. Peak accelerations were reduced because of the compressibility of the white foam (stiffness of 278.5lbs/in) and its ability to elongate the blast response. In this test, the reduction of rigidity between the hull and the frame increased peak acceleration reduction compared to Aluminum 5 (the more rigid pink foam test). Unfortunately further system oscillations were not damped by the white foam mitigating device, resulting in a large acceleration envelope.

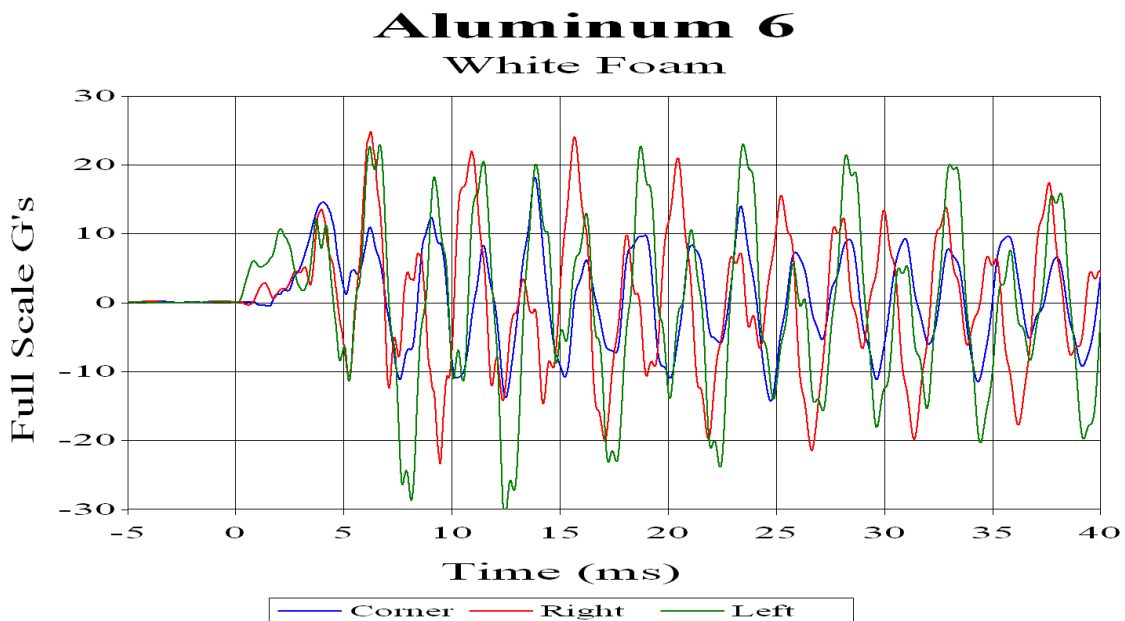


Figure 6.7: Aluminum 6 Filtered Accelerometer Data

6.1.7 Aluminum Series Peak Acceleration Overview

Based on information provided in Table 6.1 and Figure 6.8, all aluminum tests mitigated peak accelerations compared to the control. Tests 2, 3, 4, and 6 mitigated peak accelerations with the same proficiency. Test 5 also mitigated peak accelerations, but was not as proficient as the previously listed tests.

Table 6.1: Aluminum Test Series Peak Accelerations

Test	Peak Acceleration (G's)		
	Left	Right	Corner
Aluminum 1: Control Frame	39.7	N/A	N/A
Aluminum 2: Spider Frame	22.8	24.1	N/A
Aluminum 3: Sliding Hull	23.45	24.3	18.5
Aluminum 4: Spring Spider	22.5	23.7	13.6
Aluminum 5: Pink Foam	N/A	35.7	25
Aluminum 6: White Foam	23	24.8	18.17

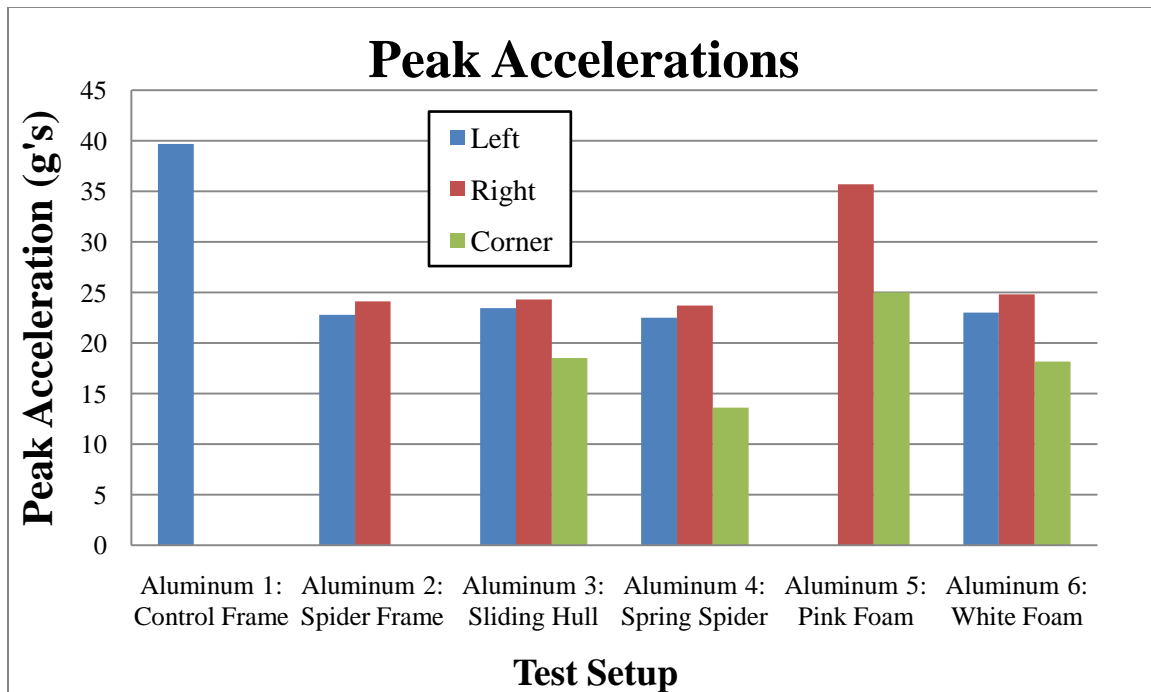


Figure 6.8: Aluminum Test Series Peak Accelerations vs. Accelerometer Position

6.1.8 Aluminum Series Acceleration Envelope Overview

Acceleration envelopes measure the time span a specific acceleration level is experienced within a test. Acceleration peaks are important, but it is the constant exposure to large accelerations that causes injury or death. Exposure times are inversely related to the magnitude of acceleration felt during that period; exposure time needed for injury decreases as acceleration magnitude increases. Based on military exposure criteria for pilot ejections (5.5mS exposure) and helicopter crashes (25mS exposure) all tests passed both exposure criteria except for the two foam tests, as seen in Table 6.2. The pink foam tests failed both exposure criteria, while the white foam test failed only the first exposure level. These long exposure levels exhibited by the foam tests are directly related to oscillations in the system during testing. Both foams did poor jobs damping system oscillations after peak accelerations were observed. Tests 2 and 4 did the best job damping further system accelerations. Aluminum 2 was able to divert blast energy away from the frame by allowing horizontal motions of the hull to be less restricted. This allowed the hull to deform more naturally, rather than forcing a deformation response based on rigidly securing the hull with bolts. Aluminum 4 reduced the acceleration envelope through dissociation of the hull and the frame shortly after the blast; peak positive accelerations launched the frame away from the hull when the hull experienced its first deceleration. This scenario is dangerous, yet interesting, because if the trajectory of the frame can be controlled the crew may experience less time in the blast path. Aluminum 3 resulted in an acceleration envelope comparable to the control test, but avoidable contact between the hull and the bolts connected to the frame was a driving

force behind this. If these interactions can be avoided there is possibility for acceleration envelope reduction, resulting in a more successful test specimen.

Incorporating both peak acceleration data and acceleration envelope information, tests can be compared for their overall mitigation properties. Considering that tests 2, 3, 4, and 6 had the lowest peak accelerations and tests 2 and 4 had the shortest acceleration envelopes above 23g's it can be concluded that tests 2 and 4 were the most proficient at mitigation acceleration delivered to the frame.

Table 6.2: Aluminum Series Acceleration Envelope Data

Test	Width of Acceleration Envelope \geq 23g's (mS)	Military Exposure Criteria	
		5.5mS	25mS
Aluminum 1	4.57	Pass	Pass
Aluminum 2	1.95	Pass	Pass
Aluminum 3	4.63	Pass	Pass
Aluminum 4	1.115	Pass	Pass
Aluminum 5	30.876	Fail	Fail
Aluminum 6	11.22	Fail	Pass

6.2 Steel Test Series

6.2.1 Steel 1: Control Frame

Acceleration data from the first test of the steel series can be seen in Figure 6.9 below. Peak accelerations found in this test were 142.2g's (Left), 152g's (Right), and 93.95g's (Corner). These accelerations are extremely large, and pose an immediate threat to a human occupant. It is clear that no mitigation provides a worst case scenario for this test series in terms of peak accelerations recorded during a blast. In this case, energy from a blast travels relatively unimpeded to the frame of the vehicle causing a more violent response than cases where energy is diverted or absorbed by mitigating materials.

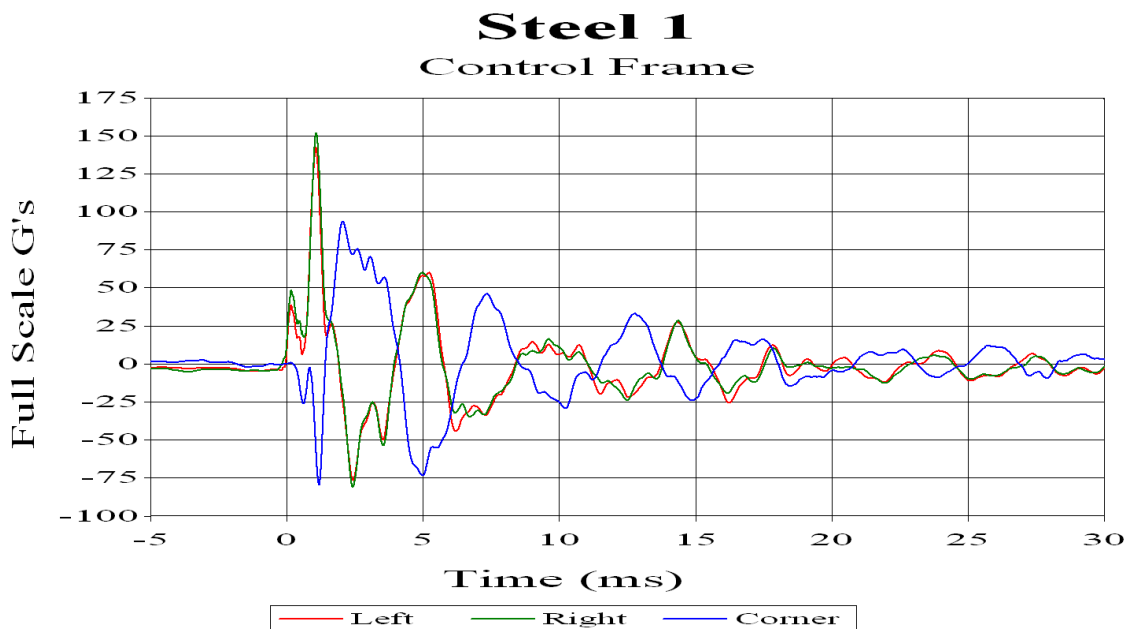


Figure 6.9: Steel 1 Filtered Acceleration Data

6.2.2 Steel 2: Pink Foam

Acceleration data from the second test of the steel series can be seen in Figure 6.10 below. Peak accelerations were found to be 105.9g's (Left), 106.8g's (Right), and 67.35g's (Corner). Acceleration peaks were reduced by 25.3% (Left), 29.6% (Right), and 28.3% (Corner). The pink foam absorbed initial peak accelerations; however subsequent acceleration peaks are higher than those found in the control test for this series. Peak accelerations are important to consider, but it is the prolonged exposure to intense accelerations that results in injury or death. This test performed admirably in mitigating accelerations within the first 5ms of the blast, but seems to have failed in damping further accelerations after that point. The failure of the pink foam to damp out accelerations will be discussed later in this section, as it applies to increased bodily harm to passengers.

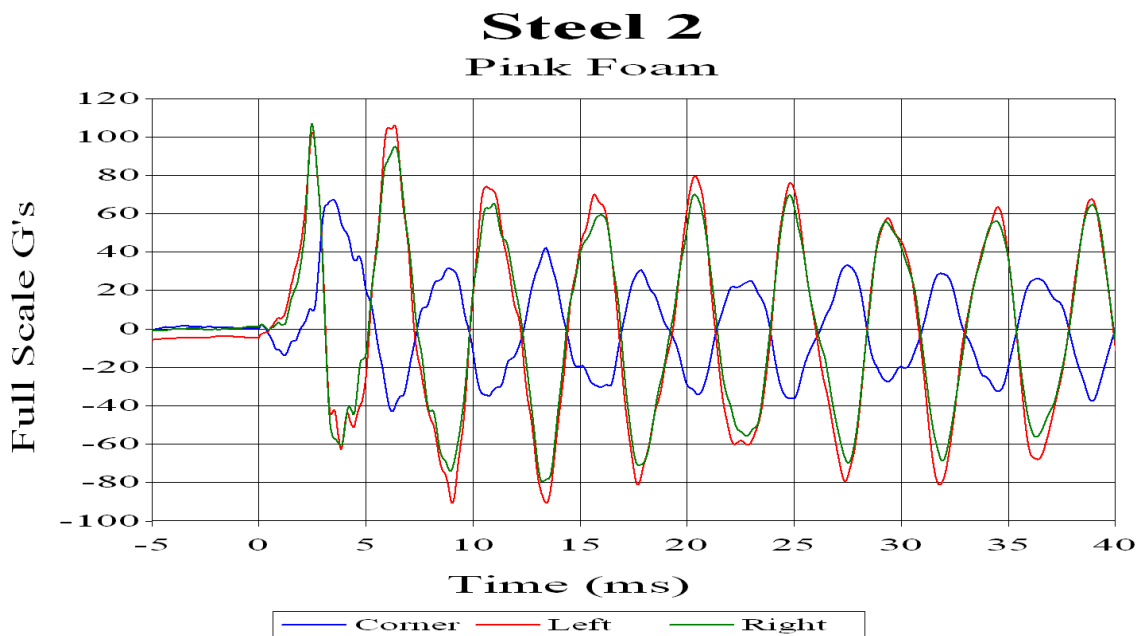


Figure 6.10: Steel 2 Filtered Acceleration Data

6.2.3 Steel 3: 3/16" Single Coil Springs

Acceleration data from the third test of the steel series can be seen in Figure 6.11 on the following page. Corner acceleration data was cut at 9.5mS due to drift of accelerometer data. Peak accelerations were found to be 137.2g's (Left), 138.54g's (Right), and 72.4g's (Corner). Though peak accelerations were found to lower in this test compared to the control, there was not a large disparity between the two tests. Right and left frame acceleration peaks were reduced by 9% and 3% respectively, while corner acceleration was reduced by 22.5%. The low percent peak acceleration reductions compared to the control can be explained by the displacement direction associated with the aluminum springs. Aluminum rods utilized as springs would displace in the vertical direction during a blast, directly into or away from the frame.

The springs were rigid enough to cause significant energy transfer to the frame upon deforming themselves. There was some reduction of energy, but according to the data most of the blast energy was transferred to the frame before being absorbed by spring deformation. This is quite feasible, because of the speeds involved in shock propagation through metals. An elastic or even plastic response by the springs in scenario is bypassed by the blast energy, leaving the frame vulnerable. In this test it is more likely that the hull motion caused an initial pulse that was only partially absorbed by the springs before being transmitted to the frame.

This shows that deformation directions of the mitigating systems are important to frame response. It also shows that reducing hull-frame interactions during the early portions of the blast is crucial to reducing acceleration peaks. It is important to ensure that the hull and frame are not bound by non-damping objects that deform in an

oscillating pattern. In this test, the springs deformed in an opening and closing manner, increasing the duration of the system response as seen in the graph below. In this format, this was not ideal because the acceleration envelope has been widened, which will be discussed later in this section.

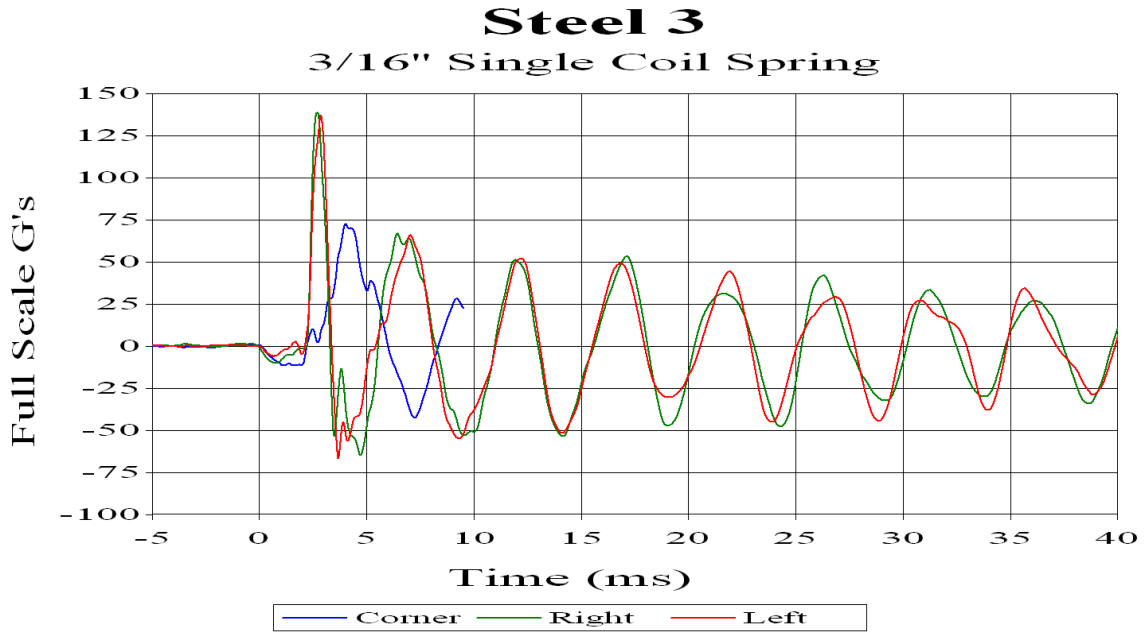


Figure 6.11: Steel 3 Filtered Acceleration Data

6.2.4 Steel 4: 3/16" Single Coil Springs + Foam Coating

Acceleration data from the fourth test of the steel series can be seen in Figure 6.12 below. Here foam was utilized to improve the damping of oscillations seen in test Steel 3. Peak accelerations were found to be 129.1g's (Left), 127.1g's (Right), and 79.1g's (Corner). These peak acceleration values improve upon those seen in test Steel 3, which shows the addition of foam increased the mitigation properties of the system. Peak accelerations were reduced by 9.5% (Left), 16.5% (Right), and 15.8% (Corner) when compared against the control test of this series. More blast energy was lost in the foam spring combination than the springs alone. This could be due to the increased stiffness of the system or the diversion of energy into the foam material itself.

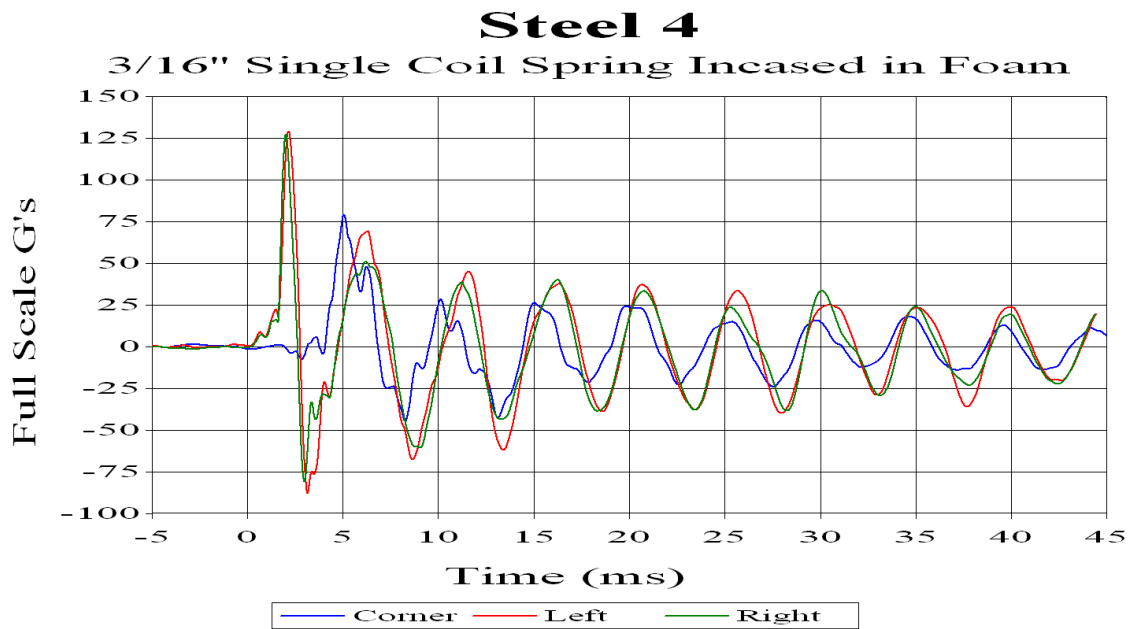


Figure 6.12: Steel 4 Filtered Acceleration Data

Though further oscillations of the frame were clearly damped in this test compared to test Steel 3, there still is an issue with the width of the acceleration envelope at large acceleration values. To improve further upon this design a better damping material than foam must be utilized in the system, or the aluminum spring design discontinued. Though results lean towards a discontinuation of the spring design as it applies to acceleration mitigation, not all possibilities have been explored. A spring system, where each oscillation is damped significantly would still pose as a feasible concept. This system would, unlike the aluminum spring system, have to accommodate the initial motion of the hull in a way where frame response is not dependent on the initial deformation, response of the hull. The ideal system would combine: free motion of the hull early in the blast, accommodations so the hull does not contact the frame directly as it displaces upward, and damping of any residual oscillation after energy has been transferred to the specimen.

6.2.5 Steel 5: Polyurethane-Polyurea Coated Hull

Acceleration data from the fifth test of the steel series can be seen in Figure 6.13 below. Peak accelerations were found to be 105.92g's (Left), 107.9g's (Right), and 66.66g's (Corner). Peak acceleration reduction was found to be 26% (Left), 29% (Left), and 29.4% (Corner) when compared to the control frame of this series. These acceleration values demonstrate the positive mitigation affects of coating a hull with a polyurethane-polyurea blended material. In this test, blast energy was not transferred in its entirety to the frame because of the damping properties of the coating material. This material also appears to have elicited a more elastic response of the hull based on deformation after testing compared to every other hull in this series. The damping properties of this material also decreased acceleration envelope width, as seen in the figure below.

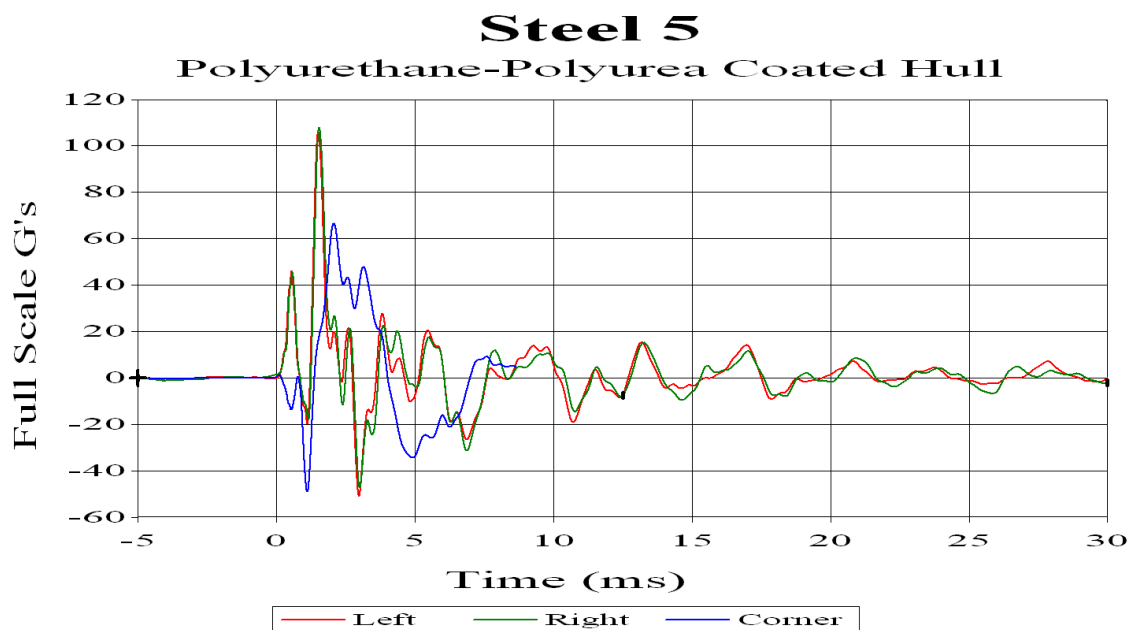


Figure 6.13: Steel 5 Filtered Acceleration Data

6.2.6 Steel 6: Steel Cable Isolators

Acceleration data from the sixth test of the steel series can be seen in Figure 6.14 below. Corner accelerometer data was cut at 11.4mS due to drift error. Peak accelerations were found to be 104g's (Left), 109.2g's (Right), and 57g's (Corner). Acceleration peaks were reduced by 26.9% (Left), 28.16% (Right), and 39.33% (Corner). Based on these values, the steel cable isolators mitigated acceleration successfully. This was due to the allowance of relatively free motion of the hull early in the blast. Though the isolators did oscillate during the test, these oscillations were damped out more successfully than previous tests because of the internal friction associated with cable strands rubbing with each oscillation [22].

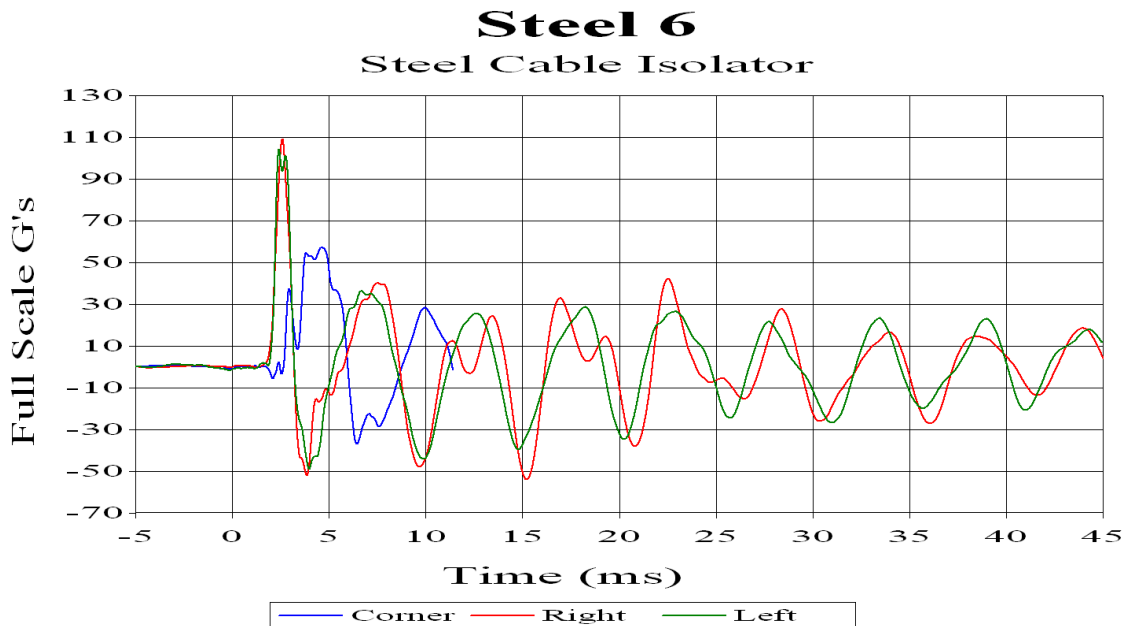


Figure 6.14: Steel 6 Filtered Acceleration Data

6.2.7 Steel Series Peak Acceleration Overview

Based on the information provided in Table 6.4, Figure 6.15 below it's clear that steel test 2,5, and 6 mitigated acceleration peaks with the most proficiency. Tests will now be analyzed for their acceleration envelope reduction properties.

Table 6.3: Steel Test Series Peak Acceleration Data

Test	Peak Acceleration (G's)		
	Left	Right	Corner
Steel 1	142.4	152	93.95
Steel 2	105.9	106.8	67.35
Steel 3	137.2	138.54	72.4
Steel 4	129.1	127.1	79.1
Steel 5	105.92	107.9	66.66
Steel 6	104.1	109.2	57

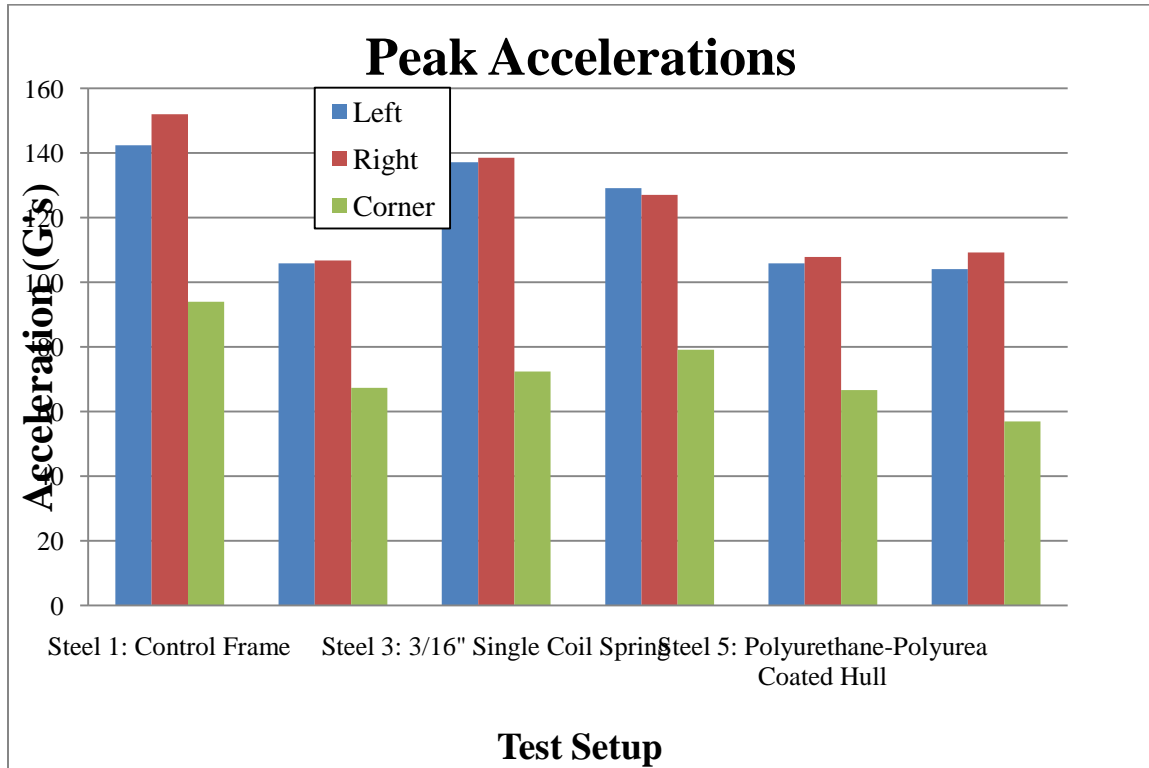


Figure 6.15: Steel Test Series Peak Acceleration v. Accelerometer Position

6.2.8 Steel Series Acceleration Envelope Overview

All tests in this series failed the first exposure criteria, based on 5.5mS of exposure to 23g's or more. However, Steel 5 came close to damping out accelerations to avoid this level. The polyurethane-polyurea coated hull performed by far the best at eliminating exposure times to large accelerations, seen in Table 6.4. This was due to two things: forced elastic response to the hull reducing deformations received during first few milliseconds of the blast, and the damping of any hull movement after that point. These two factors limited the energy the frame received from the hull due to blast effects. The pink foam test (Steel 2) failed both exposure criteria, as seen in the aluminum series. Tests involving aluminum springs (Steel 3 and Steel 4) also had large exposure times to accelerations greater than or equal to 23g's. This was due to the oscillatory behavior of the springs, with little damping (though Steel 4 performed better due to damping effects of the foam coating). Steel 1 and Steel 6 passed the 25mS exposure criteria, but as previously stated failed the more stringent exposure criteria. Steel 1 failed the 5.5mS criteria because peak accelerations were too high, and even good damping characteristics would be strained to reduce these large accelerations to below 23g's within 5.5mS. Steel 6 failed the 5.5mS criteria due to system oscillations, though these oscillations were damped more proficiently than any other test exhibiting an oscillatory behavior of the mitigating devices. This damping, as previously discussed, was due to energy loss from friction of steel cable elements.

Peak accelerations and acceleration envelope data can now be combined and analyzed. It was previously found that tests 2, 5, and 6 reduced peak accelerations with the most proficiency. Tests 5, 1, and 6 (starting with the best) were the most proficient in

reducing the profile of the acceleration envelope greater than or equal to 23g's. Based on these pieces of information, Steel 5 was the most proficient at reducing both peak accelerations and acceleration envelope width at large acceleration values. Steel 6 was as proficient at reducing peak accelerations, but did not damp oscillations as well as Steel 5, resulting in a wider acceleration envelope at large acceleration values.

Table 6.4: Steel Series Acceleration Envelope Data

Test	Width of Acceleration Envelope \geq 23g's (mS)	Military Exposure Criteria	
		5.5mS	25mS
Steel 1	16.25	Fail	Pass
Steel 2	100+	Fail	Fail
Steel 3	54.6255	Fail	Fail
Steel 4	33.532	Fail	Fail
Steel 5	6.716	Fail	Pass
Steel 6	23.8	Fail	Pass

6.3 Pocket Plate Series

6.3.1 Pocket Plate 1: Pocket Plate Control

Acceleration data from the first test of the pocket plate series can be seen in Figure 6.16 below. Corner accelerations were found to be unnaturally large in comparison to previous tests due to the hull hitting the frame close to where the corner accelerometer was located. This contact causes large acceleration spikes, as seen on the blue curve at approximately 2ms. Peak accelerations were found to be 110 g's (corner), 93 g's (right), and 103.3 g's (left). The interesting difference in this test is that the corner accelerometer peaks prior the right and left frame accelerometers. This can be attributed to the hull frame contact which did not occur in previous tests.

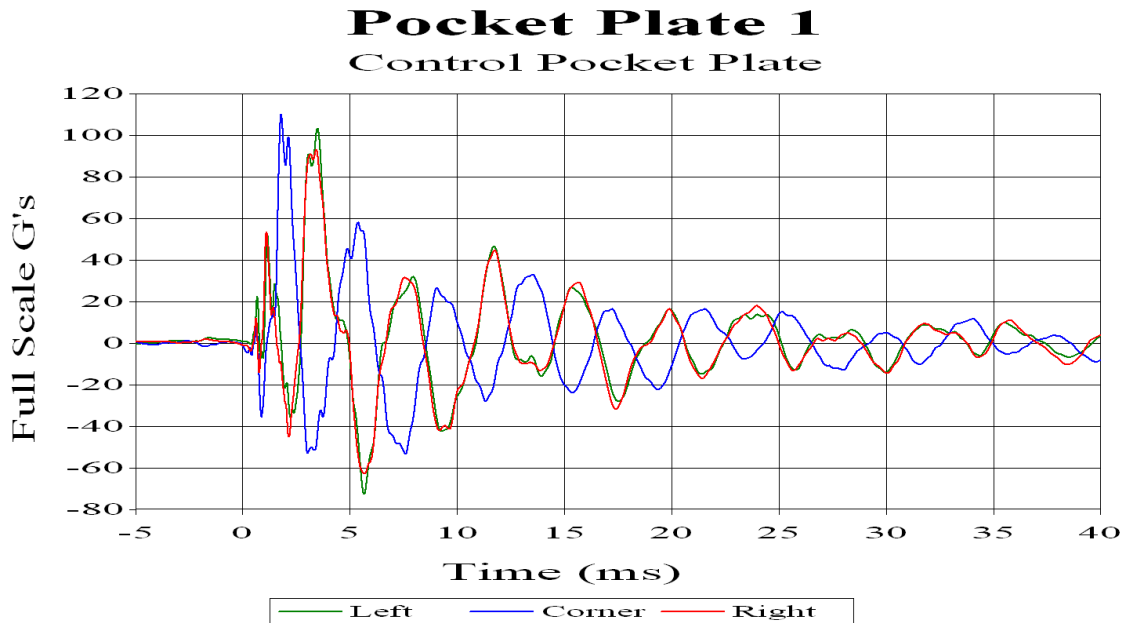


Figure 6.16: Pocket Plate 1 Filtered Acceleration Data

6.3.2 Pocket Plate 2: 3/16" Single Coil Spring Pocket Plate

Acceleration data from the second test of the pocket plate series can be seen in Figure 6.17 below. Corner accelerations were again found to be unnaturally large due to the hull hitting the frame close to where the corner accelerometer was located. This contact causes large acceleration spikes, as seen on the red curve at approximately 2ms. Peak accelerations were found to be 129.07 g's (corner) and 95.96 g's (left). Corner accelerations are higher in this test compared to Pocket Plate 1 because the connection between the hull and the frame is less stiff in this test, allowing for the hull to contact the frame with a higher velocity. Besides from the large acceleration spike for the corner accelerometer, mitigation effects in this test do not appear to have performed any better than the control for this series.

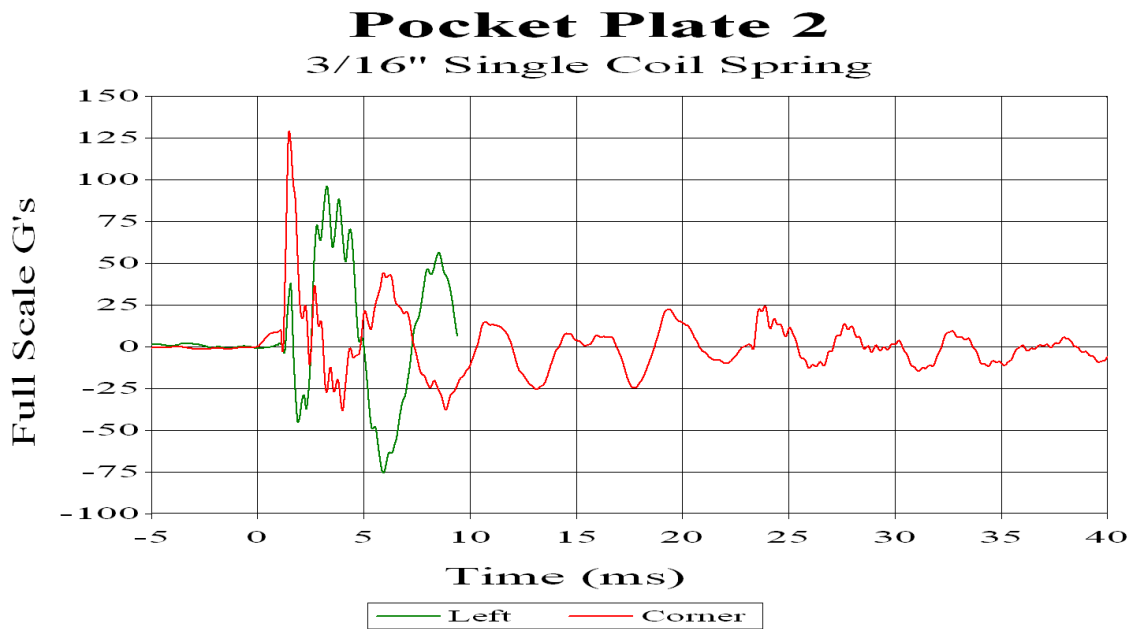


Figure 6.17: Pocket Plate 2 Filtered Acceleration Data

6.3.3 Pocket Plate 3: 1/8" Single Coil Spring Pocket Plate

Acceleration data from the first test of the pocket plate series can be seen in Figure 6.18 below. Peak accelerations were found to be 110 g's (corner), 93 g's (right), and 103.3 g's (left). Peak corner accelerations have been reduced in this test compared to others in this series, because of the introduction of a layer of foam where the hull contacts the frame. It was decided that the contact between the hull and the frame could not be avoided with this test setup, so a half inch layer of white foam (the same foam used in Aluminum 6) was used to reduce the impulse delivered to the frame by the hull upon impact. It was thought that the foam would slow the hull because the foam must be compressed in its entirety before the hull can reach the frame.

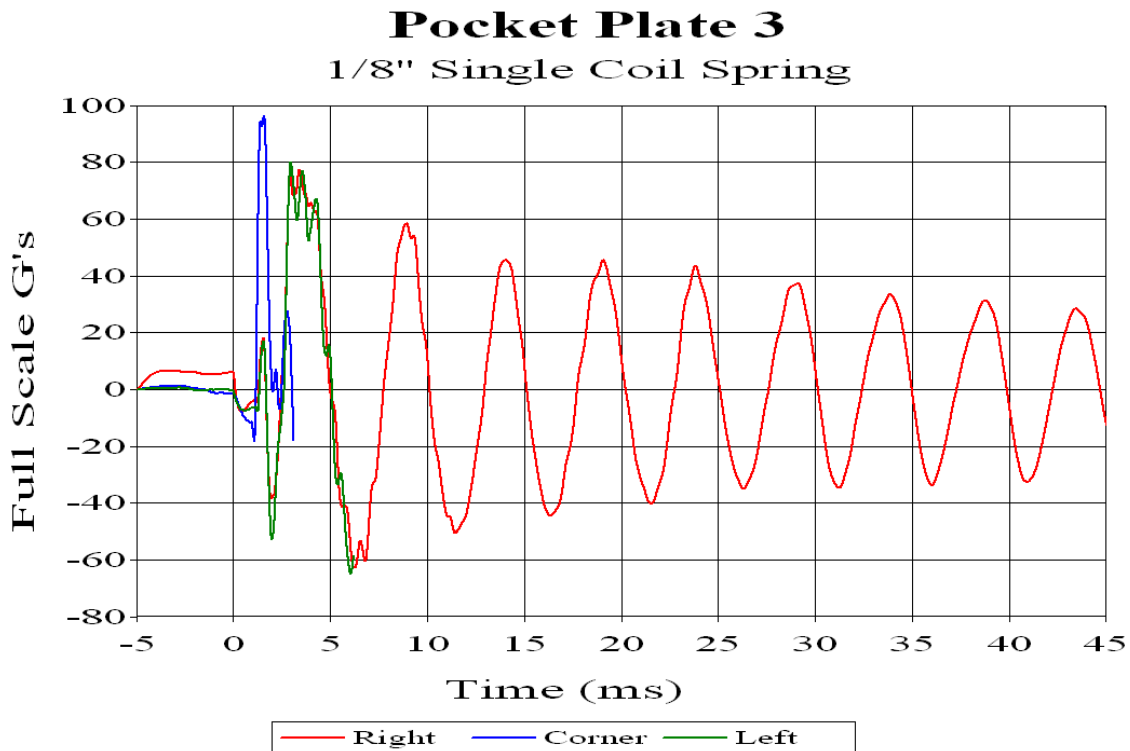


Figure 6.18: Pocket Plate 3 Filtered Acceleration Data

6.3.4 Pocket Plate Series Peak Acceleration Overview

Peak accelerations for all tests in the Pocket Plate Series can be seen in Table 6.5 and Figure 6.19 below. Based on peak accelerations, it can be seen that 3/16” single coil springs were not successful in mitigating accelerations for this test setup. The 1/8” single coil springs however were successful in reducing accelerations at least 20% in all instances. The most significant improvement can be seen in the peak corner accelerations, where the 1/8” springs reduced peak acceleration values by at least 12% when compared to other tests in this series.

Table 6.5: Pocket Plate Series Peak Acceleration Data

Test Setup	Peak Acceleration (G's)		
	Left	Right	Corner
Pocket Plate 1	103.3	93	110
Pocket Plate 2	95.96	N/A	129.07
Pocket Plate 3	80.06	77.57	96.34

Pocket Plate 1 accelerations can be compared directly to the first test of the steel series (Steel 1: Control Frame). The only variable between the two tests was the orientation of the hull (Steel 1 was orientated convex down; Pocket Plate 1 was orientated concave down). Peak accelerations of the right and left frame were found to be approximately 33% lower for Pocket Plate 1, though corner accelerations were found to be 18% higher (due to previously discussed hull frame contact). If corner accelerations can be lowered for the control pocket plate test (solving the problem of the hull hitting

the frame), then it would be a superior design in reducing peak accelerations than the steel control frame test. It can be inferred that this is possible, based on the corner acceleration reduction seen in the third pocket plate test that utilized foam to slow the hull before it contacts the frame.

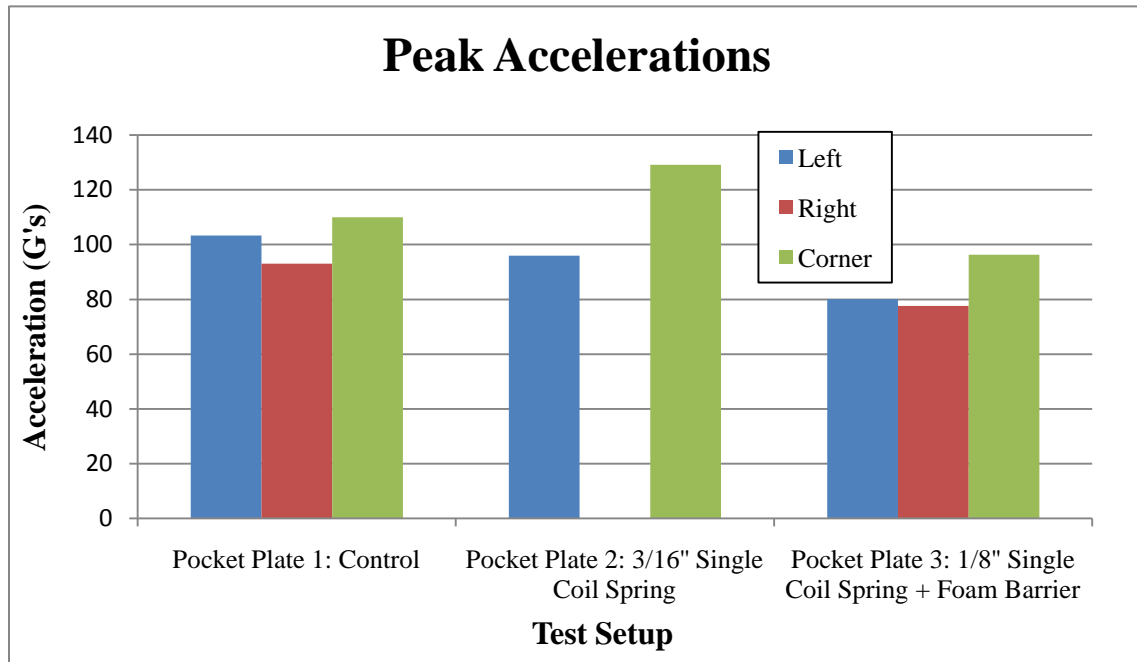


Figure 6.19: Pocket Plate Series Peak Acceleration v. Accelerometer Position

6.3.5 Pocket Plate Series Acceleration Envelope Overview

All three pocket plate tests failed the more stringent exposure time criteria (5.5mS); however tests Pocket Plate 1 and Pocket Plate 2 passed the 25mS criteria, as seen in Table 6.6. Pocket Plate 1 exhibited lower peak accelerations than Steel 1, with similar damping aspects, resulting in slightly lower exposure times. Pocket Plate 2 exhibited accelerations over 23g's for 21.24mS. This is larger than the control for this

series because of the oscillatory behavior of the system. However, because peak accelerations for this test were lower than other aluminum spring tests, the oscillations dropped below 23g's sooner (as compared to Steel 3 and Steel 4). Pocket Plate 3, due to the lower stiffness of the 1/8'' aluminum springs, was not able to reduce oscillations easily, resulting in a large acceleration envelope.

Considering peak accelerations and acceleration envelopes, no one test flourished in both aspects. Pocket Plate 3 had the lowest peak acceleration, but the largest acceleration envelope for large acceleration values. Pocket Plate 1 exhibits the best acceleration envelope, but acceleration peaks are not as low as those in Pocket Plate 3. The fact that the control for this series exhibits the best envelope profile is cause for concern. Mitigating systems used in this test series were not effective in reducing acceleration envelope width at large acceleration values.

Table 6.6: Pocket Plate Series Acceleration Envelope Data

Test	Width of Acceleration Envelope \geq 23g's (mS)	Military Exposure Criterion	
		5.5mS	25mS
Pocket Plate 1	14.49	Fail	Pass
Pocket Plate 2	21.24	Fail	Pass
Pocket Plate 3	76.178	Fail	Fail

Chapter 7 - Conclusions

7.1 Aluminum Test Series

Based on acceleration data, it can be concluded that two of the mitigation techniques used in this test series were successful. Aluminum rods, and compression springs mitigated peak accelerations, while reducing the width of the acceleration envelope at large acceleration values. White foam and enabling the hull to slide were successful in mitigating acceleration peaks, but failed in respect to the two previously mentioned tests in regards to reducing the profile of the acceleration envelope.

It is important to note that there was dissociation of the hull and the frame in the case where compression springs were used for mitigation (Aluminum 4). For the basis of this paper, this was viewed as neither good nor bad, but must be accounted for when considering the design of the vehicle.

There were also problems associated with Aluminum 3 (Sliding Hull), where the slots allowing the hull to slide were not large enough. This caused unintended contact between the hull and the bolts connected to the frame. Further tests should be performed to see if this can be avoided, and its effects on the acceleration response of the frame.

7.2 Steel Test Series

Based on acceleration data previously discussed, it can be concluded that a polyurethane-polyurea coated hull performs the best at mitigating accelerations delivered to the frame. This material also reduces hull deformations compared to the control test (and all other tests), though this was only visually verified. Steel cable isolators performed as well as the coated hull in terms of reducing peak accelerations, but failed to reduce the profile of the acceleration envelope with the success of the coated hull.

Coating the hull of a vehicle can be applied with other mitigation techniques, such as steel cable isolators due to their differing locations of application. This should be further investigated, as well as other tests involving a polyurethane-polyurea coated hull. The coating's ability to reduce deformations should also be investigated for its ability to increase the survival probability of a vehicle involved in a blast.

7.3 Pocket Plate Series

No one test in this series performed better than others in terms of reducing peak accelerations and reducing the profile of the acceleration envelope. The mitigating systems utilized in this test series were not successful in damping oscillations of the system, causing an increase in the profile of the acceleration envelope. More mitigation techniques must be investigated with this hull orientation for conclusions to be made. This test series does show promise when comparing the data of the control test, with that control test of the steel series. This will be discussed in the next section.

Many of the problems associated with this test series arise from hull-frame contact during testing. Based on lower corner accelerations with the implementation of a foam barrier, it can be concluded that this effect can be reduced. It is also possible to redesign the frame so that there is no longer concern of contact during testing.

7.4 Combined Conclusions

For this paper, conclusions from the aluminum test series will not be compared to other test series. However, it would provide good research direction to investigate the mitigation techniques that performed well in this series under the test specifications of other series. The steel cable isolators seen in the steel series were intended to roughly simulate the response seen in the compression spring test of the aluminum series. In the steel cable isolator test, mitigating systems were bound to the specimen (unlike the compression springs). This caused oscillations in the system not seen in the compression spring test. Both of these systems were successful in their respective test series, a reason for further investigation of the spring, damper mitigation technique.

Direct comparison of the control tests of the steel and pocket plate results in conclusions of acceleration mitigation based on hull orientation. Peak accelerations of the pocket plate control were found to be approximately 33% lower than the steel control test for the right and left frame, but 18% higher at the corner of the frame. This was due to contact between the hull and the frame during testing. This contact can be reduced, seen in Pocket Plate 3, or even eliminated by redesigning the frame. The acceleration envelope was slightly shorter (at 23g's) for the pocket plate control compared to the steel control. Based on this data, it can be concluded that a concave downward hull orientation is superior to a convex downward hull orientation in regards to acceleration mitigation.

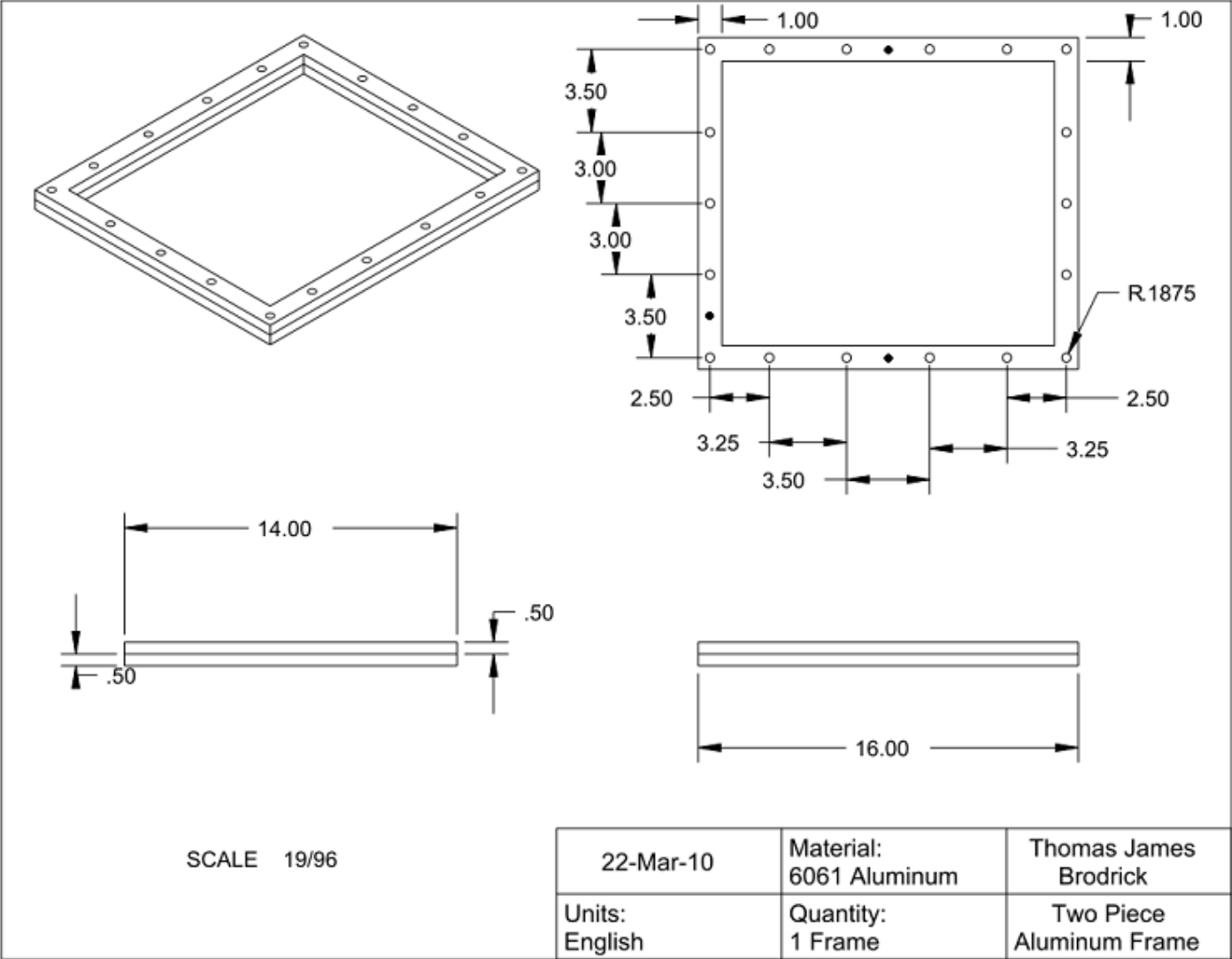
The two most important factors in mitigating accelerations to the frame were limiting hull-frame interactions early in the blast (when the hull deforms the most), and

damping responses of the system. Damping the initial response of the system can reduce plastic hull deformation, while further damping reduces the chance of system oscillations at large acceleration values. A polyurethane-polyurea coated hull was effective in reducing early blast effects, and damping residual responses. This polymer coating also reduces the chance of hull penetration by distributing deformations, retarding localization of deformations. The incorporation of structures that allow unrestricted movement of the hull, such as springs was also important. Springs that allow for free expansion, contraction of the hull were preferred. These structures exhibited less response in the vertical direction, seen as acceleration oscillations in the system. Regardless of spring specifications, a damping material must be incorporated into the system. In conclusion, the most preferred design would incorporate a polyurethane-polyurea coated hull with spring structures between the hull and the frame that have incorporated damping characteristics. These springs would allow for free movement of the hull perpendicular to the vertical, diverting oscillations away from the frame.

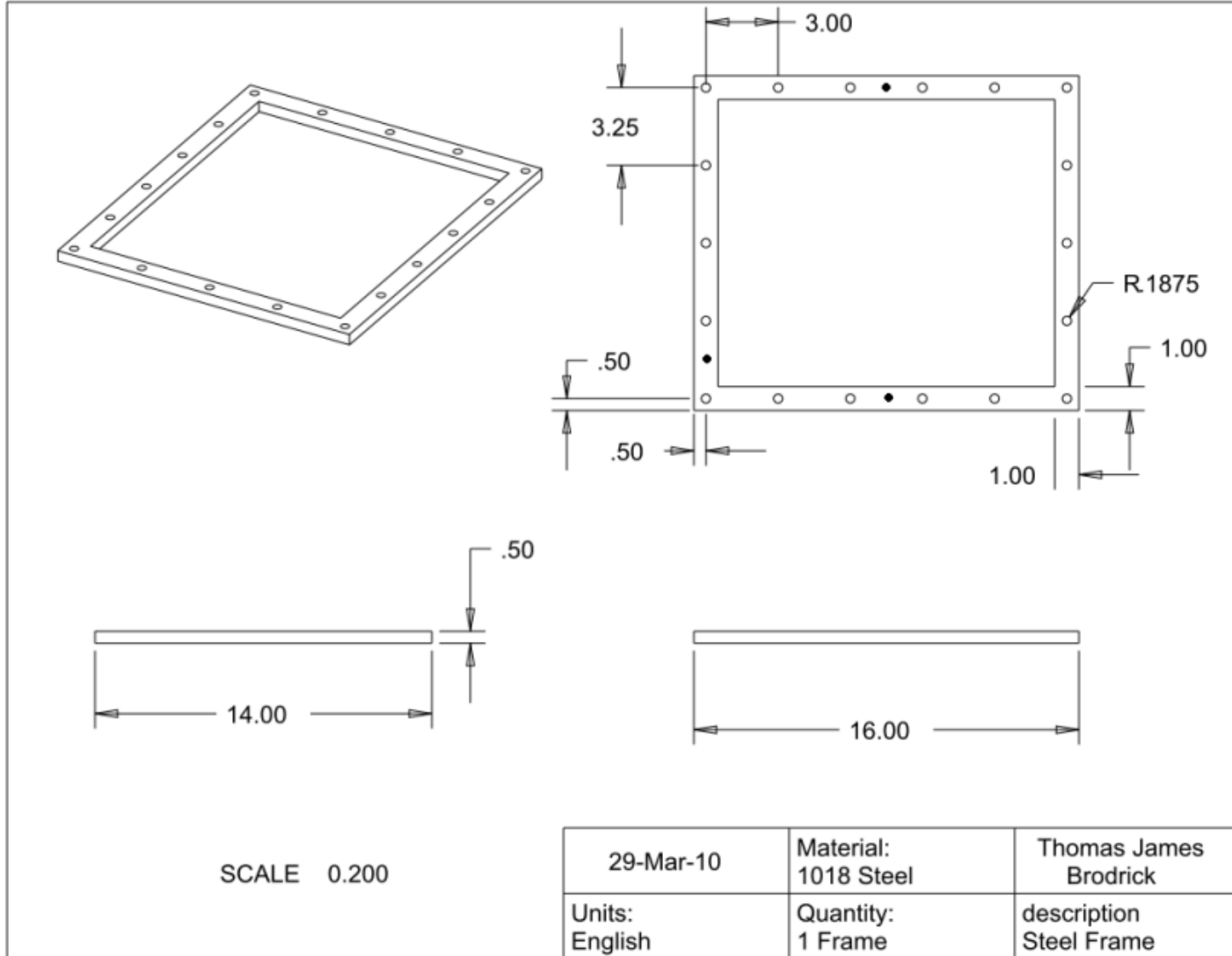
Appendix A: FS-17 Specifications [14]

Design and Specifications	
<p>Input Energy</p> <ul style="list-style-type: none"> • Battery supply for a minimum of 50 firings. • Built-in battery charger for 110 VAC • (220 available) <p>Output Energy</p> <ul style="list-style-type: none"> • 4000 volt pulse with 1500 amperes peak current into low resistance load (8.0 joules). <p>Circuit</p> <ul style="list-style-type: none"> • Regulated DC battery power supply in Control Unit. • DC to DC converter with high voltage energy storage capacitor in firing module • Triggered gap for instantaneous firing (typically less than 10 microseconds) • Meters in Control Unit to monitor module capacitor voltage and battery voltage • External or internal trigger monitor <p>Control Unit Input Connection</p> <ul style="list-style-type: none"> • U.S. Type, 3 pin plug for 110 VAC battery recharging • (Special plug for 220 VAC if required) • Safety interlock and Key Arm Switch to arm • Meter to indicate module arm voltage & discharge rate • Five-pin connector to module • Six-pin connector for accessory connection for 'Pulse Out' 	<ul style="list-style-type: none"> • External trigger pulse out • External switch closure • External breakwire • Automatic trigger • Meter to indicate battery voltage • External dimensions: 6"x7"x9" <p>Control Unit to Module Connection</p> <ul style="list-style-type: none"> • Requires 3-Conductor Shielded Cable with ground used as a shield • Maximum 2,000 feet of 20 gauge wire <p>Module</p> <ul style="list-style-type: none"> • Five pin connector for connection from Control Unit • Safety Interlock Connector • Reynolds Type 31 Coaxial output connector <p>Module to Detonator Connection</p> <ul style="list-style-type: none"> • Maximum 100 feet twin lead blasting wire (P/N 167-8559) • Maximum 300 feet Type "C" high voltage coaxial cable (P/N 167-2669) <p>Options</p> <ul style="list-style-type: none"> • FS-46 Ruggedized Module P/N 188-7065

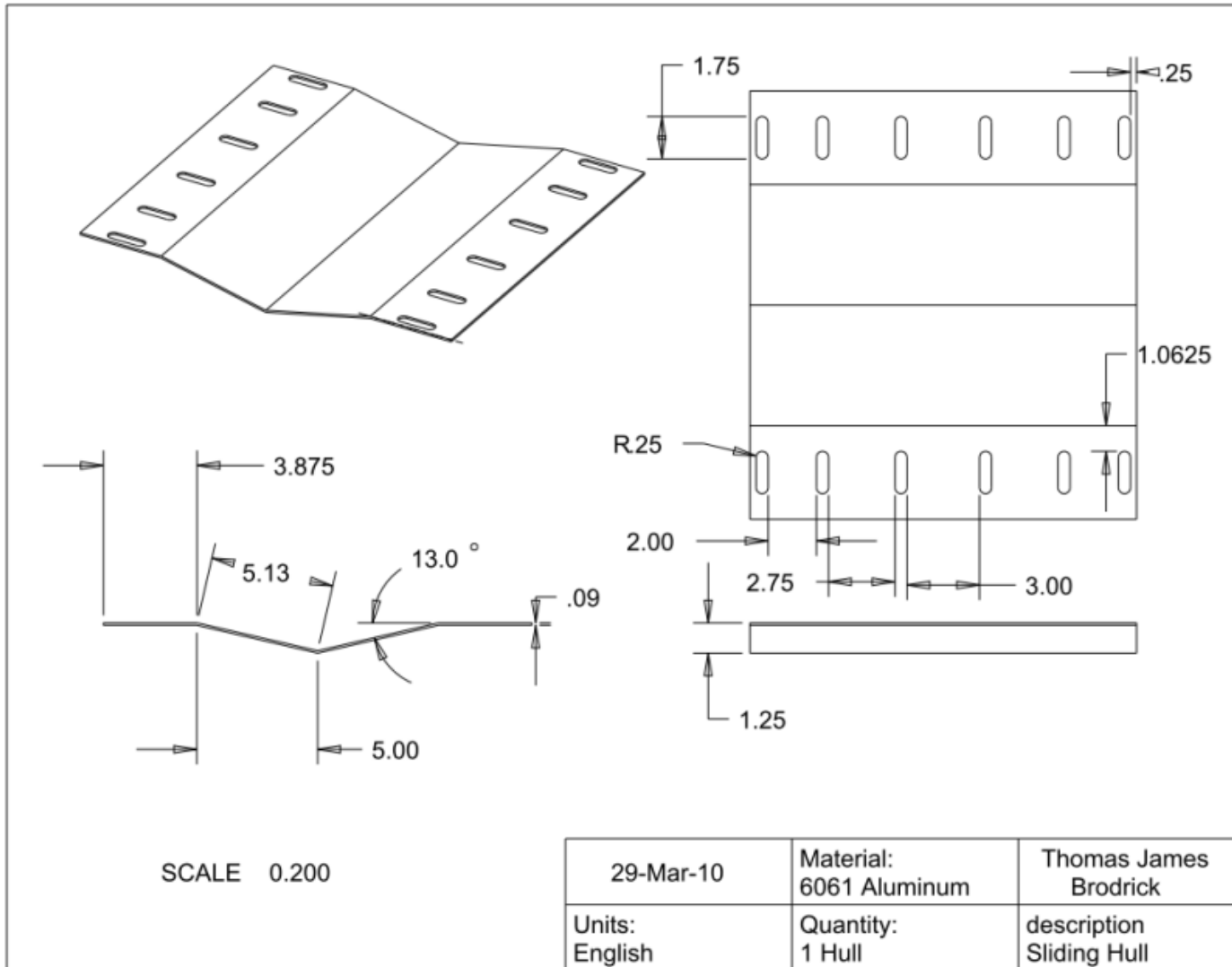
Appendix B: Aluminum Frame



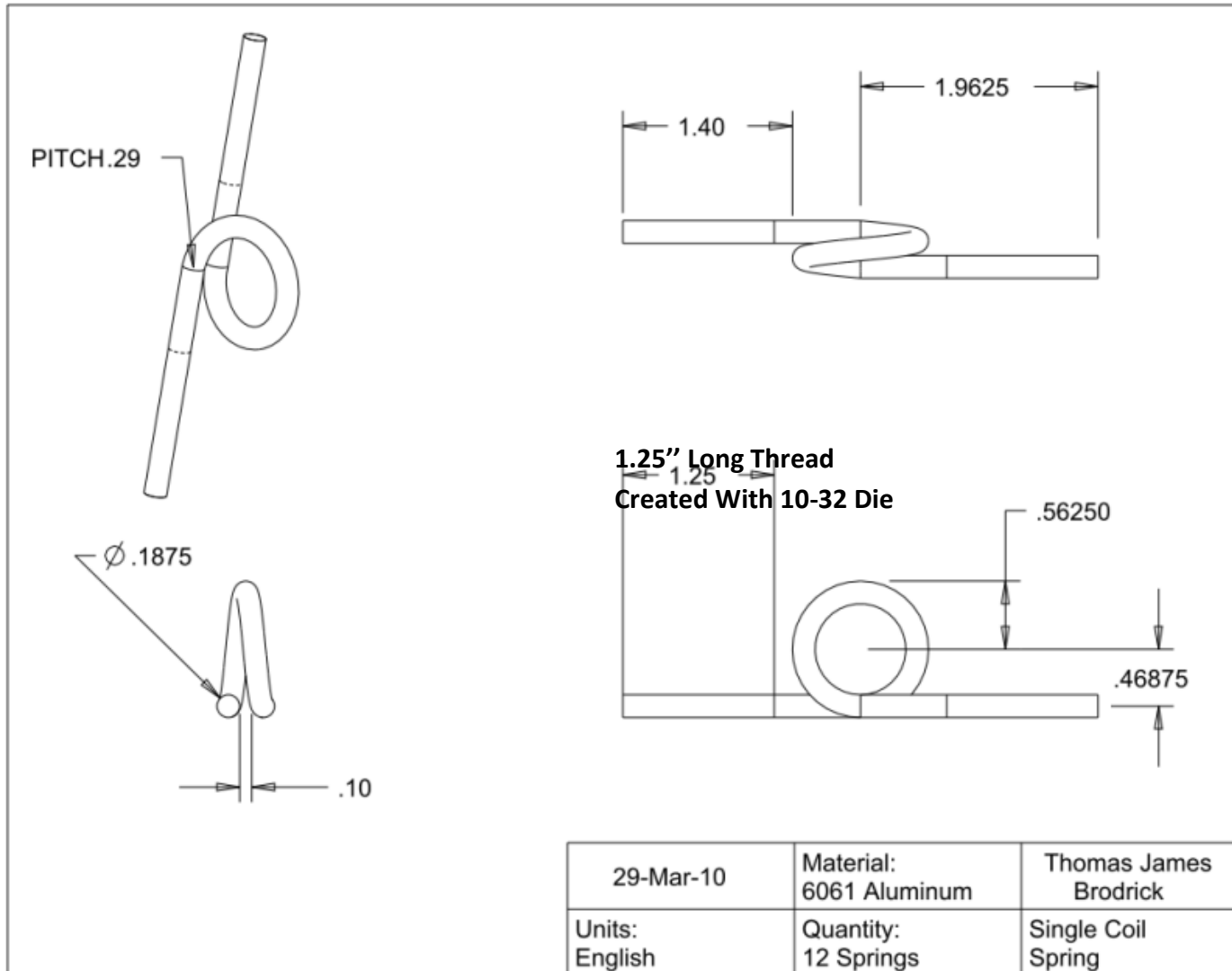
Appendix C: Steel Frame



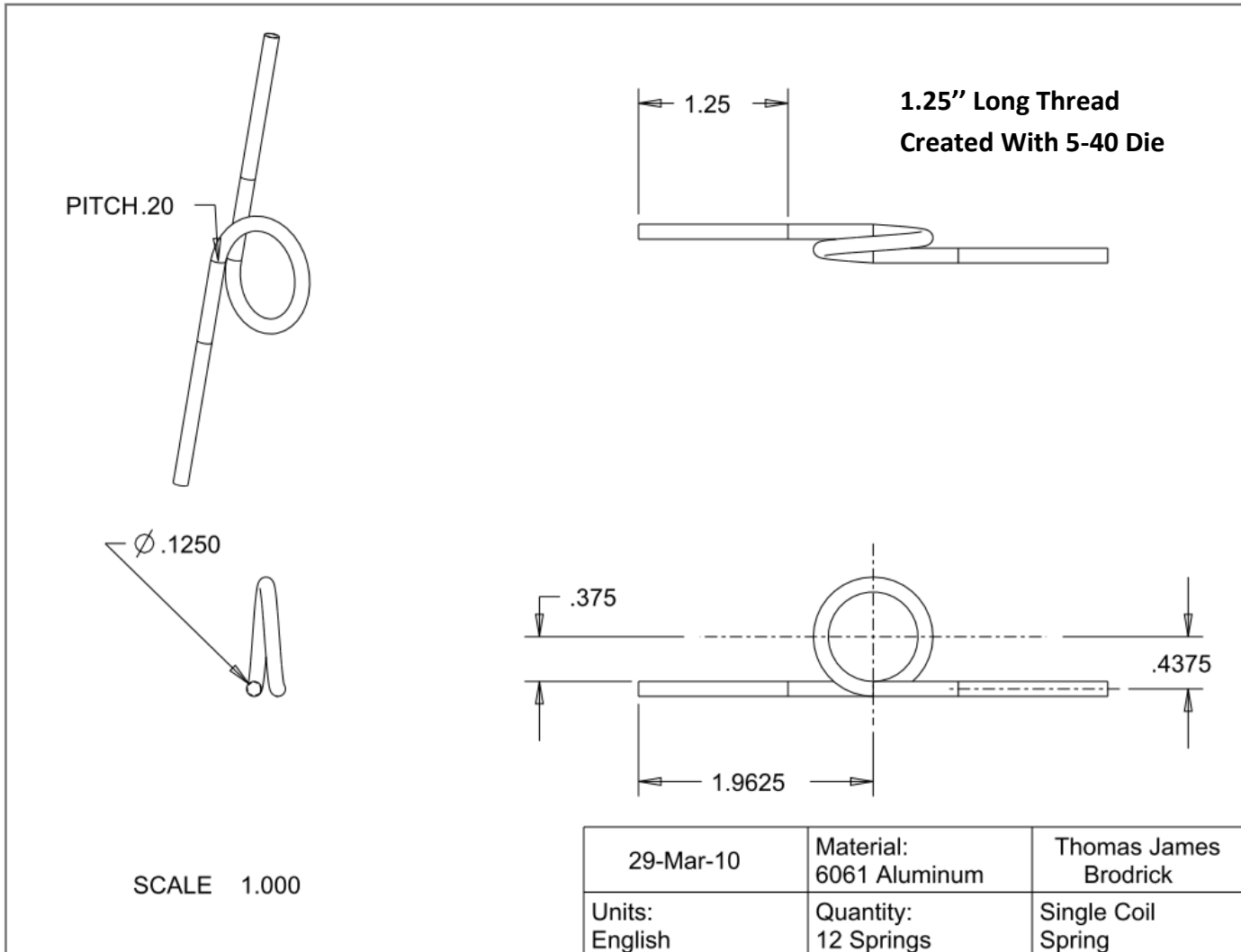
Appendix D: Sliding Hull



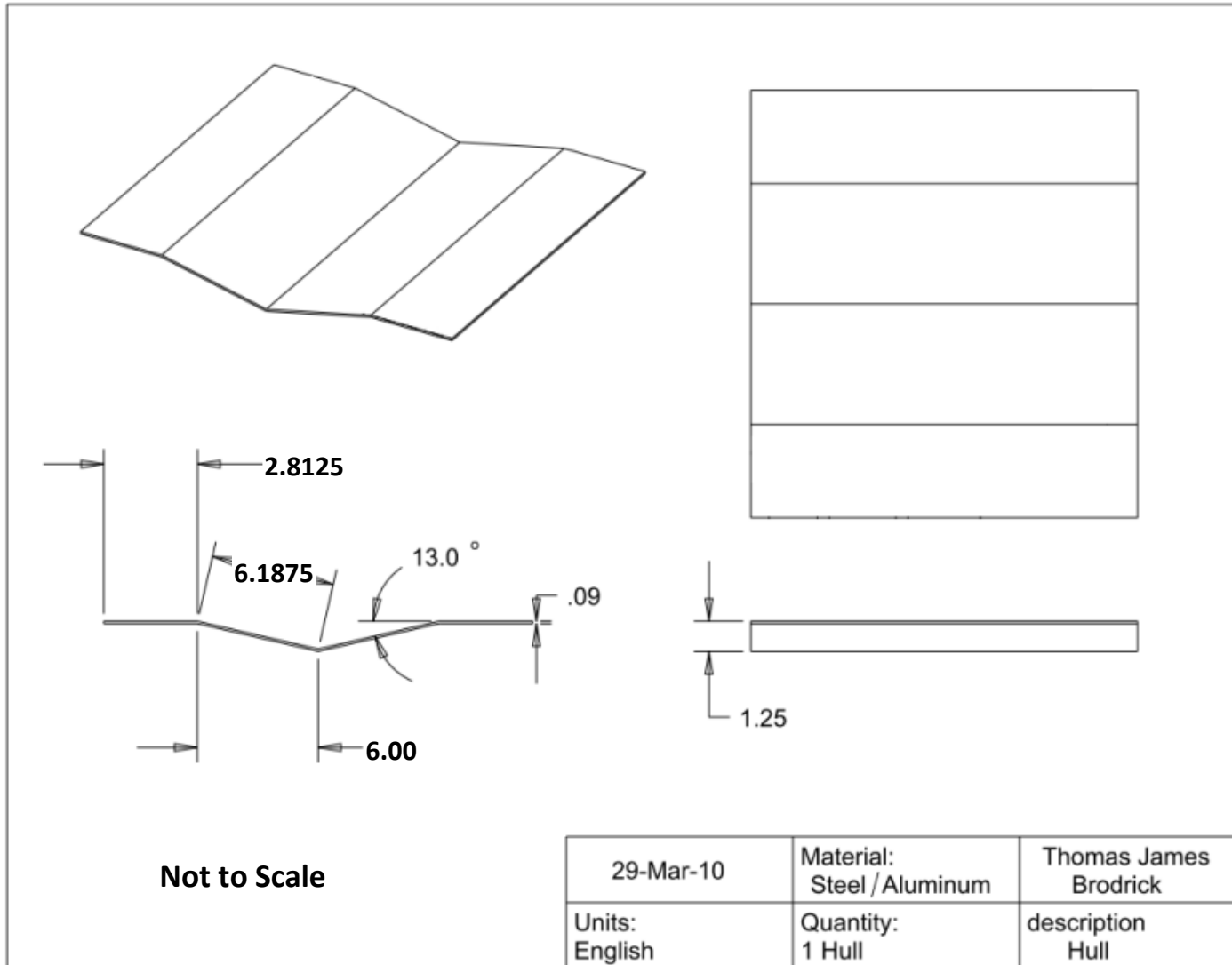
Appendix E: 3/16" Single Coil Aluminum Springs



Appendix F: 1/8" Single Coil Aluminum Springs

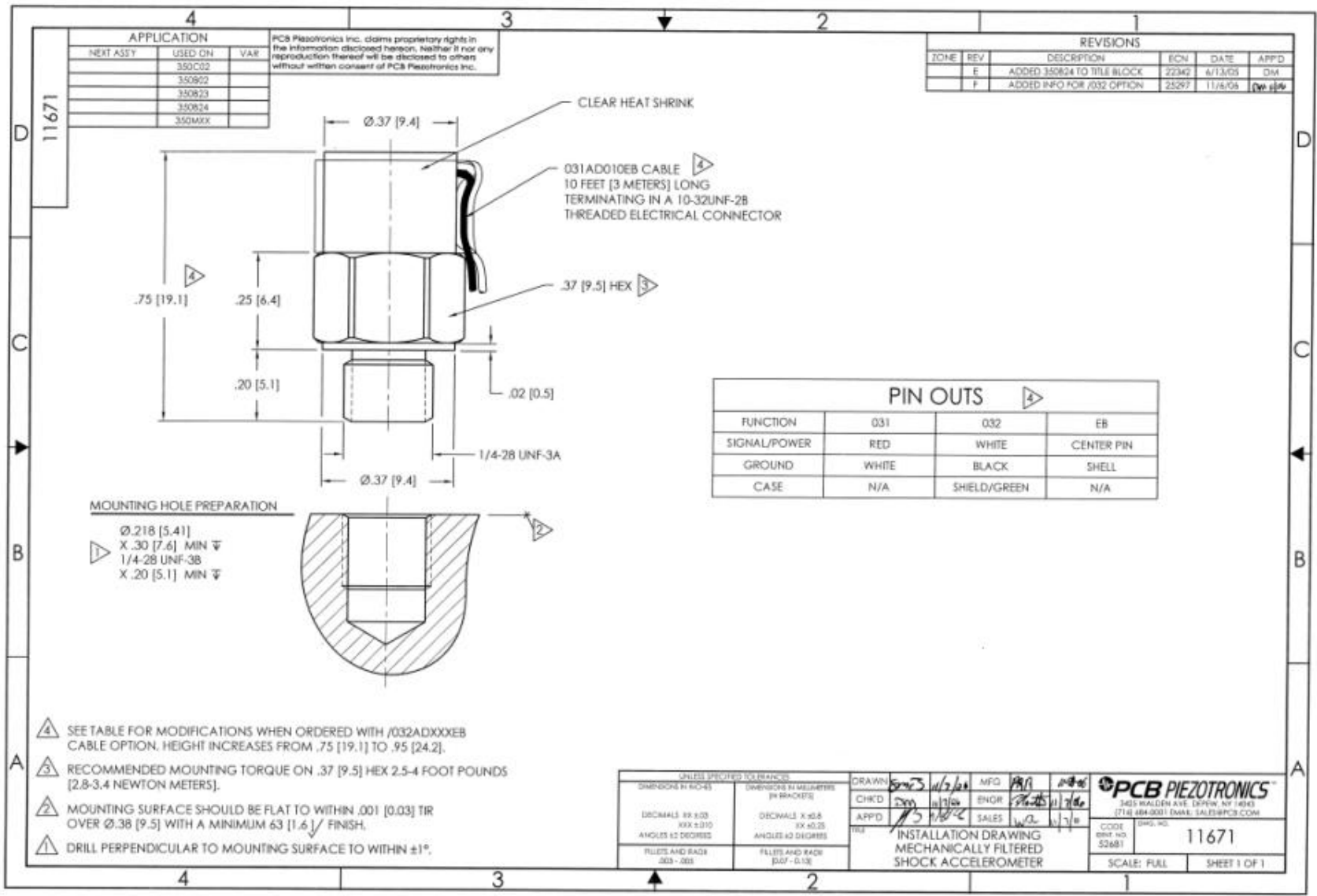


Appendix G: Steel/Aluminum Hull



Appendix H: Accelerometer Specifications [25]

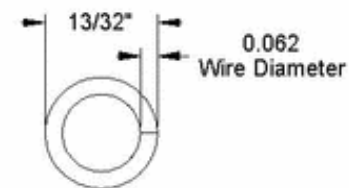
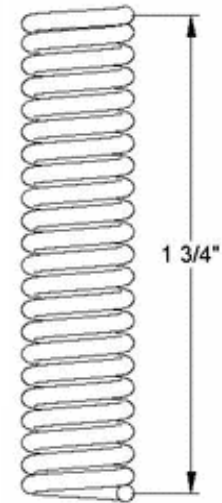
Model Number 350C02	SHEAR ICP® SHOCK ACCELEROMETER		Revision A ECN #: 28655										
Performance Sensitivity (±30 %) Measurement Range Frequency Range (±1 dB) Frequency Range (-3 dB) Electrical Filter Corner Frequency (-3 dB) Mechanical Filter Resonant Frequency Resonant Frequency Broadband Resolution (1 to 10000 Hz) Non-Linearity (per 10,000 g (98,100 m/s ²)) Transverse Sensitivity Environmental Overload Limit (Shock) Temperature Range (Operating) Temperature Range (Storage) Temperature Response Electrical Excitation Voltage Constant Current Excitation Output Impedance Output Bias Voltage Discharge Time Constant Settling Time (within 10% of bias) Electrical Isolation (Case) Physical Sensing Element Sensing Geometry Housing Material Sealing Size (Hex x Height) Weight (without cable) Electrical Connector Cable Length Cable Type Mounting Thread	ENGLISH 0.1 mV/g ±50000 g pk 4 to 10000 Hz 2 to 25000 Hz 13 kHz 23 kHz ≥100 kHz 0.5 g rms ≤2.5 % ≤7 % ±150000 g pk 0 to +150 °F -40 to +200 °F See Graph 20 to 30 VDC 2 to 20 mA ≤200 ohm 8 to 14 VDC 0.10 sec <1 sec >1000000 ohm Ceramic Shear Titanium Hermetic 0.375 in x 0.75 in 0.15 oz Integral Cable 10 ft 031 Twisted Pair 1/4-28 Male	SI 0.01 mV/(m/s ²) ±490000 m/s ² pk 4 to 10000 Hz 2 to 25000 Hz 13 kHz 23 kHz ≥100 kHz 4.9 m/s ² rms ≤2.5 % ≤7 % ±1471500 m/s ² pk -18 to +66 °C -40 to +93 °C See Graph 20 to 30 VDC 2 to 20 mA ≤200 ohm 8 to 14 VDC 0.10 sec <1 sec >1000000 ohm Ceramic Shear Titanium Hermetic 9.5 mm x 19.1 mm 4.2 gm Integral Cable 3.05 m 031 Twisted Pair 1/4-28 Male	Optional Versions (Optional versions have identical specifications and accessories as listed for standard model except where noted below. More than one option maybe used.) M - Metric Mount Mounting Thread M6 x 0.75 Male (M6 x 0.75 Male) Notes [1] Typical. [2] Typical corner frequency for coupled electrical and mechanical filters. [3] Electrical filter is a second order filter. [4] Amplitude at resonance is +9 dB. [5] See PCB Declaration of Conformance PS023 for details. Supplied Accessories ACS-22 NIST Traceable frequency response (100Hz to ±1 dB point) (1)										
			<table border="1"> <tr> <td>Entered: BLS</td> <td>Engineer: BAM</td> <td>Sales: WDC</td> <td>Approved: JJB</td> <td>Spec Number:</td> </tr> <tr> <td>Date: 04/23/2008</td> <td>Date: 04/23/2008</td> <td>Date: 04/23/2008</td> <td>Date: 04/23/2008</td> <td style="text-align: center;">31119</td> </tr> </table>	Entered: BLS	Engineer: BAM	Sales: WDC	Approved: JJB	Spec Number:	Date: 04/23/2008	Date: 04/23/2008	Date: 04/23/2008	Date: 04/23/2008	31119
Entered: BLS	Engineer: BAM	Sales: WDC	Approved: JJB	Spec Number:									
Date: 04/23/2008	Date: 04/23/2008	Date: 04/23/2008	Date: 04/23/2008	31119									
			<p style="text-align: center;"> </p> <p style="text-align: center;">Typical Sensitivity Deviation vs Temperature</p>										
<p><i>All specifications are at room temperature unless otherwise specified.</i> In the interest of constant product improvement, we reserve the right to change specifications without notice. ICP® is a registered trademark of PCB group, Inc.</p>			<p> </p> <p> 3425 Walden Avenue Depew, NY 14043 UNITED STATES Phone: 888-684-0013 Fax: 716-685-3886 E-mail: vibration@pcb.com Web site: www.pcb.com </p>										



Appendix I: Compression Spring Information [20]

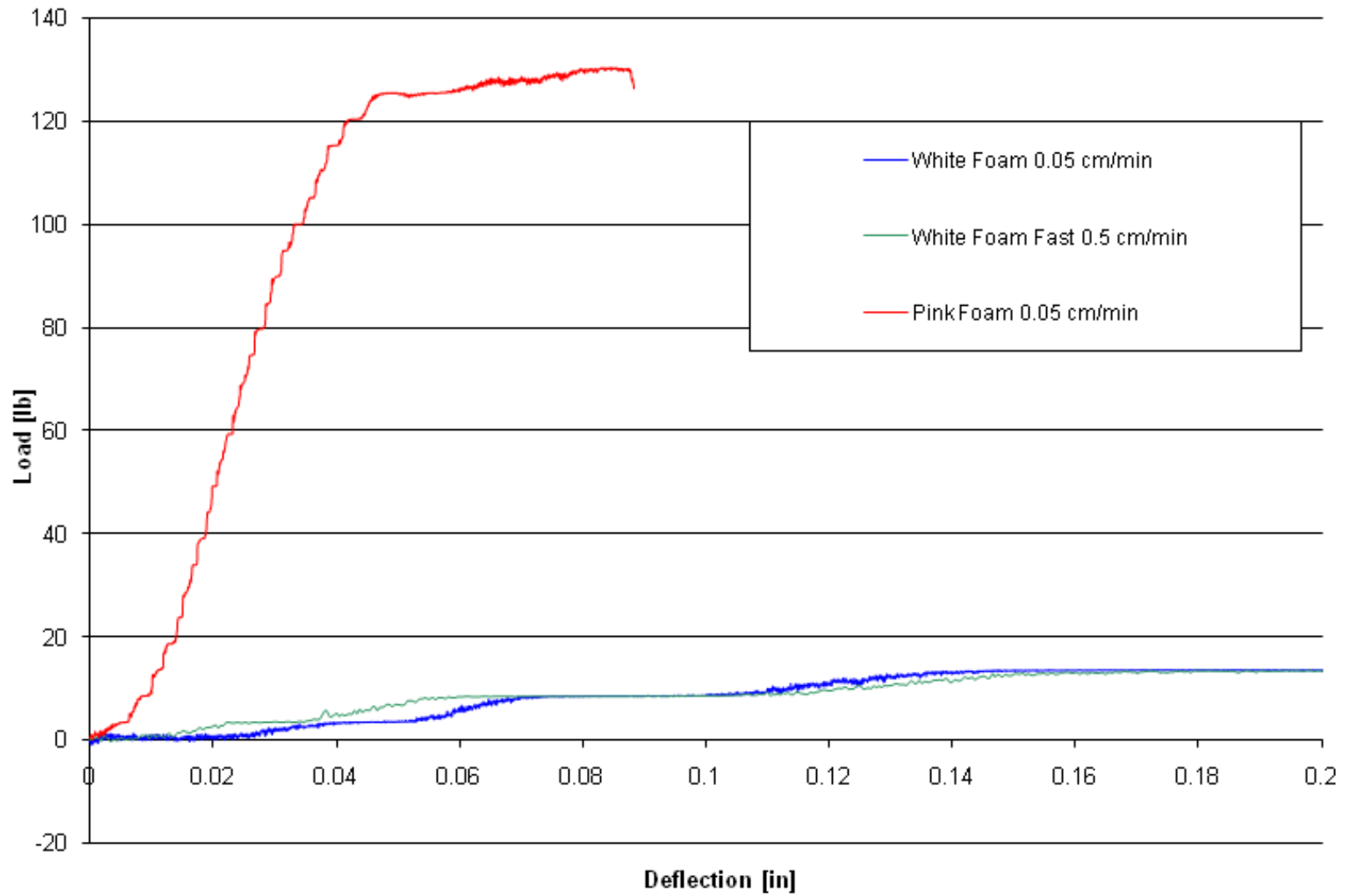
Part Number: [9657K113](#)

Type	Compression Springs
Material	Steel
Steel Type	Zinc-Plated Spring-Tempered Steel
System of Measurement	Inch
Outside Diameter	13/32"
Wire Size	.062"
Overall Length	1-3/4"
Compressed Length	1.38"
Ends	Closed
Wire Type	Round Wire
Load	17.73 lbs.
Deflection at Load	.37"
Rate	47.44 lbs./inch
Specifications Met	Not Rated



 http://www.mcmaster.com © 2005 McMaster-Carr Supply Company		PART NUMBER	9657K113
		Zinc-Plated Spring-Tempered Steel Compression Spring	
<small>Unless otherwise specified, dimensions are in inches. Information in this drawing is provided for reference only.</small>			

Appendix J: Foam - Load v. Deflection Curves



Appendix K: Aluminum 6061-T6 Material Properties [26]

	Metric	English
Density	2.7 grams/cubic cm	.0975 lb/cubic in
Ultimate Tensile Strength	310 MPa	45000psi
Yield Strength	276MPa	40000psi
Modulus of Elasticity	68.9Gpa	10000ksi
Poisson's Ratio	.33	.33
Shear Modulus	26Gpa	3770ksi
Shear Strength	207Mpa	30000psi

Appendix L: 1018 Steel Material Properties [27]

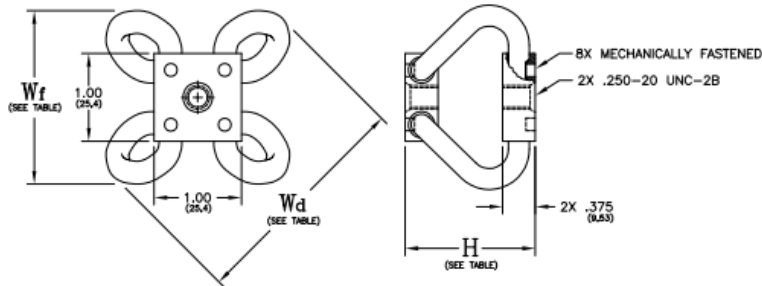
	Metric	English
Density	7.87 grams/cubic cm	.284 lb/cubic in
Ultimate Tensile Strength	475 MPa	68900 psi
Yield Strength	275 MPa	39900 psi
Modulus of Elasticity	205 Gpa	29700 ksi
Poisson's Ratio	.29	.29
Shear Modulus	80 Gpa	11600 ksi

Appendix M: Steel Cable Isolators [22]

DESIGN DATA

• SM7 SERIES • 7/32" DIAMETER CABLE

SHOCK & VIBRATION ISOLATORS



PART NUMBER	DIMENSIONS, in.			ISOLATOR WEIGHT
	H ±.04	Wf (REF)	Wd (REF)	
SM7 - 165 - A	1.65 (41.9)	2.25 (57.2)	3.00 (76.2)	2.5oz (71gms)
SM7 - 185 - A	1.85 (47.0)	2.50 (63.5)	3.25 (82.8)	2.6oz (73gms)
SM7 - 215 - A	2.15 (54.6)	2.75 (69.9)	3.60 (91.4)	2.7oz (76gms)

FEATURES:

- ALL METAL CONSTRUCTION
- UNEQUALLED TEMP. RANGE -200°F TO 500°F
- THREE AXIS CAPABILITY
- MAINTENANCE FREE
- FAIL SAFE DESIGN
- HIGH DAMPING: C/Cc ≈ .20
- EXCEPTIONAL RELIABILITY

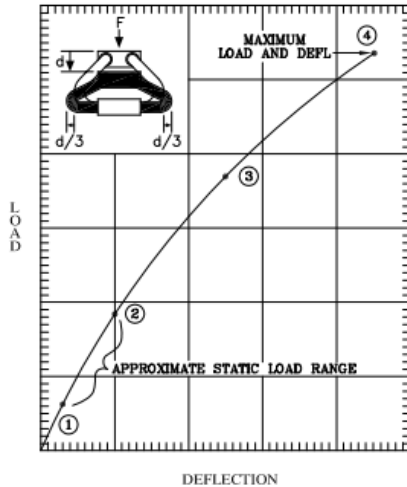
MATERIALS/FINISHES:

- CABLE: 300 SERIES SS PER MIL-W-83420 OR RR-W-410
- INSERTS: 300 SERIES SS PER NAS1130-4-10
- RETAINER BARS: 8063-T52 ALUM ALLOY/CHEM FILM IAW MIL-C-5541, CLASS 1A

NOTES:

- 1) ALL DIMENSIONS IN PARENTHESIS ARE METRIC (mm).
- 2) SPECIALS AVAILABLE UPON REQUEST (MATERIALS, SIZE, MOUNTING HOLES, FINISH, ETC...)

COMPRESSION



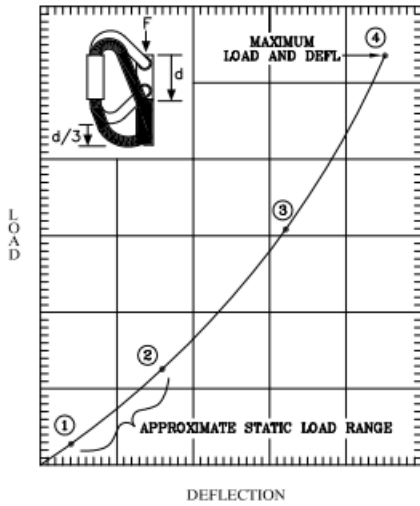
PART NO.	①		②		③		④		K _v (VIBE) (lbs/in)	K _s (SHOCK) (lbs/in)
	LOAD (lbs)	DEFL (in)	LOAD (lbs)	DEFL (in)	LOAD (lbs)	DEFL (in)	LOAD (lbs)	DEFL (in)		
SM7-165-A	7.2	.04	14.5	.10	46.0	.50	67.0	.90	155	93
SM7-185-A	4.8	.04	9.6	.10	32.0	.60	48.0	1.10	102	53
SM7-215-A	3.2	.04	5.6	.10	24.0	.70	35.0	1.30	61	34

TOLL FREE : 888-ISOLATOR
 FAX : (631) 491-5672
 WEB SITE : www.isolator.com
 E-MAIL : sales@isolator.com
 CAGE : 07007



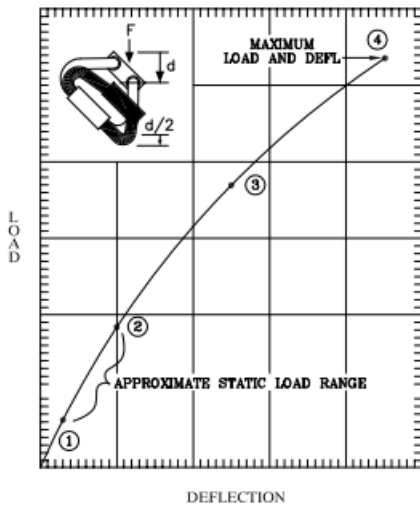
PERFORMANCE DATA • **SM7 SERIES** • 7/32" DIAMETER CABLE
SHOCK & VIBRATION ISOLATORS

ROLL



PART NO.	①		②		③		④		K_V (VIBE) (lbs/in)	K_R (SHOCK) (lbs/in)
	LOAD (lbs)	DEFL (in)	LOAD (lbs)	DEFL (in)	LOAD (lbs)	DEFL (in)	LOAD (lbs)	DEFL (in)		
SM7-165-A	4.0	.04	6.4	.10	27.0	.50	59.0	.90	74	54
SM7-185-A	2.4	.04	4.0	.10	19.0	.60	42.0	1.10	46	32
SM7-215-A	1.6	.04	3.2	.10	16.0	.70	35.0	1.30	34	22

45° COMPRESSION/ROLL



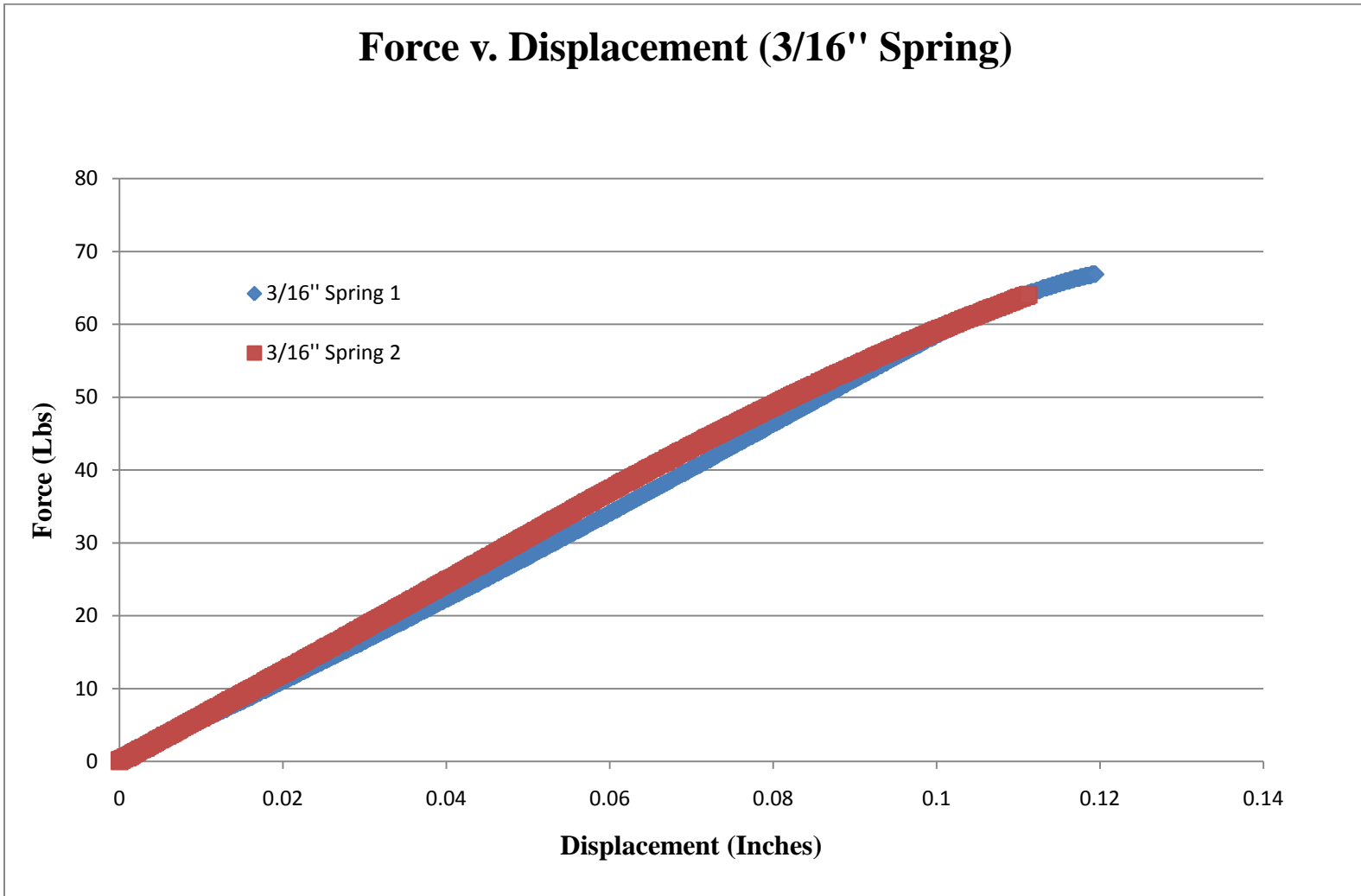
PART NO.	①		②		③		④		K_V (VIBE) (lbs/in)	K_R (SHOCK) (lbs/in)
	LOAD (lbs)	DEFL (in)	LOAD (lbs)	DEFL (in)	LOAD (lbs)	DEFL (in)	LOAD (lbs)	DEFL (in)		
SM7-165-A	5.6	.04	9.6	.10	37.0	.70	51.0	1.25	109	53
SM7-185-A	3.2	.04	6.4	.10	27.0	.85	38.0	1.50	69	32
SM7-215-A	2.4	.04	4.0	.10	21.0	1.00	35.0	1.80	45	21

TOLL FREE : 888-ISOLATOR
FAX : (631) 491-5672
WEB SITE : www.isolator.com
E-MAIL : sales@isolator.com
CAGE : 07QQ7

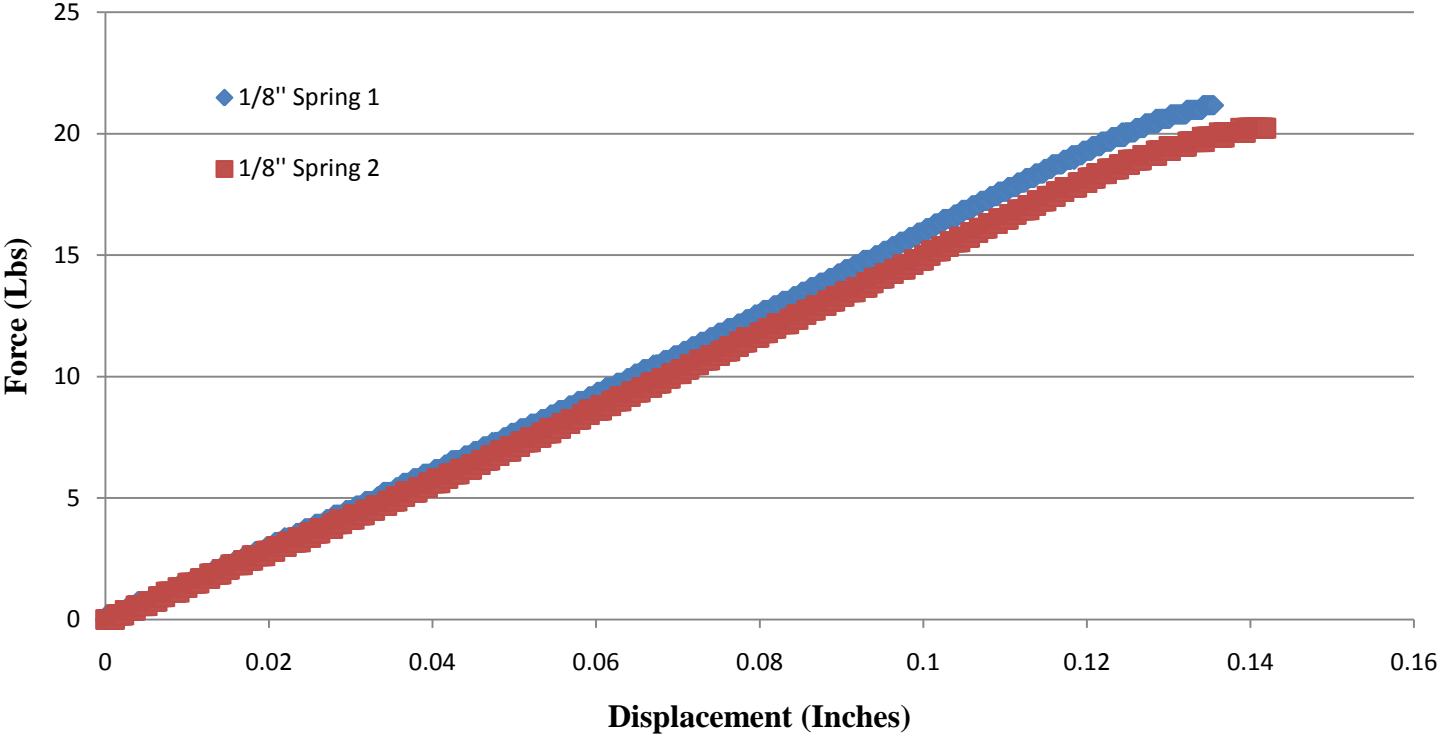


Appendix N: Tensile Tests for Spring Specimens

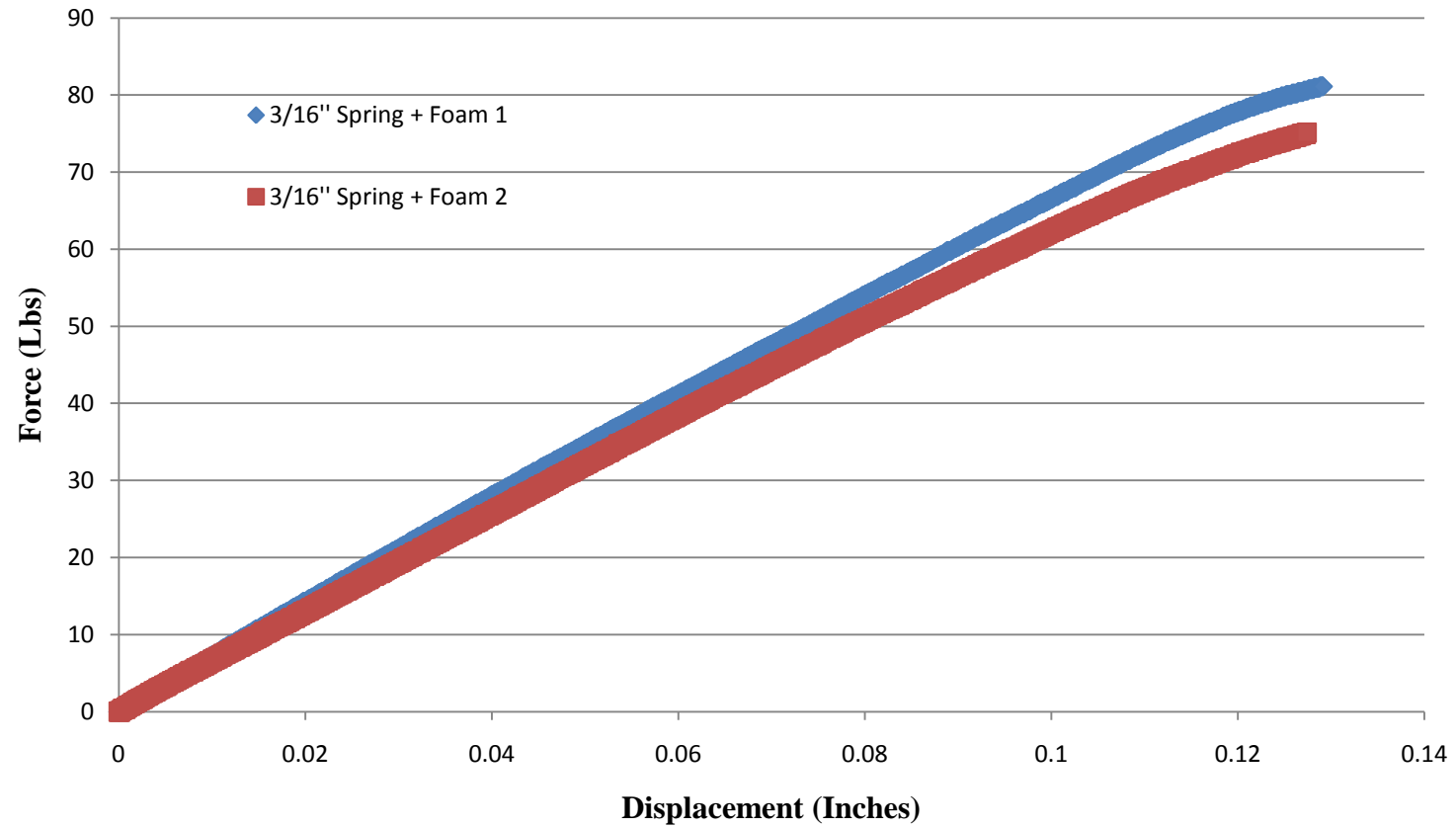
Force v. Displacement (3/16" Spring)



Force v. Displacement (1/8" Spring)



Force v. Displacement (3/16" Spring + Great Stuff Foam)



Appendix O: Data Verification (Accelerometer vs. Camera)

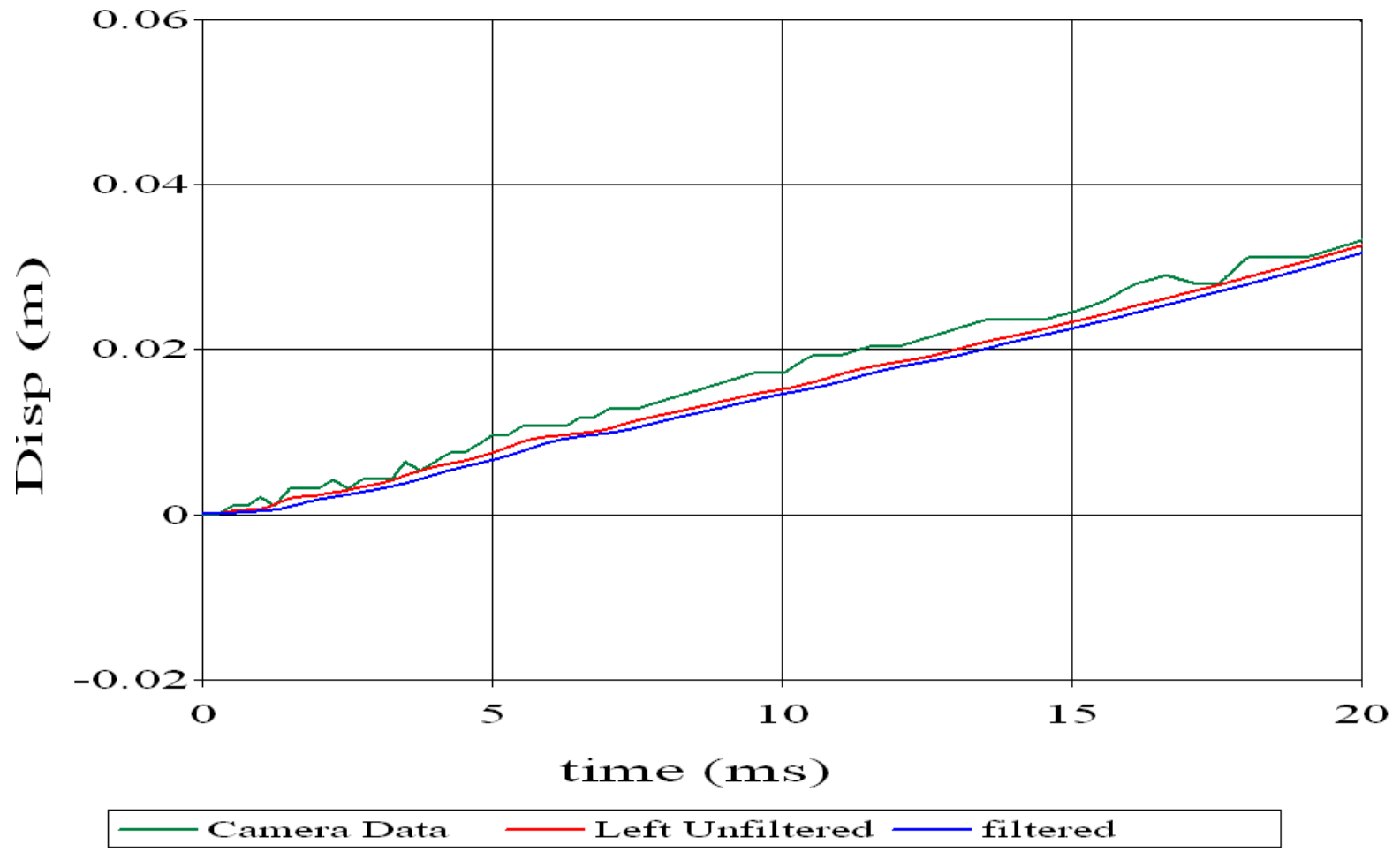
NOTES

- Graphs shown are only those that were verified. Examples of graphs that were not verified can be seen in Figure 5.6.
- * Refers to verifications assumed by displacements from other tests. Aluminum 5 video was corrupt, so accelerometer data was compared to Aluminum 6. These tests were very similar in nature.

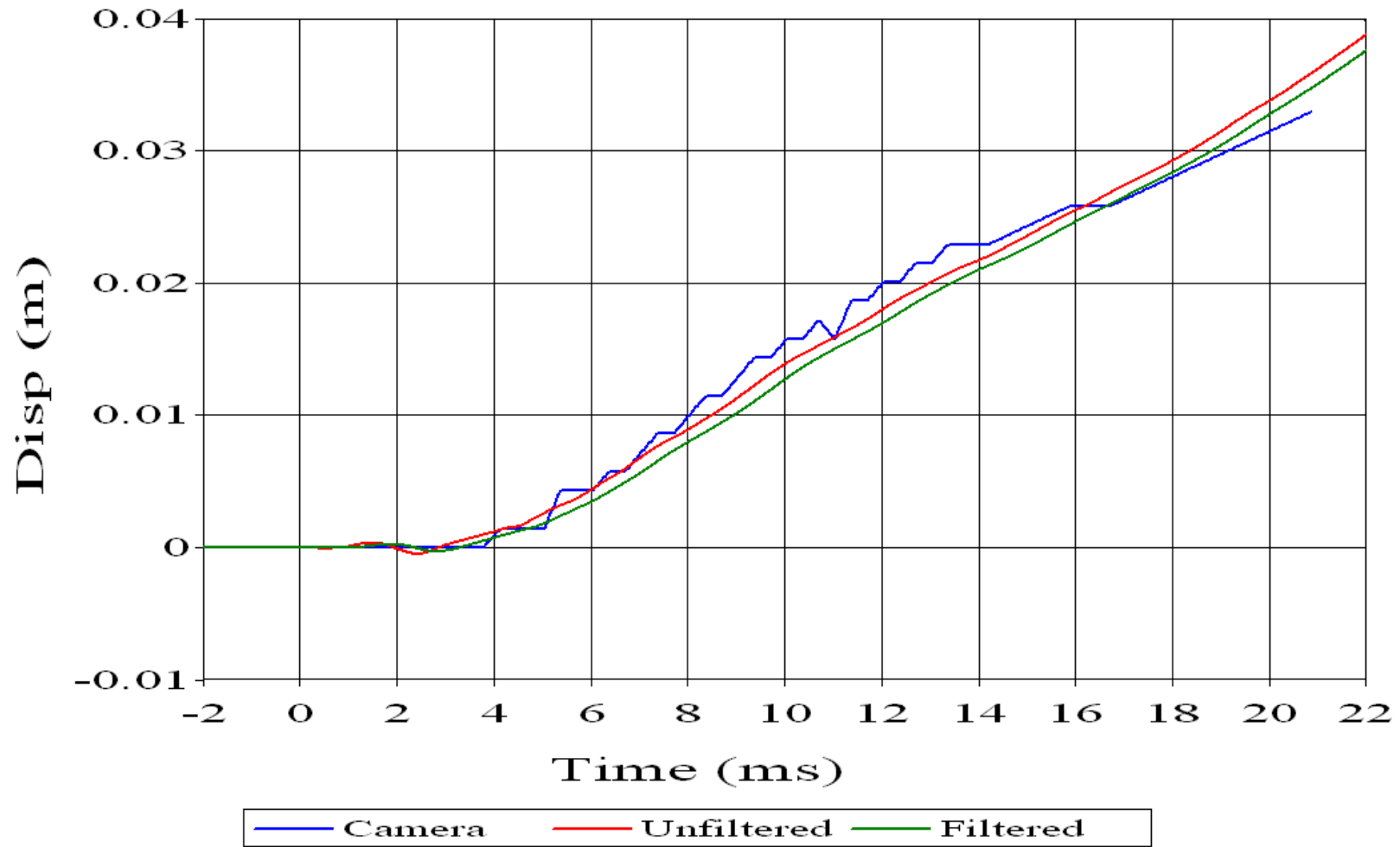
Table O.0.1: Accelerometer Verification

	Right Accelerometer	Left Accelerometer	Corner Accelerometer
Aluminum 1	Incorrect	Verified	Incorrect
Aluminum 2	Verified	Verified to 6.4mS	Incorrect
Aluminum 3	Verified	Verified to 5mS	Verified to 4.5mS
Aluminum 4	Verified	Verified	Verified
Aluminum 5	*Assumed	Incorrect	*Assumed
Aluminum 6	Verified	Verified	Verified
Steel 1	Verified	Verified	Verified
Steel 2	Verified	Verified	Verified
Steel 3	Verified	Verified	Verified to 9.5mS
Steel 4	Verified	Verified	Verified
Steel 5	Verified	Verified	Verified to 8.7mS
Steel 6	Verified	Verified	Verified to 11.4mS
Pocket Plate	Verified	Verified	Verified
Pocket Plate	Incorrect	Verified to 9.4mS	Verified
Pocket Plate	Verified	Verified to 6.2mS	Verified to 3.1mS

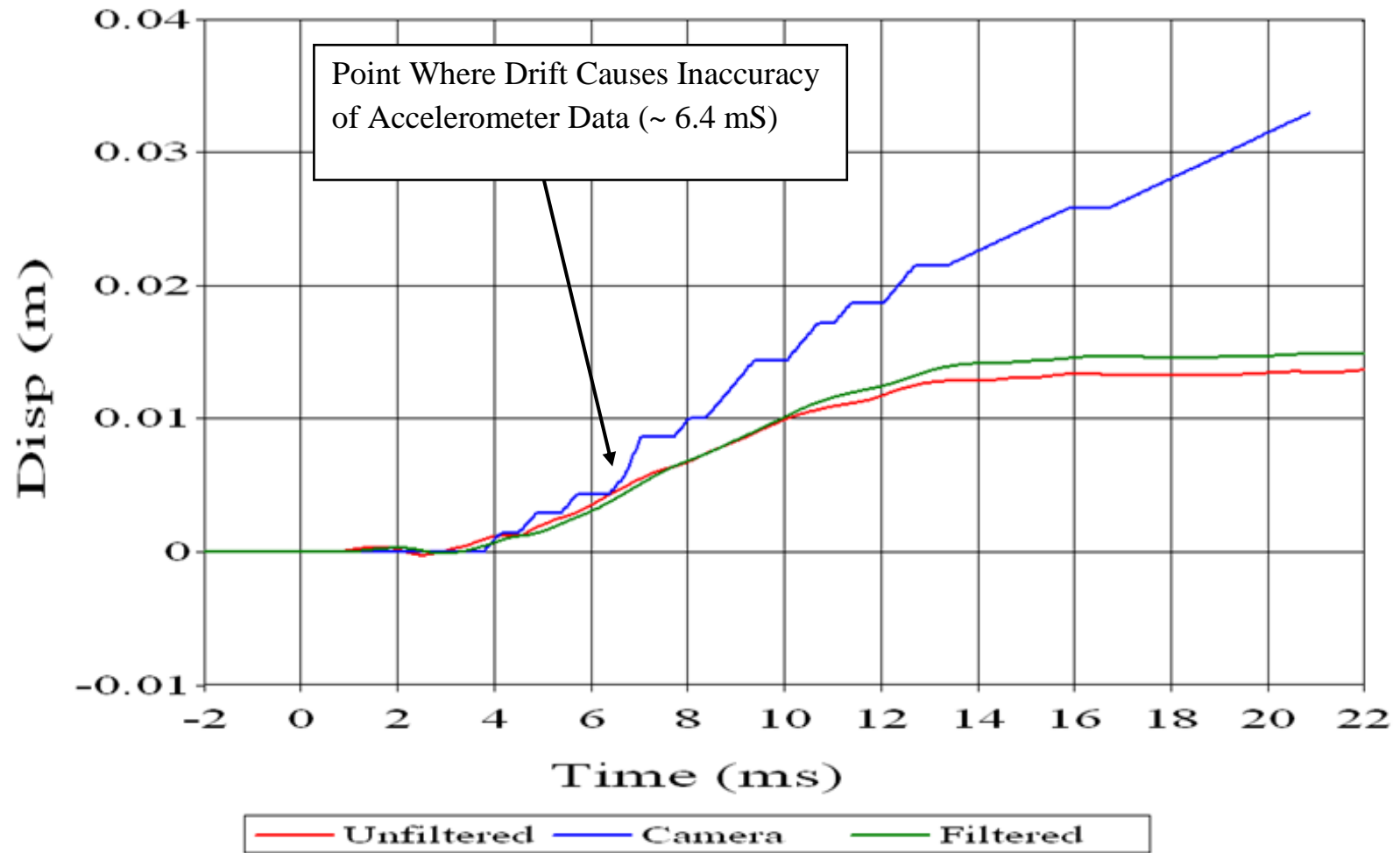
Aluminum 1 (Left Frame)



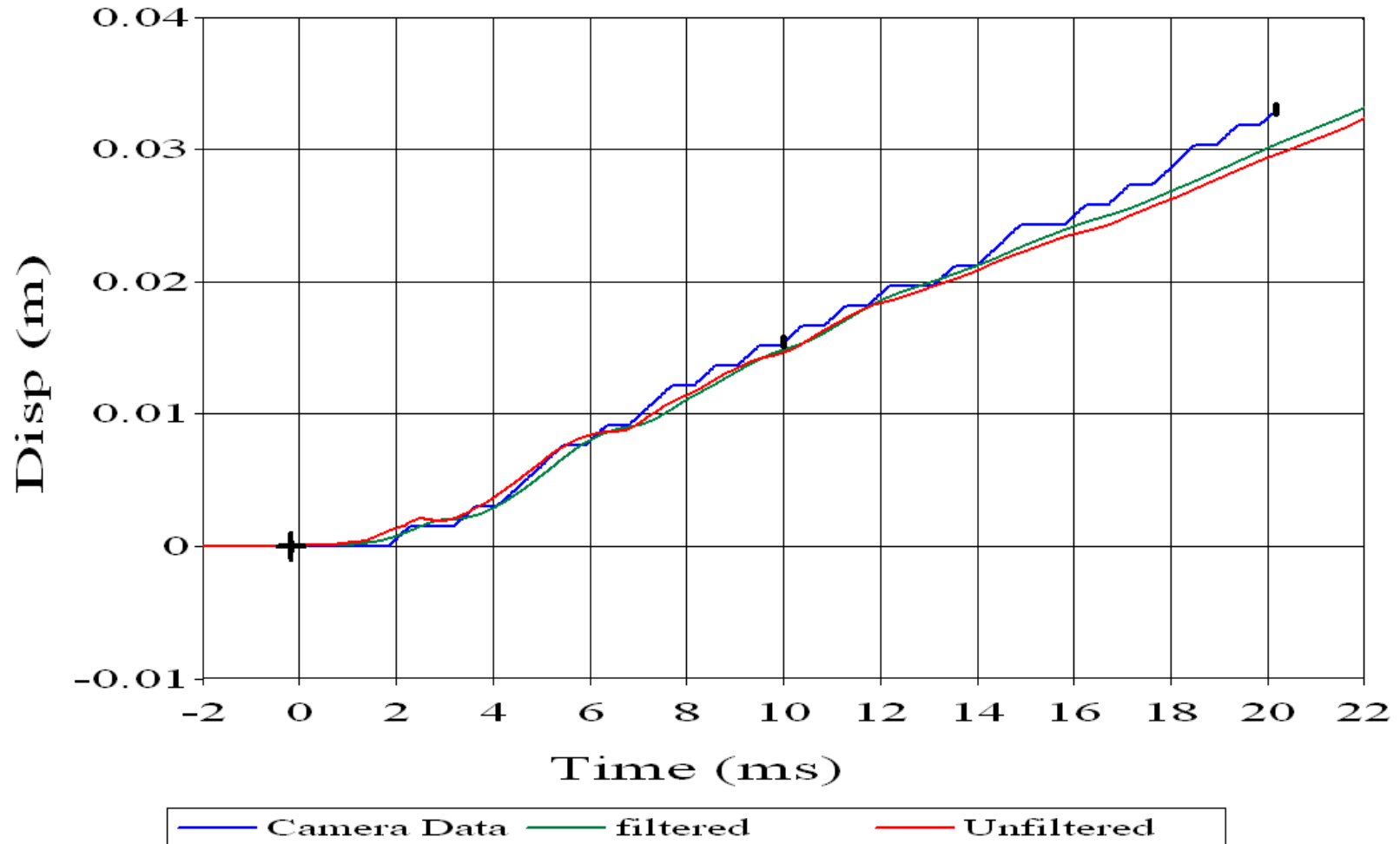
Aluminum 2 (Right Frame)



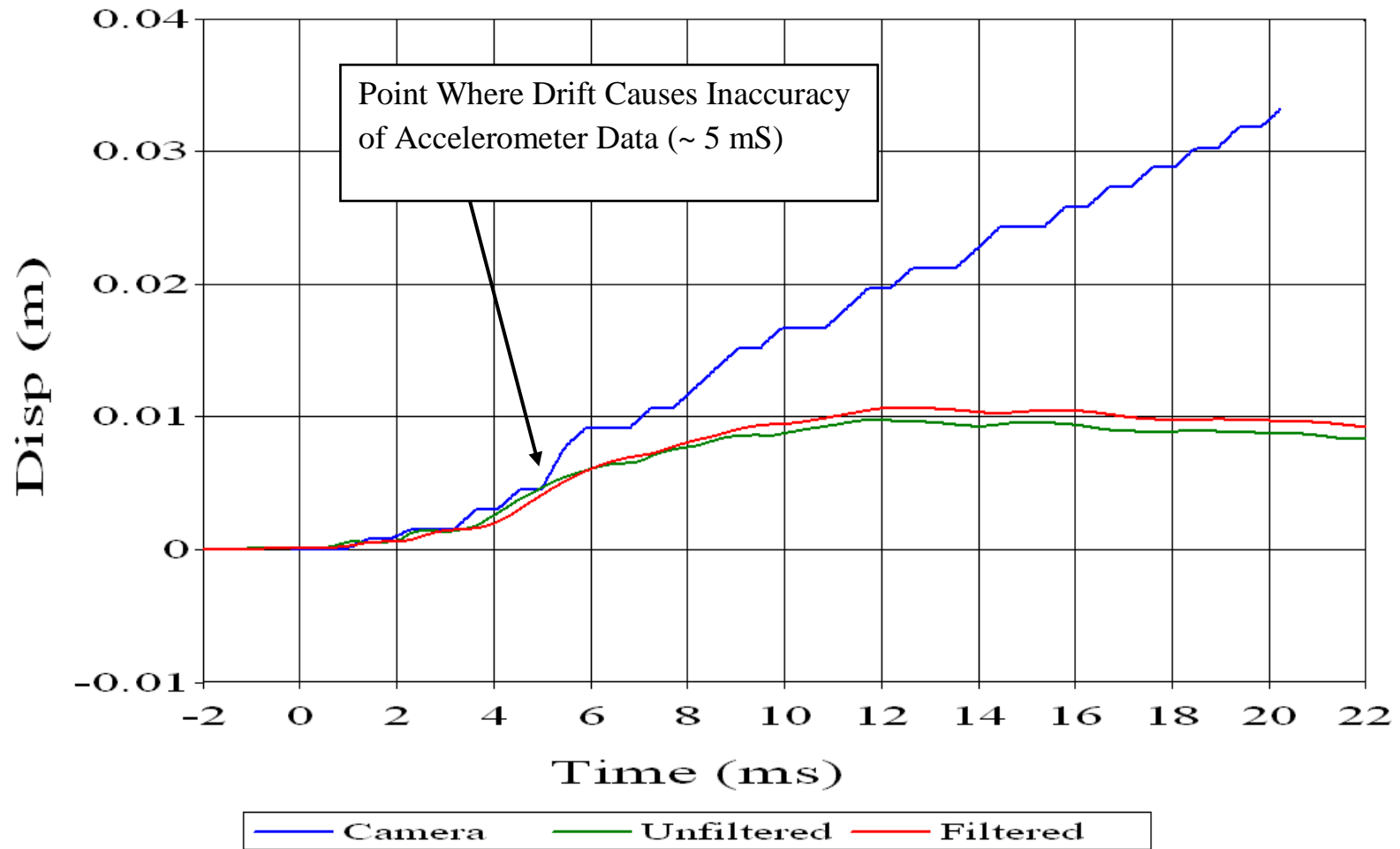
Aluminum 2 (Left Frame)



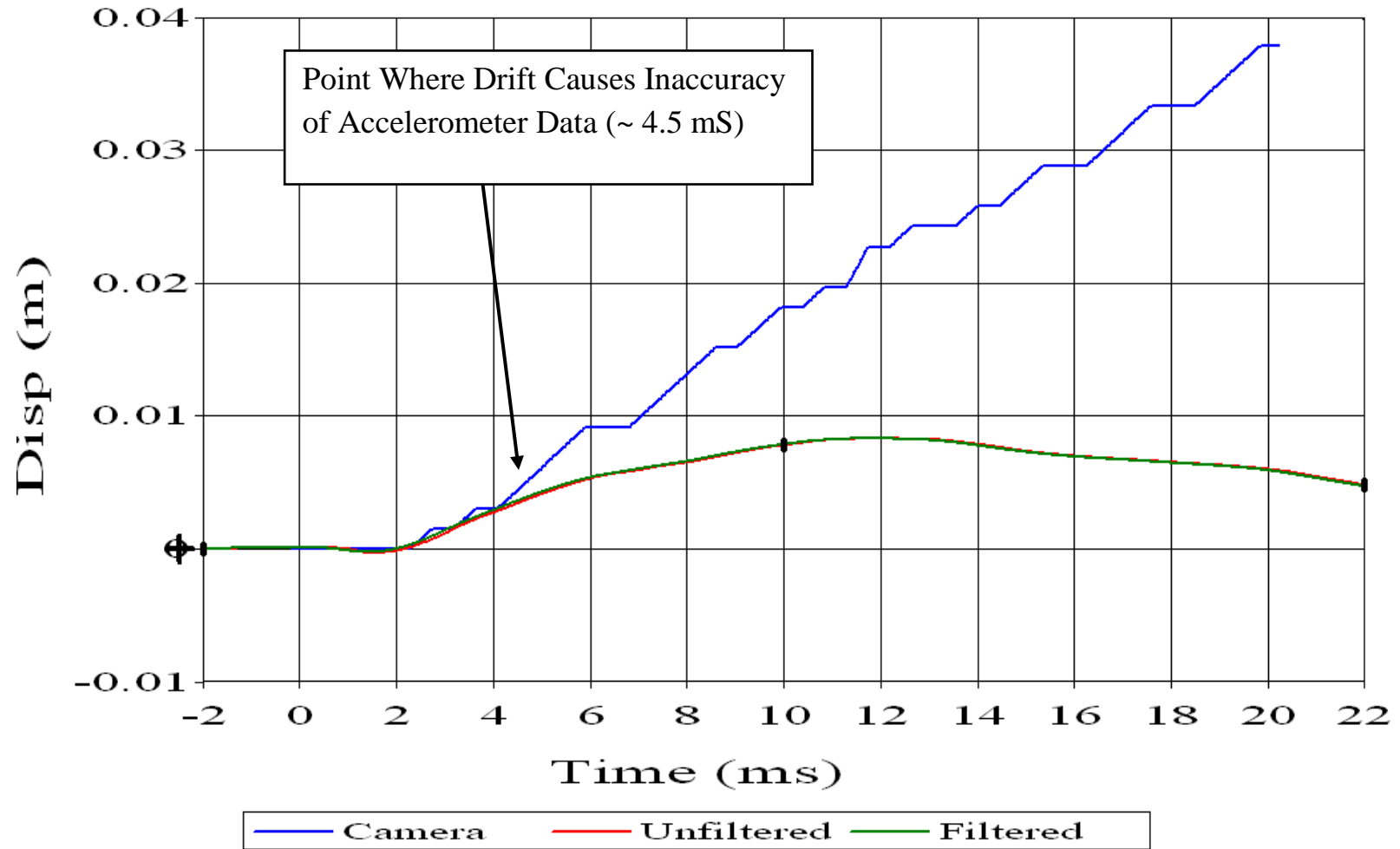
Aluminum 3 (Right Frame)



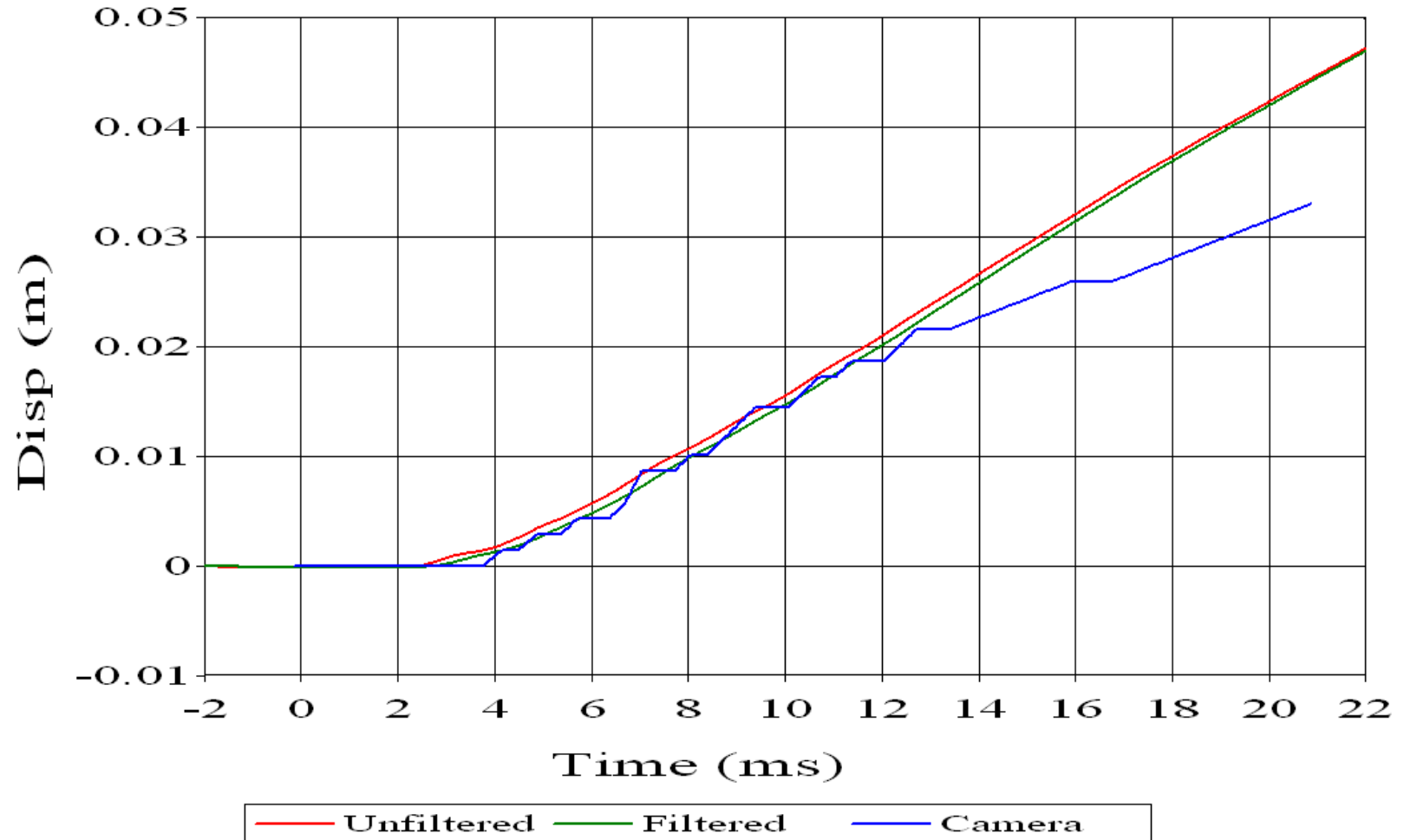
Aluminum 3 (Left Frame)



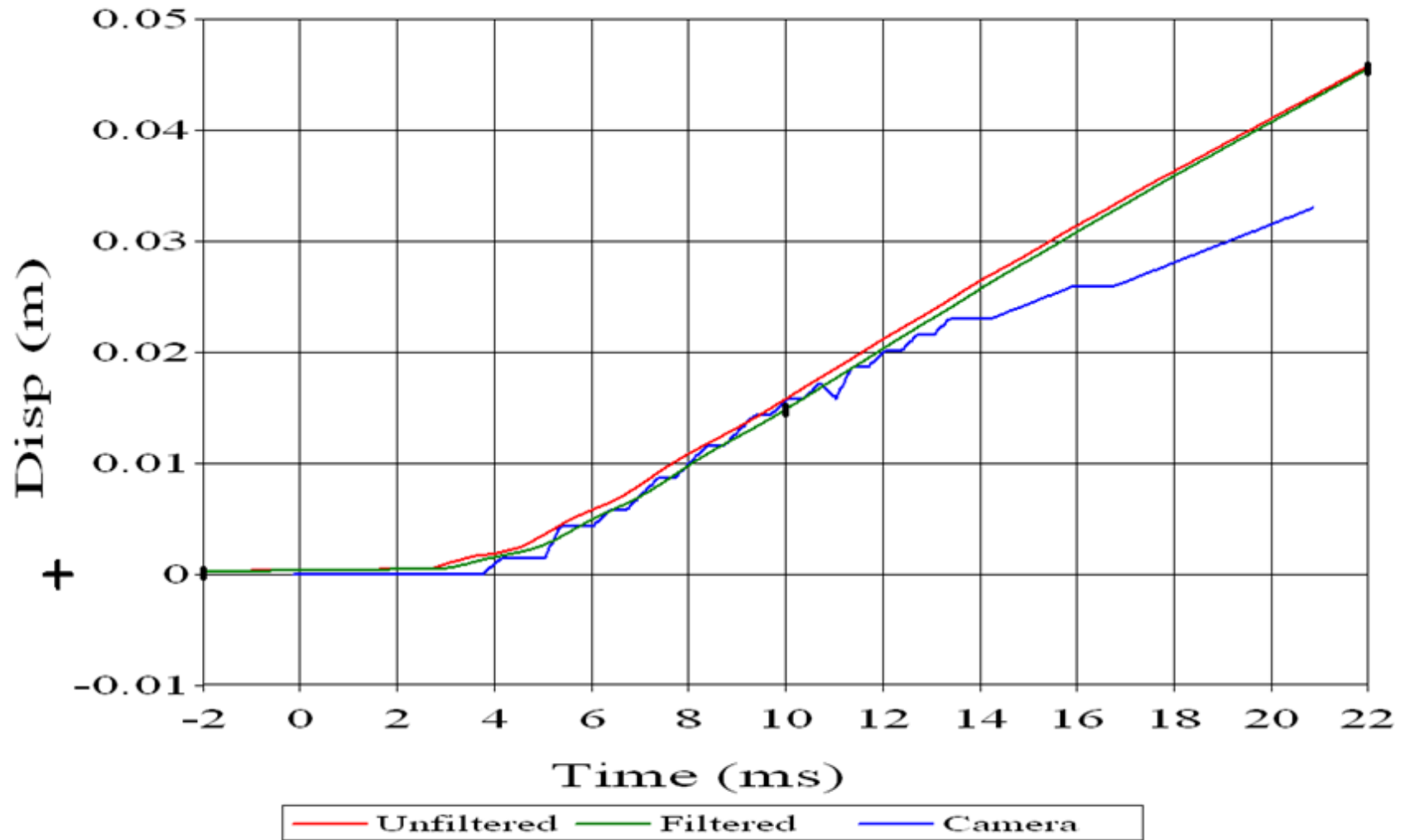
Aluminum 3 (Corner Frame)



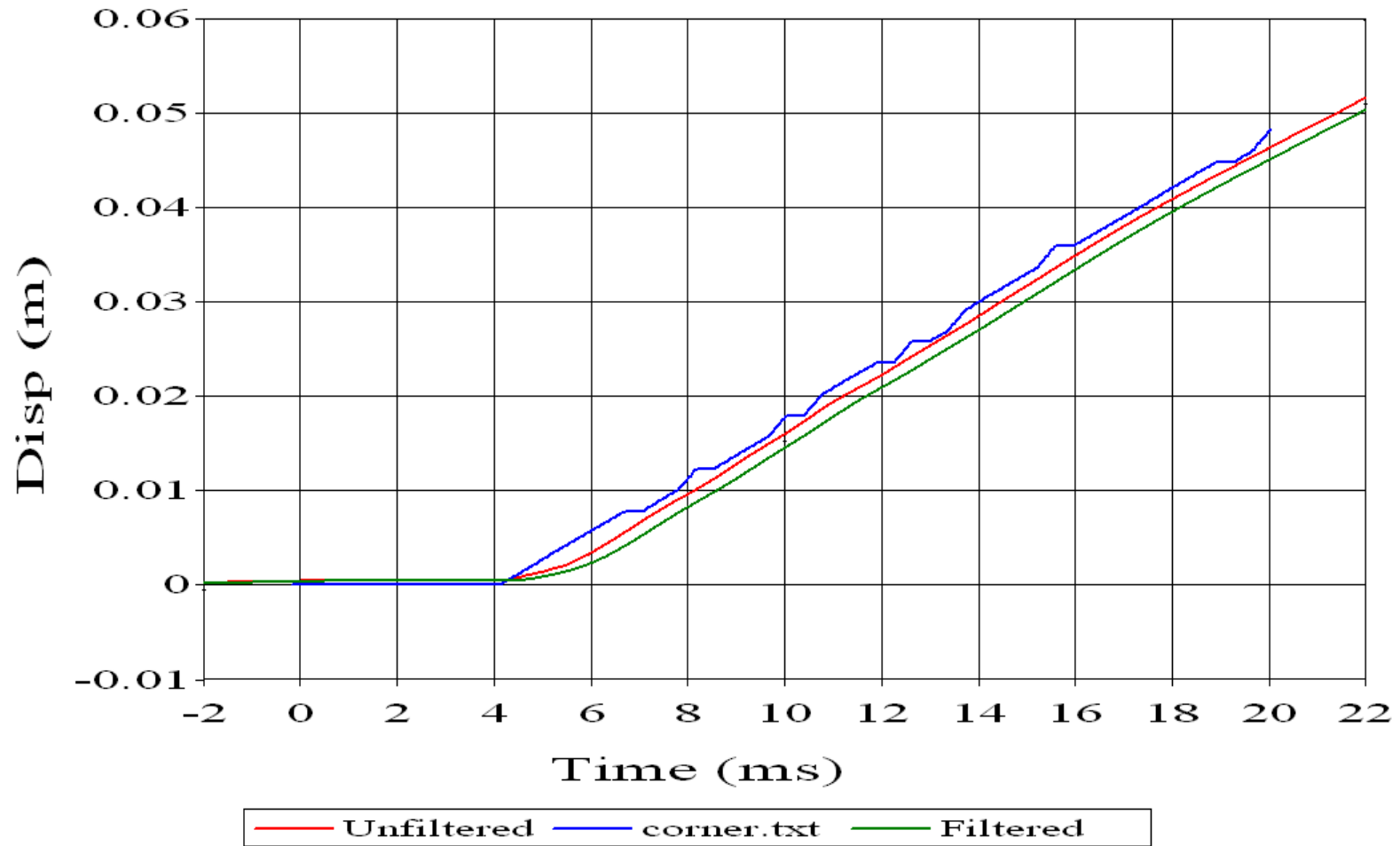
Aluminum 4 (Left Frame)



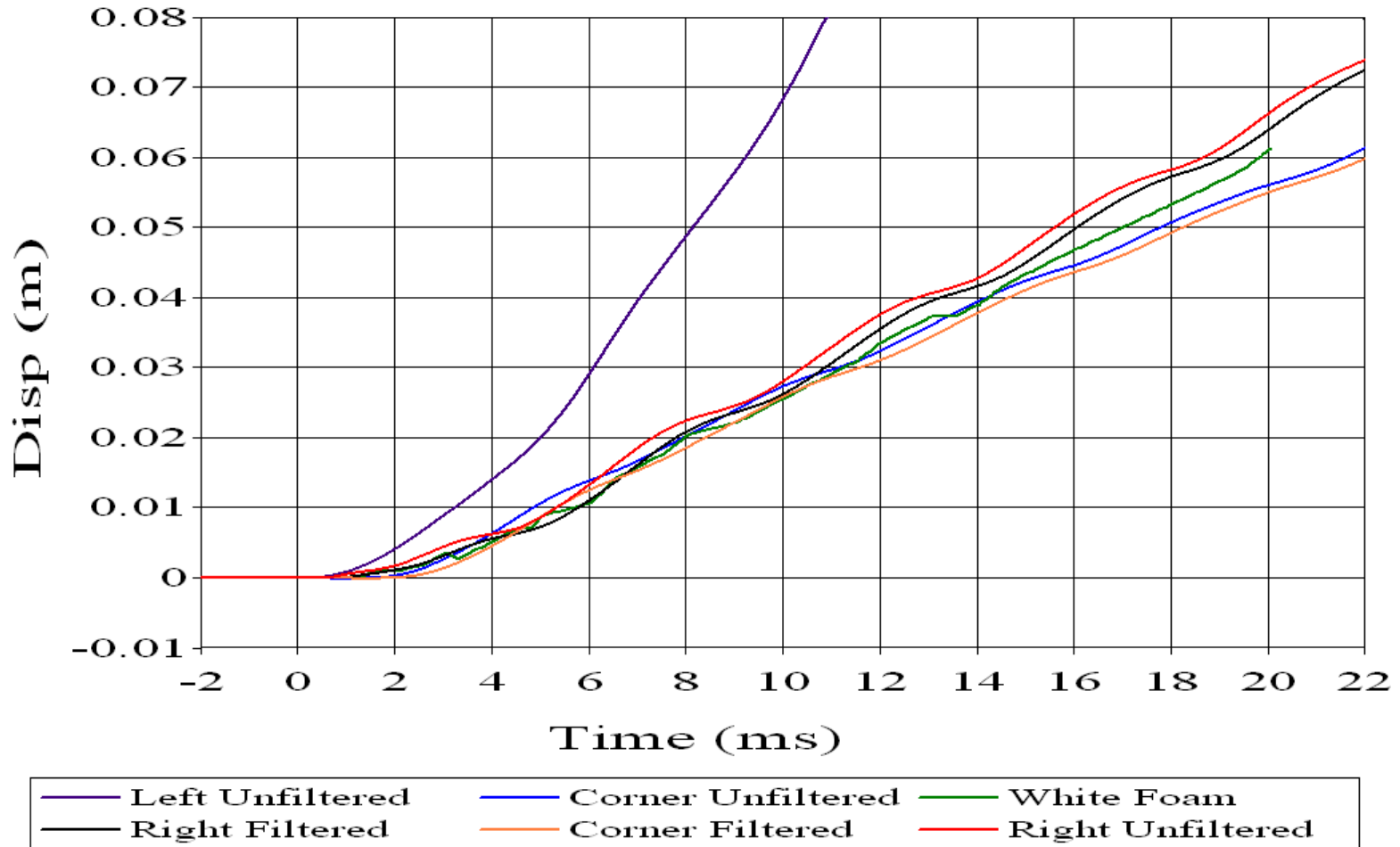
Aluminum 4 (Right Frame)



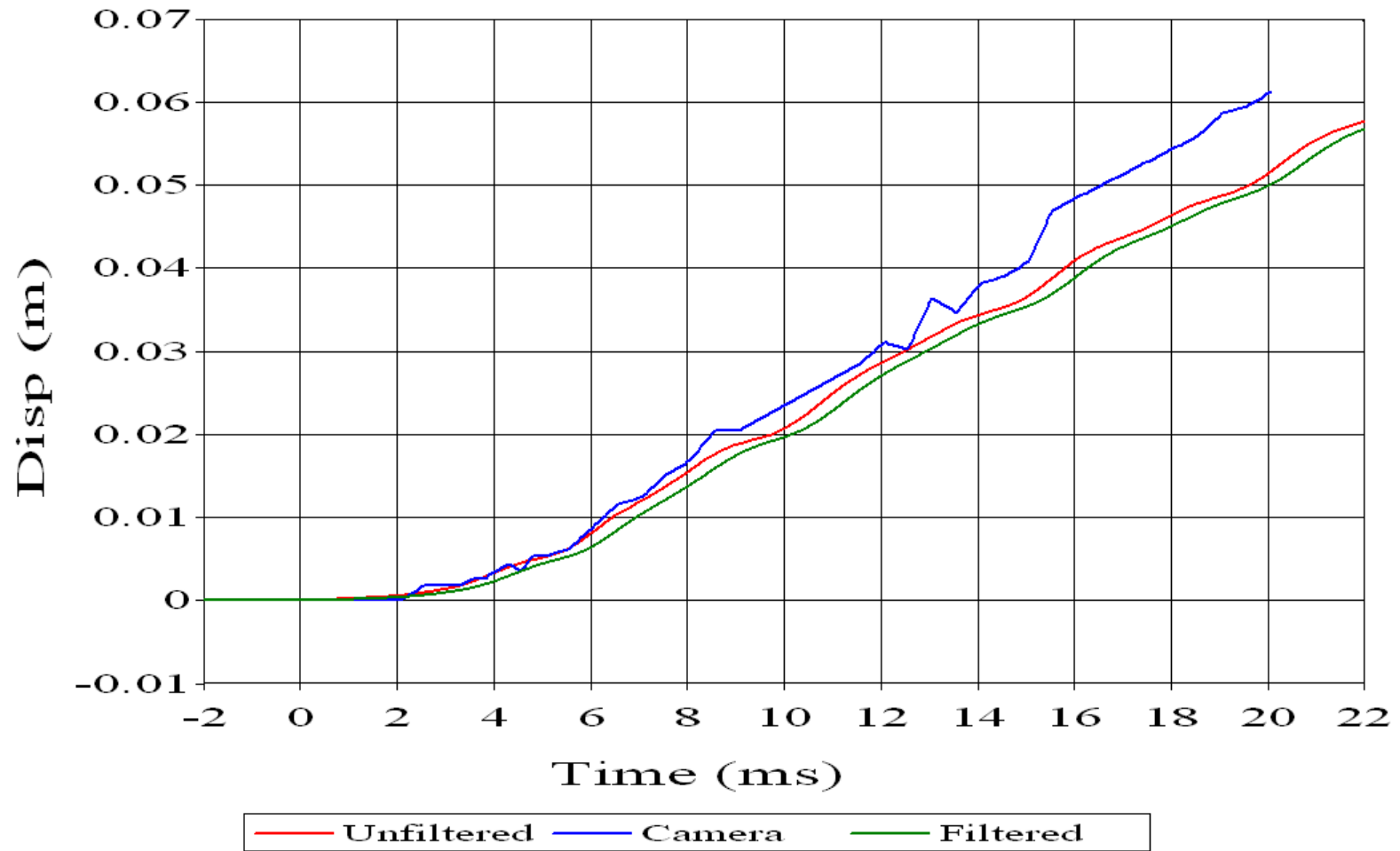
Aluminum 4 (Corner Frame)



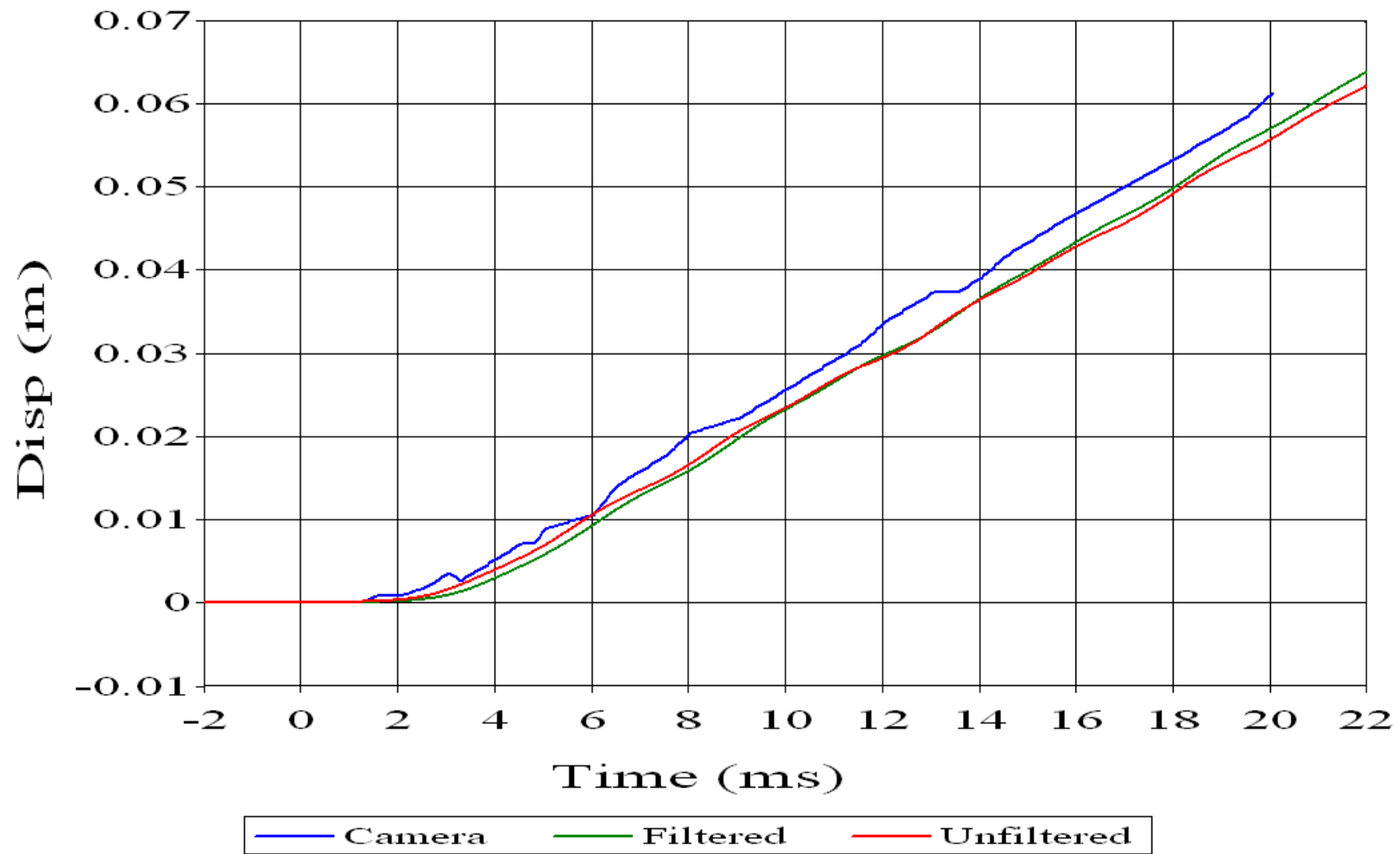
Aluminum 5 Displacement



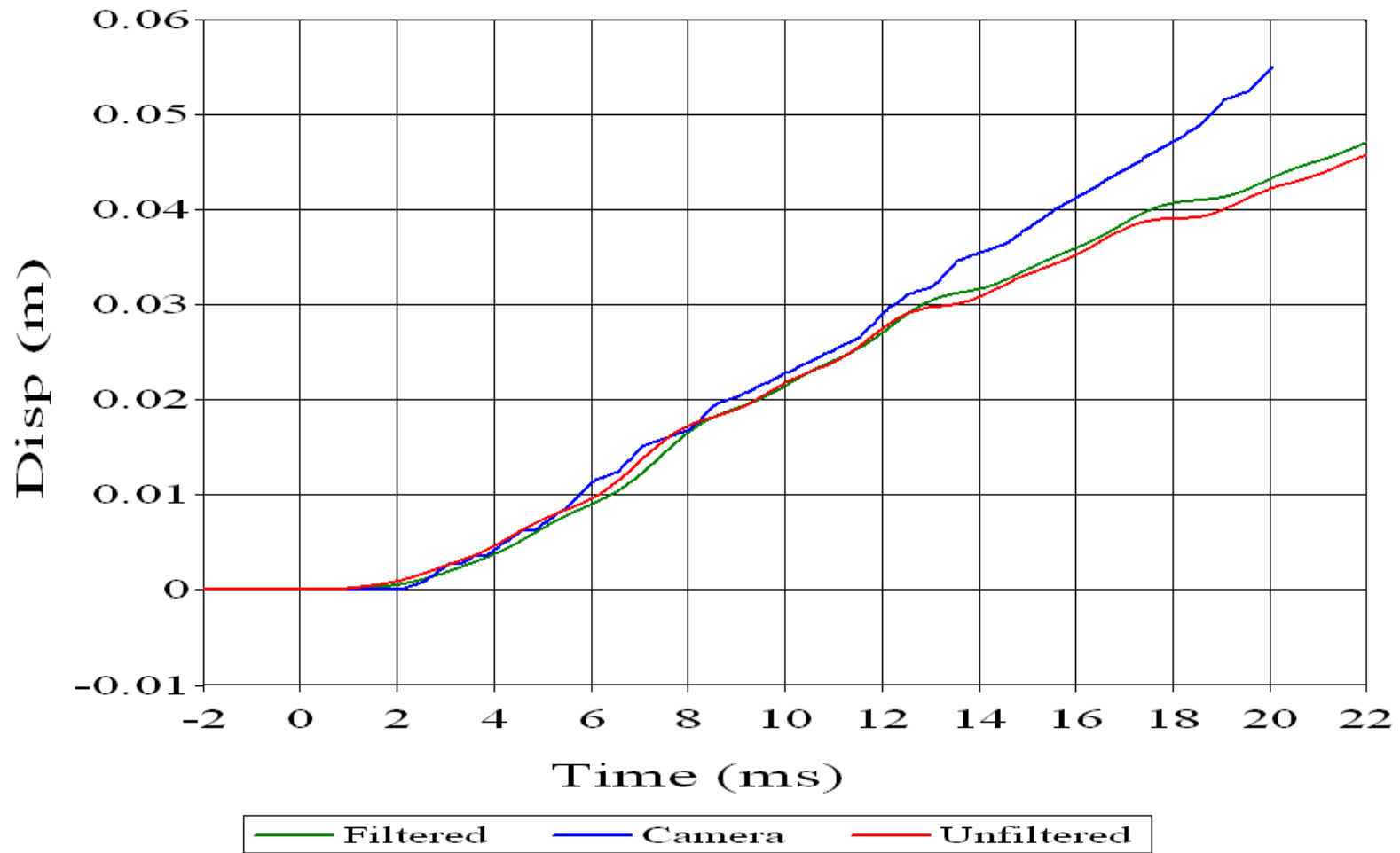
Aluminum 6 (Right Frame)



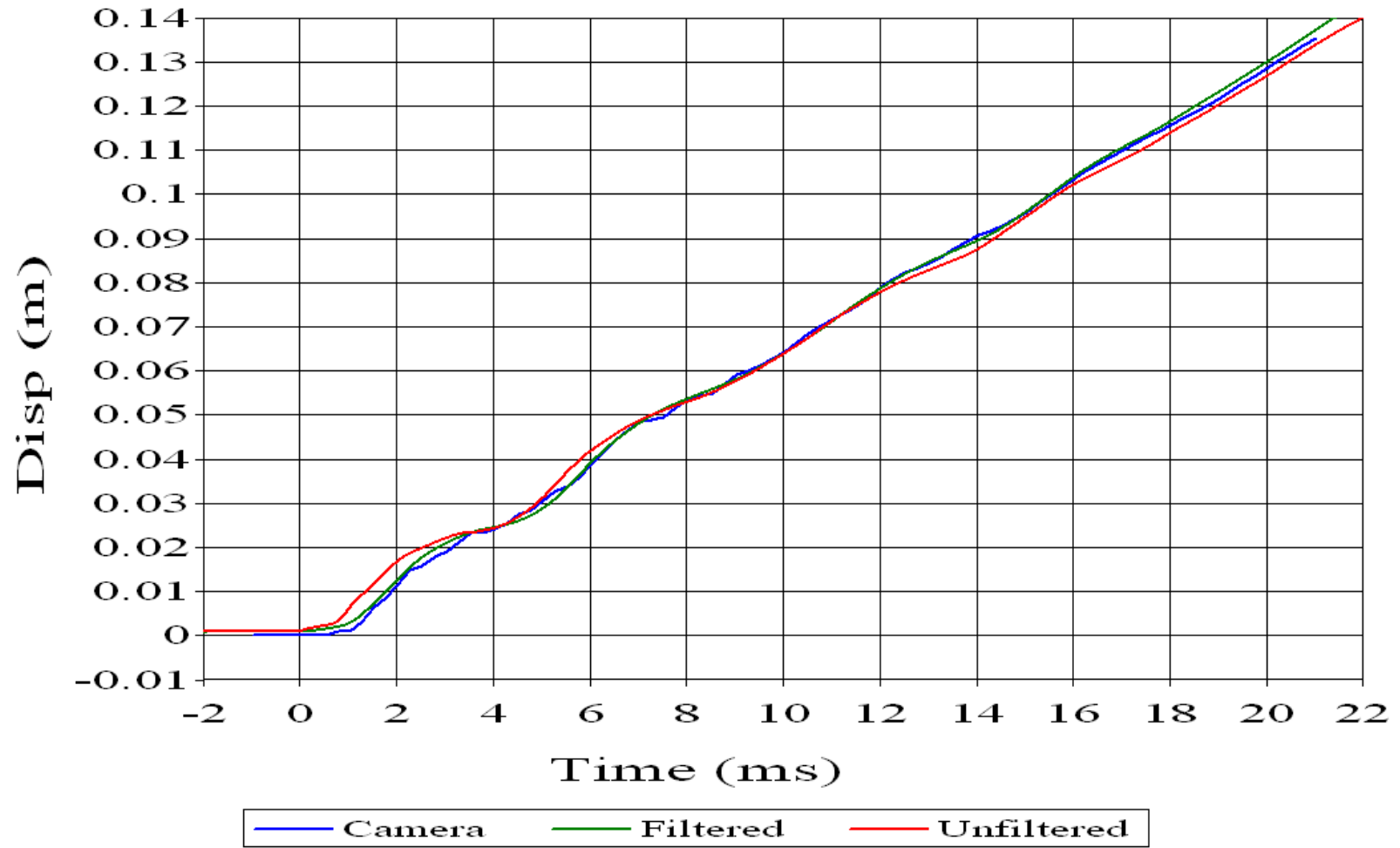
Aluminum 6 (Left Frame)



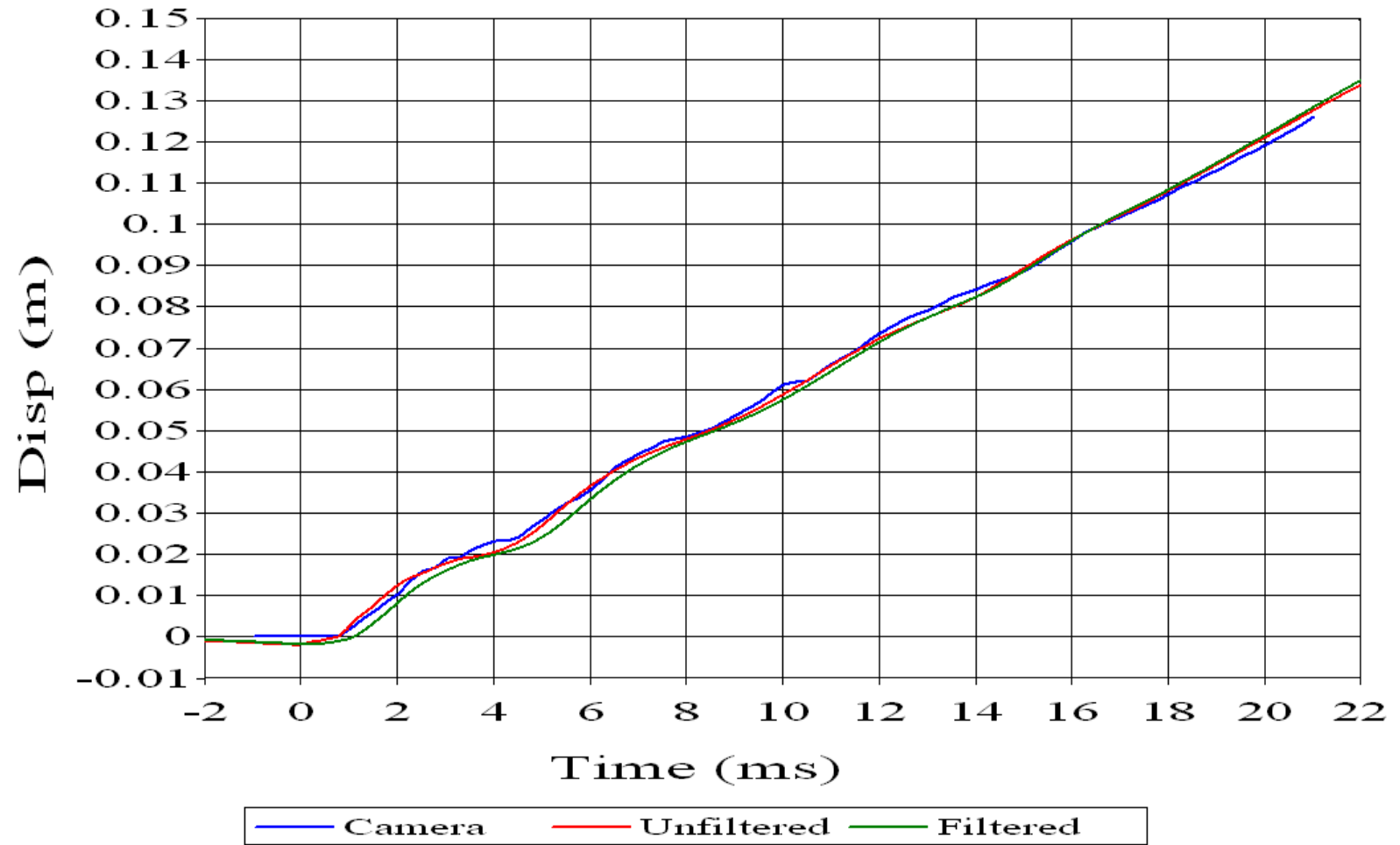
Aluminum 6 (Corner Frame)



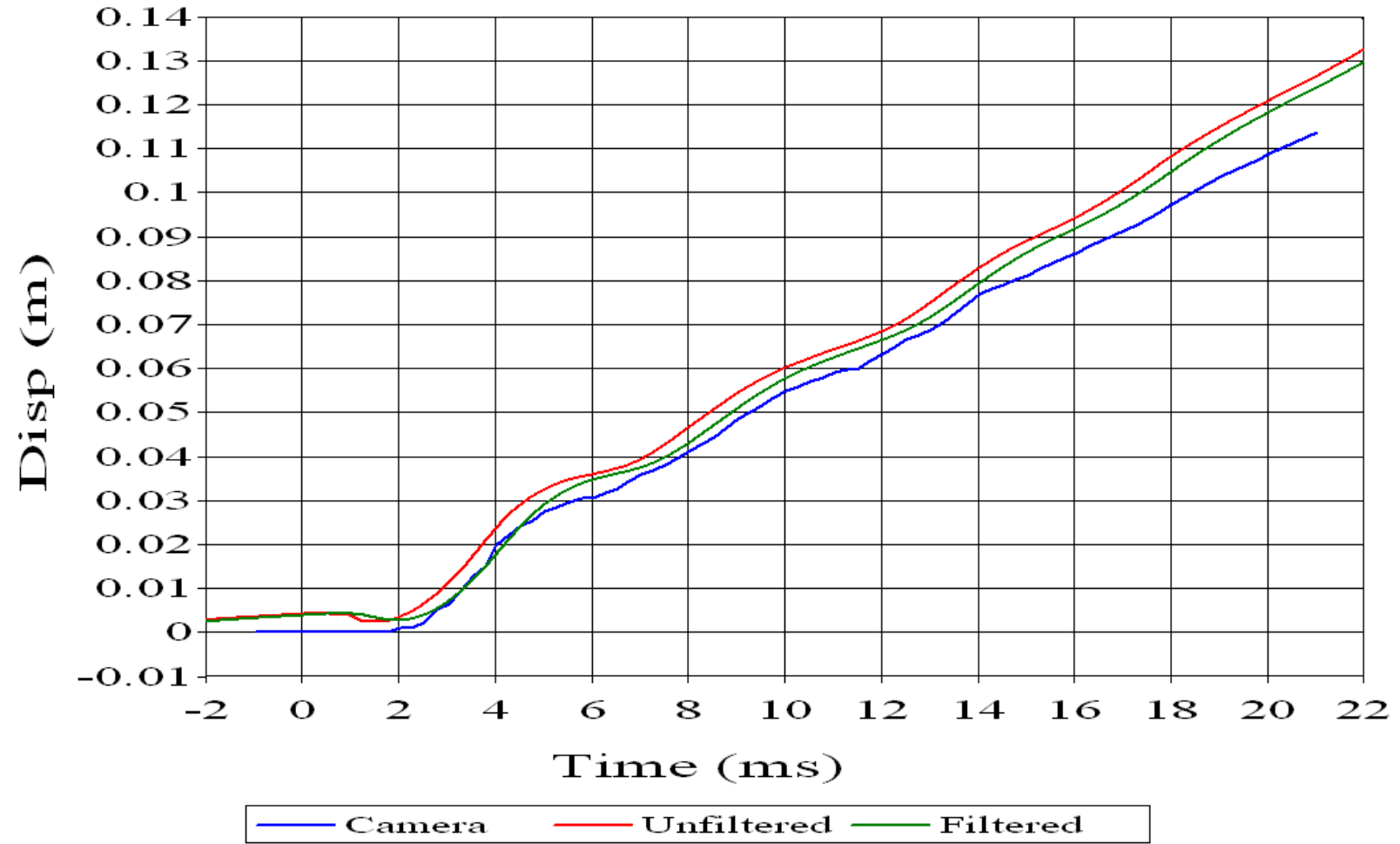
Steel 1 (Left Frame)



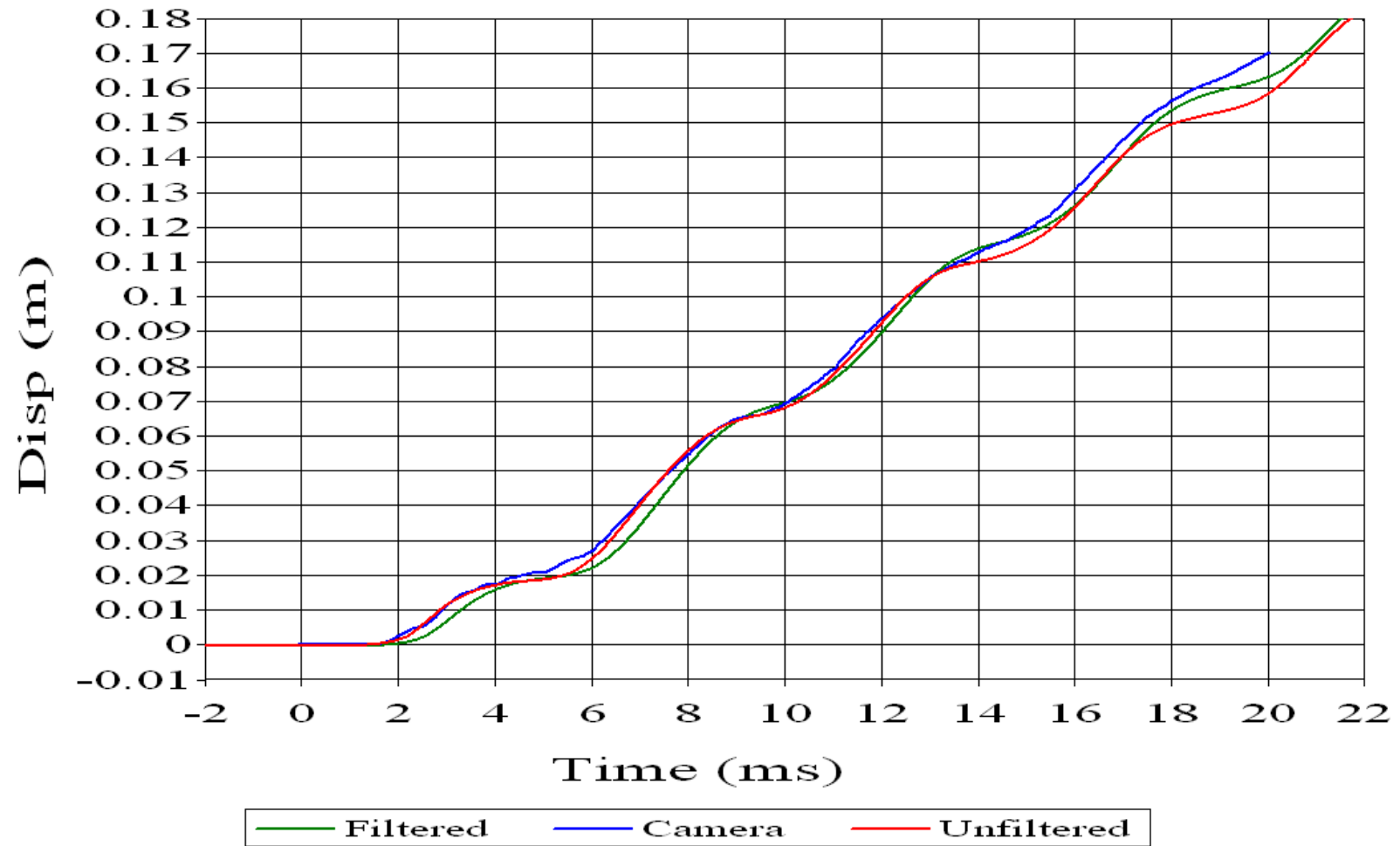
Steel 1 (Right Frame)



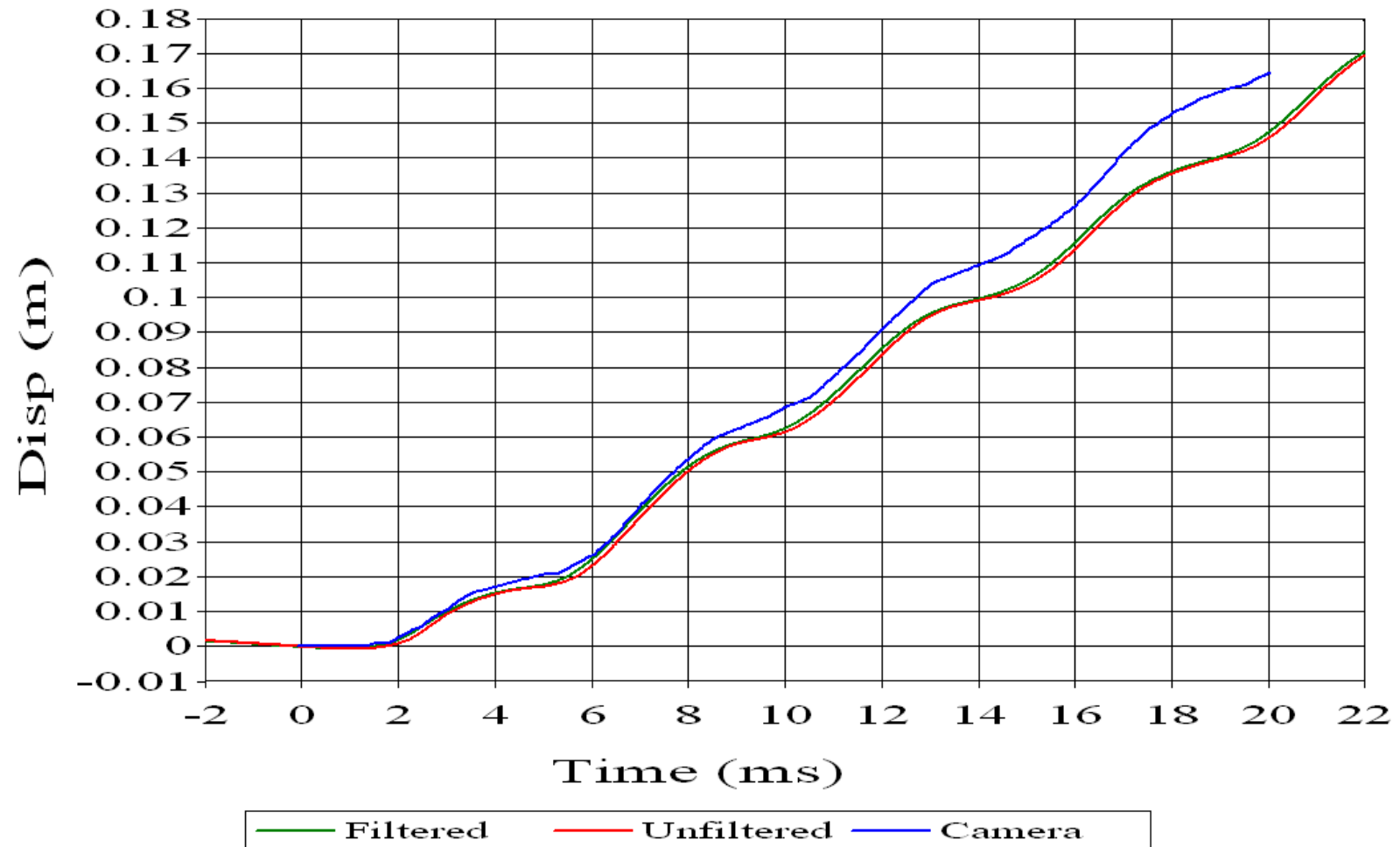
Steel 1 (Corner Frame)



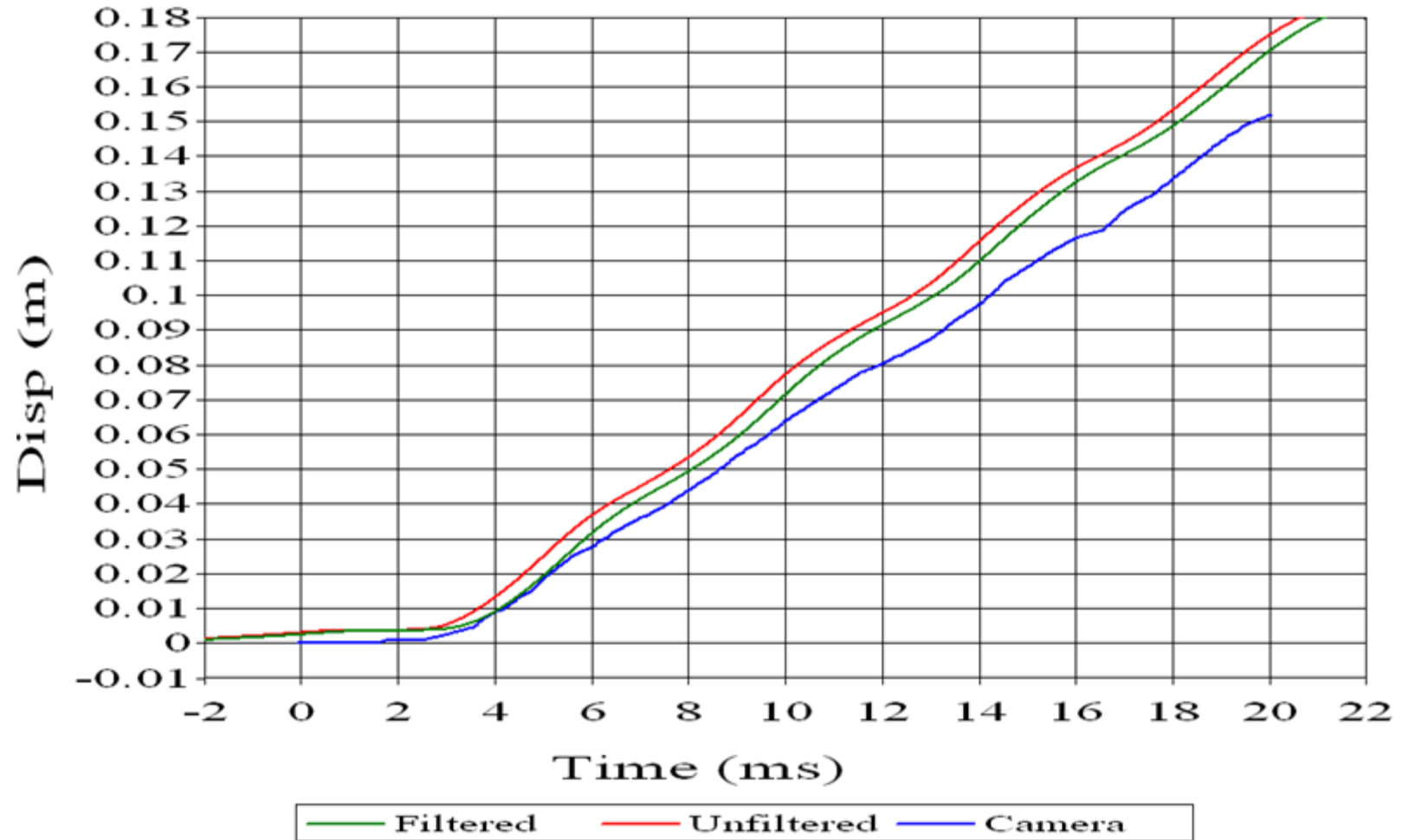
Steel 2 (Right Frame)



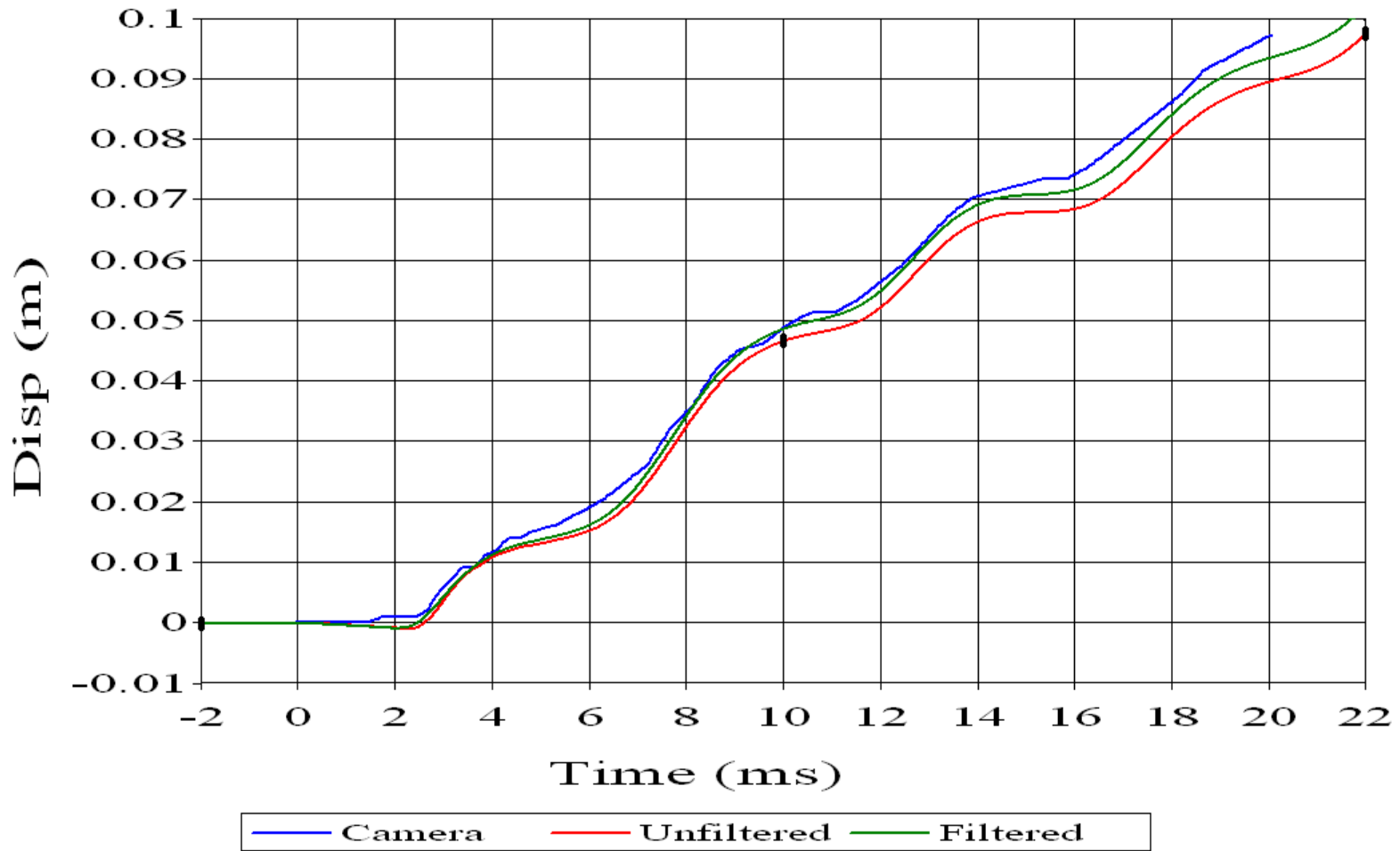
Steel 2 (Left Frame)



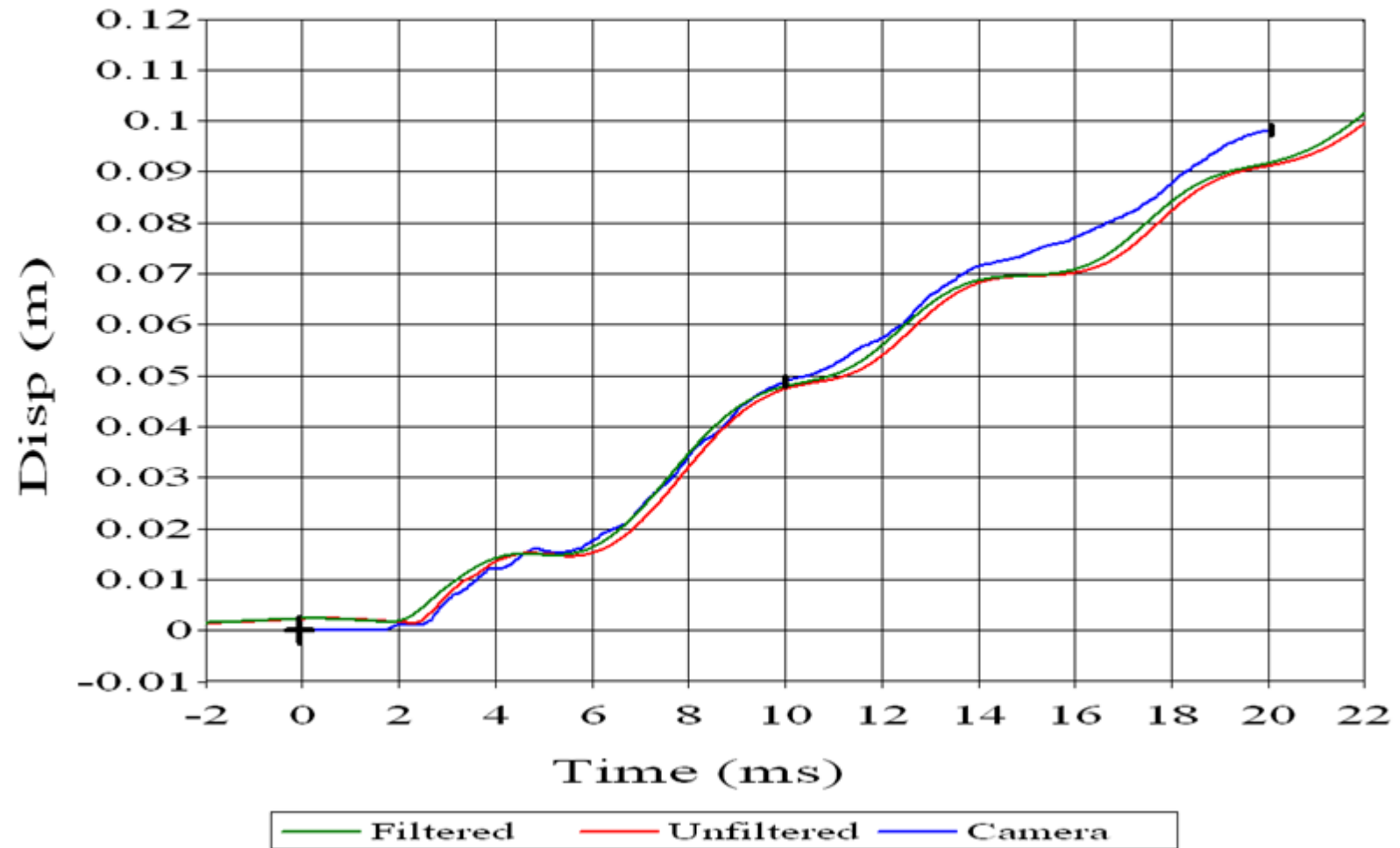
Steel 2 (Corner Frame)



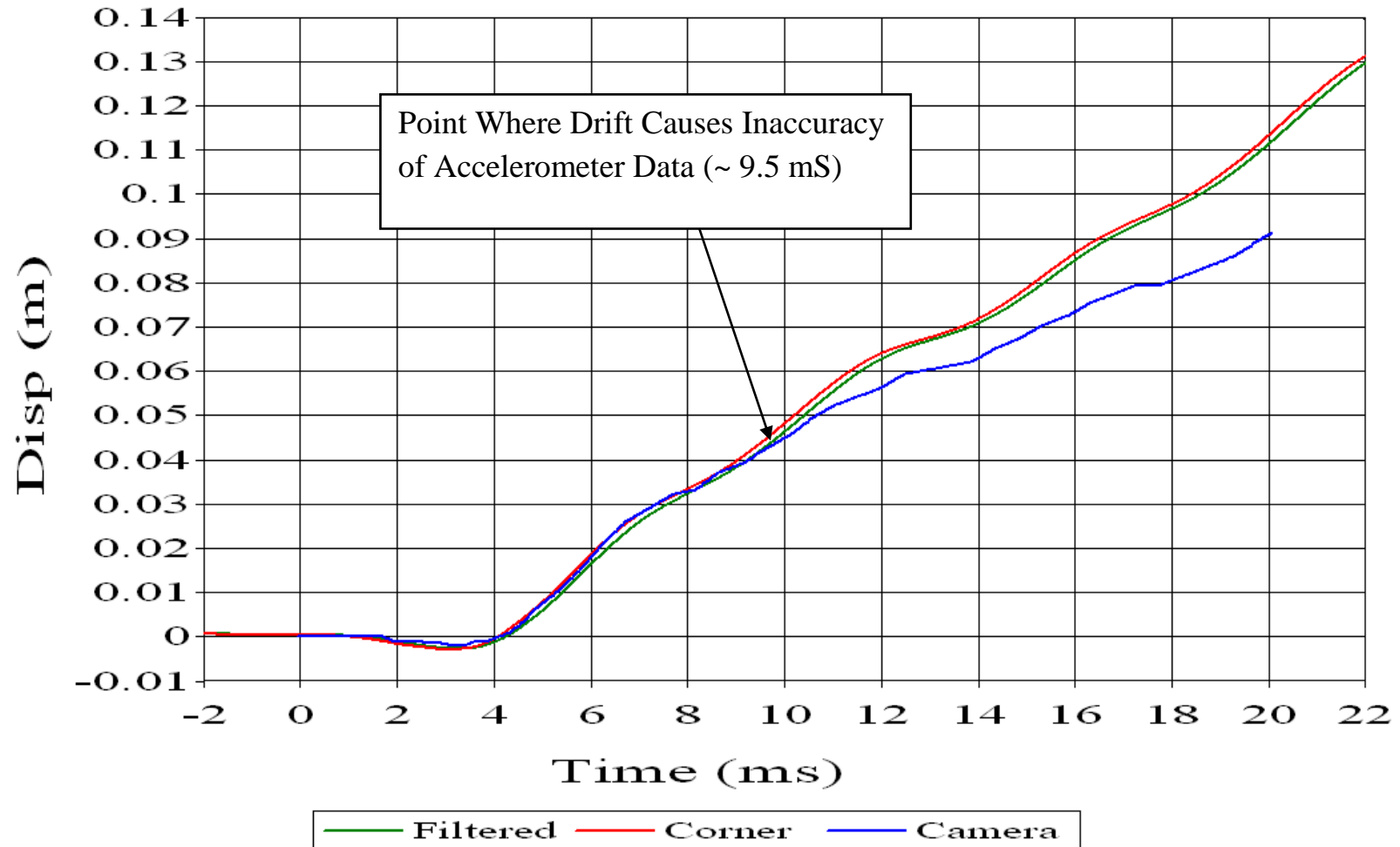
Steel 3 (Left Frame)



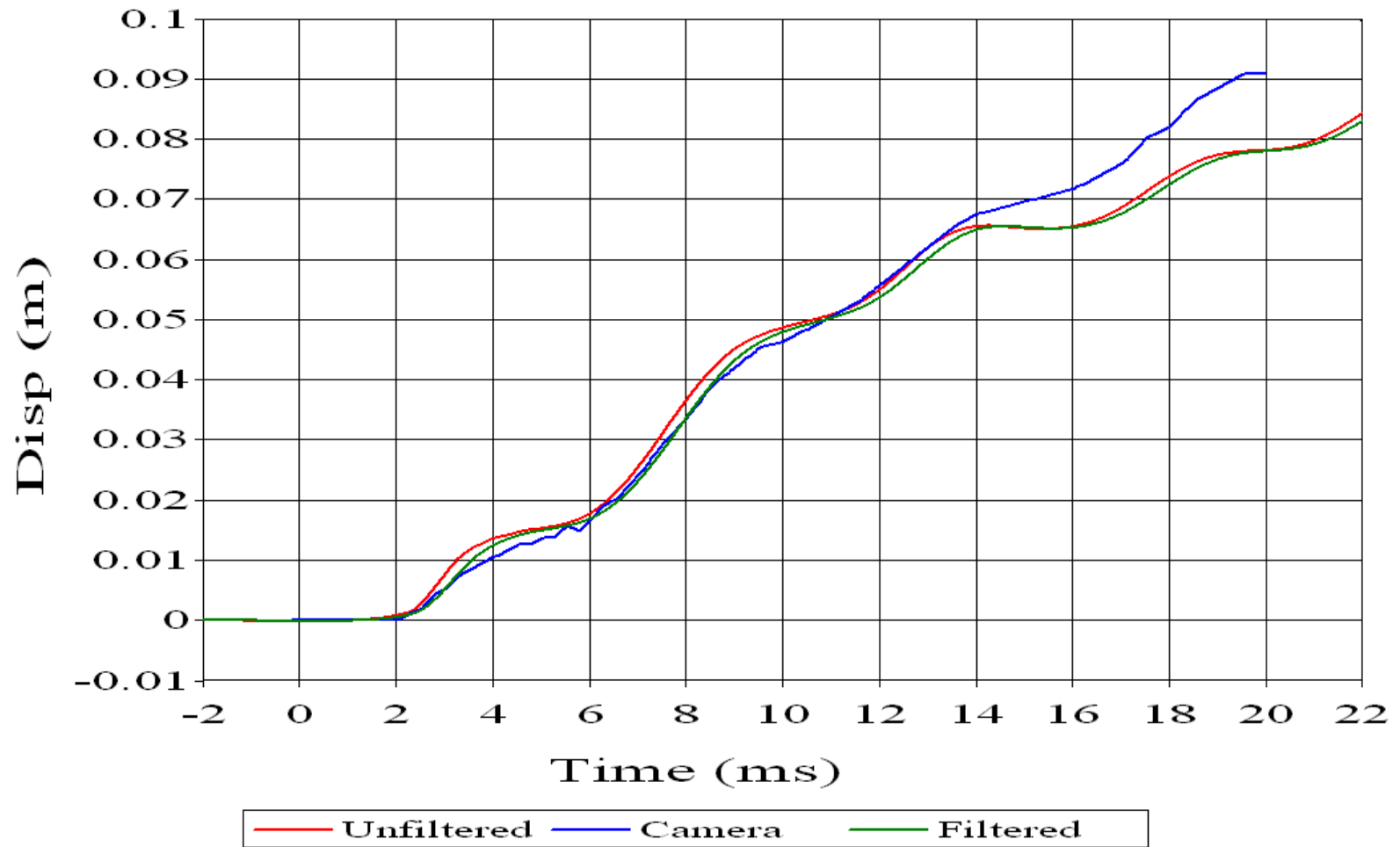
Steel 3 (Right Frame)



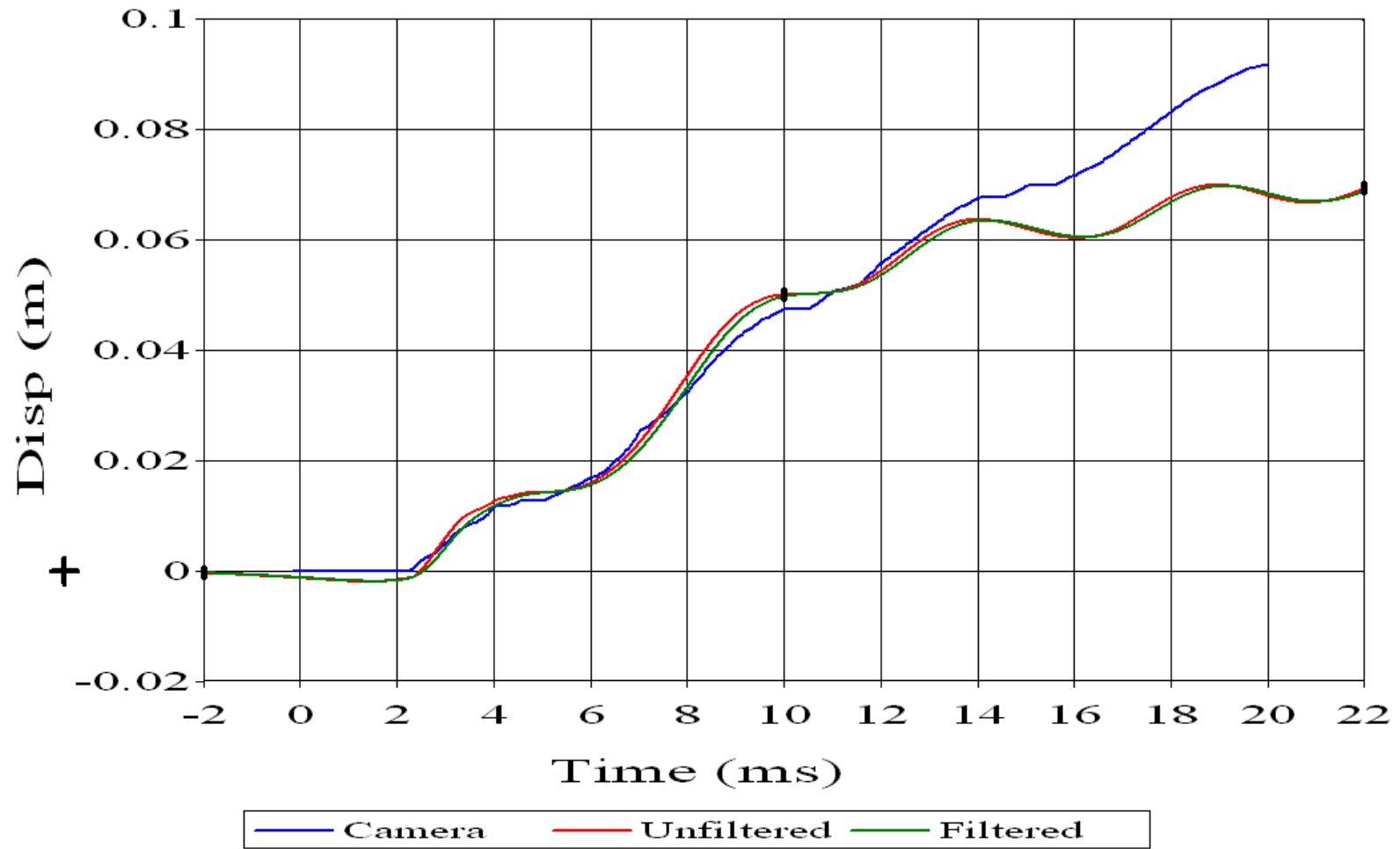
Steel 3 (Corner Frame)



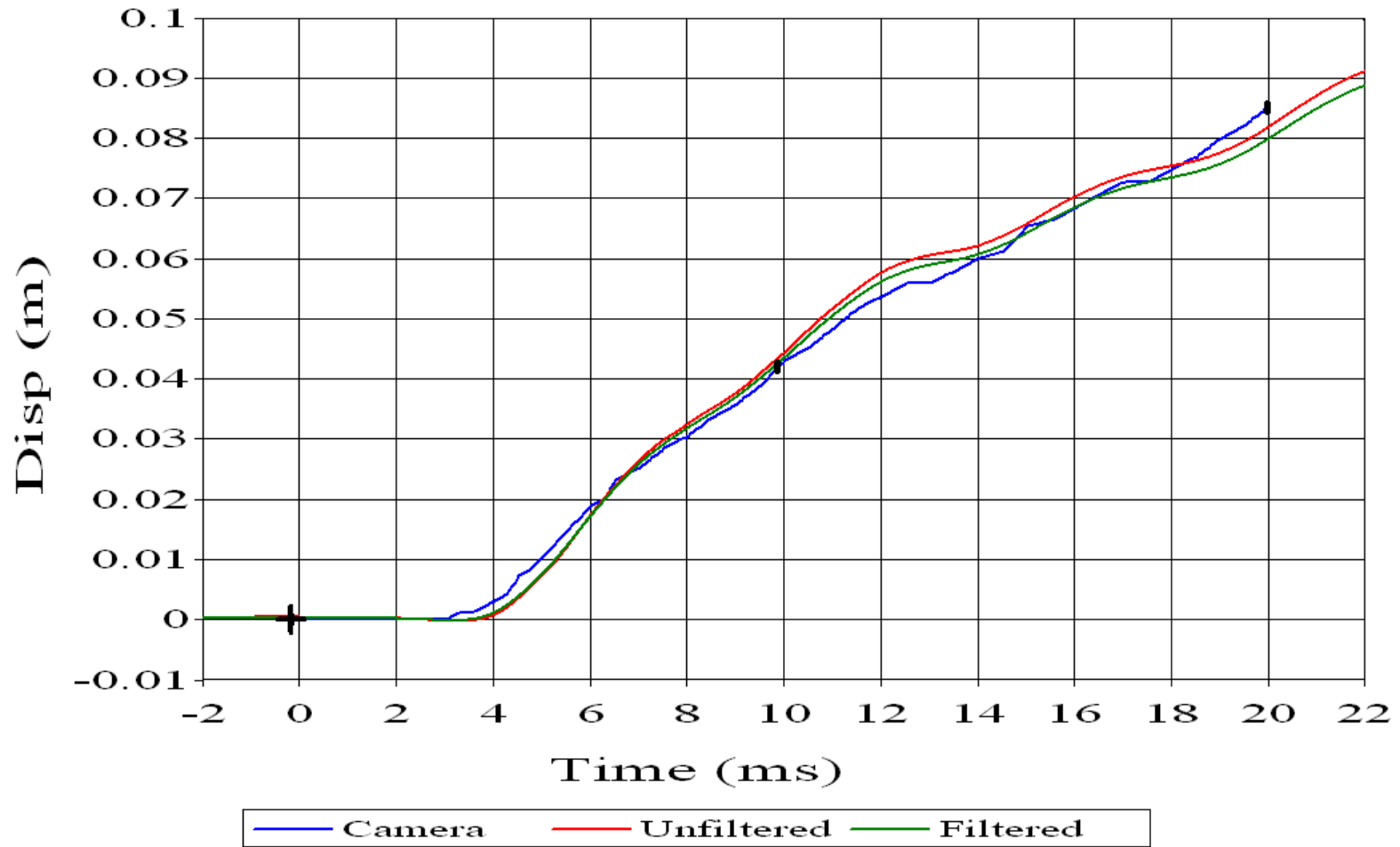
Steel 4 (Left Frame)



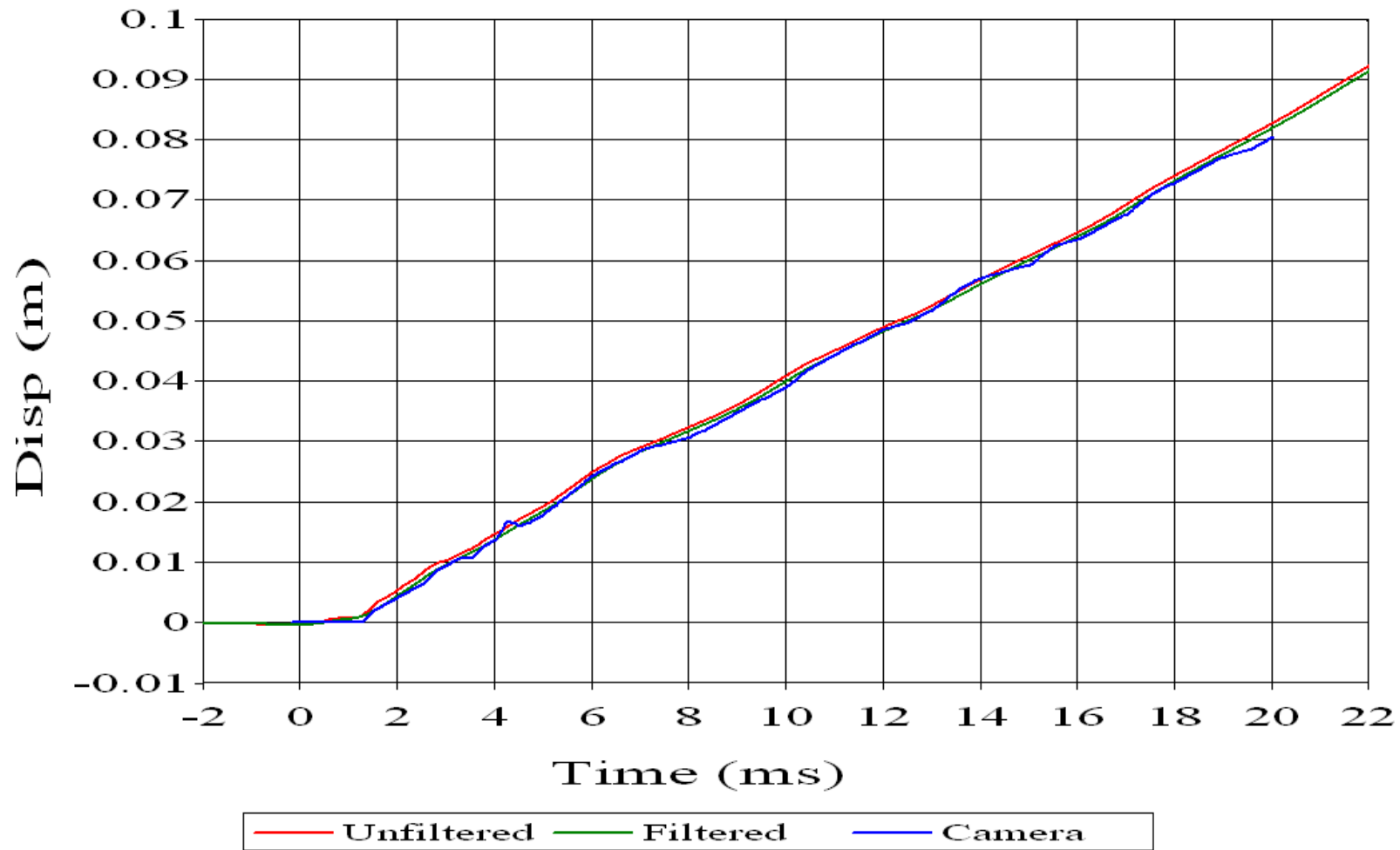
Steel 4 (Right Frame)



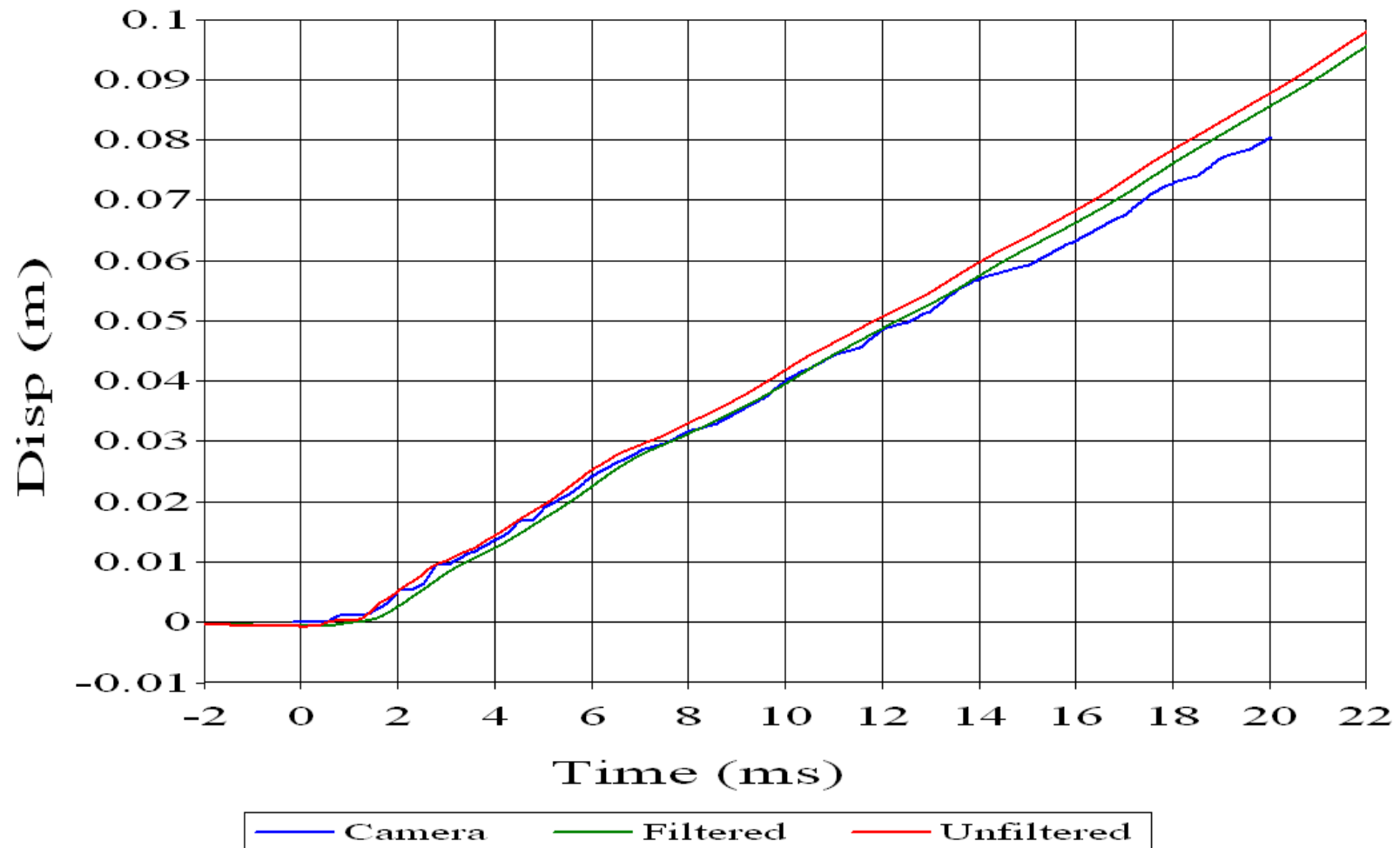
Steel 4 (Corner Frame)



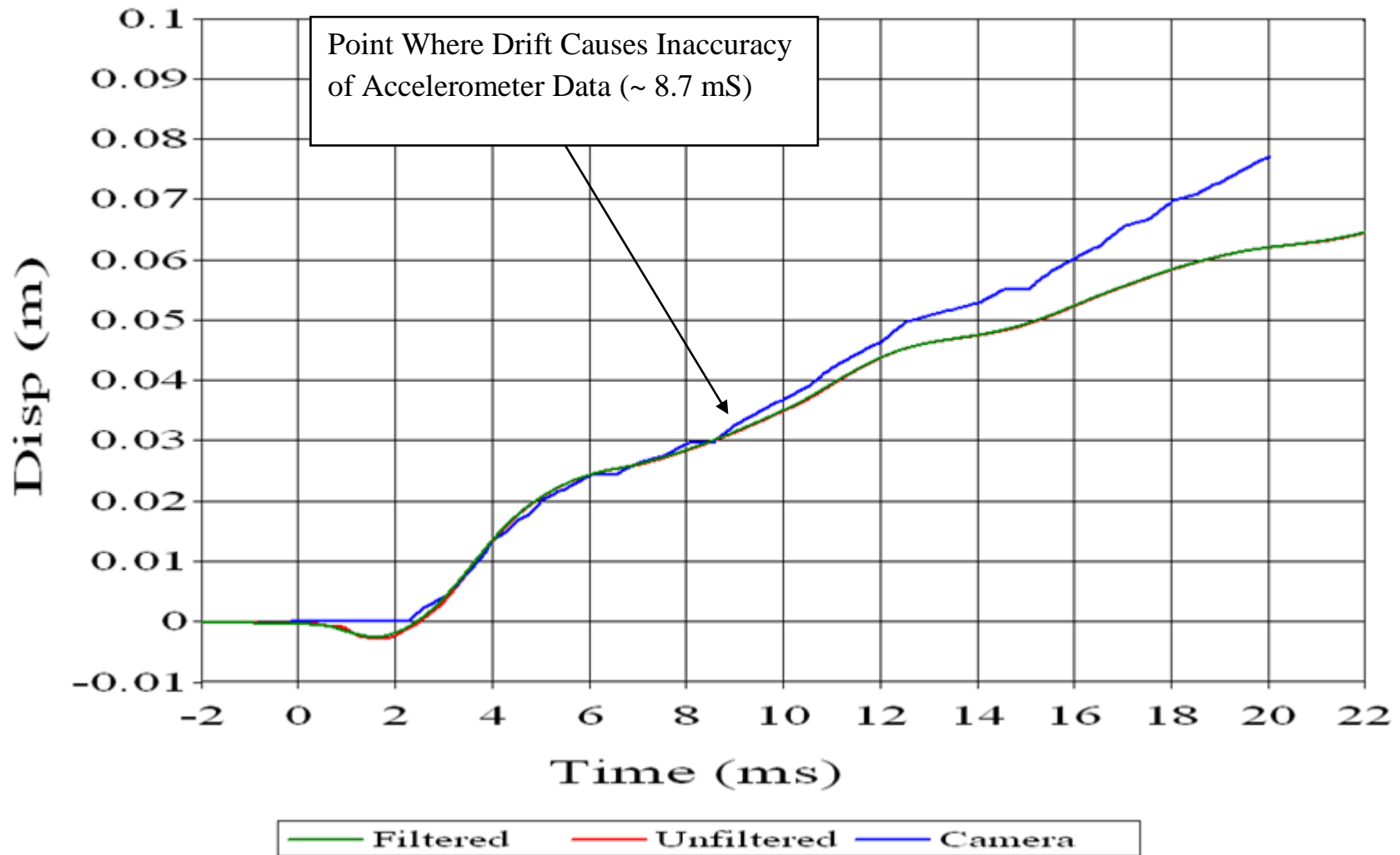
Steel 5 (Left Frame)



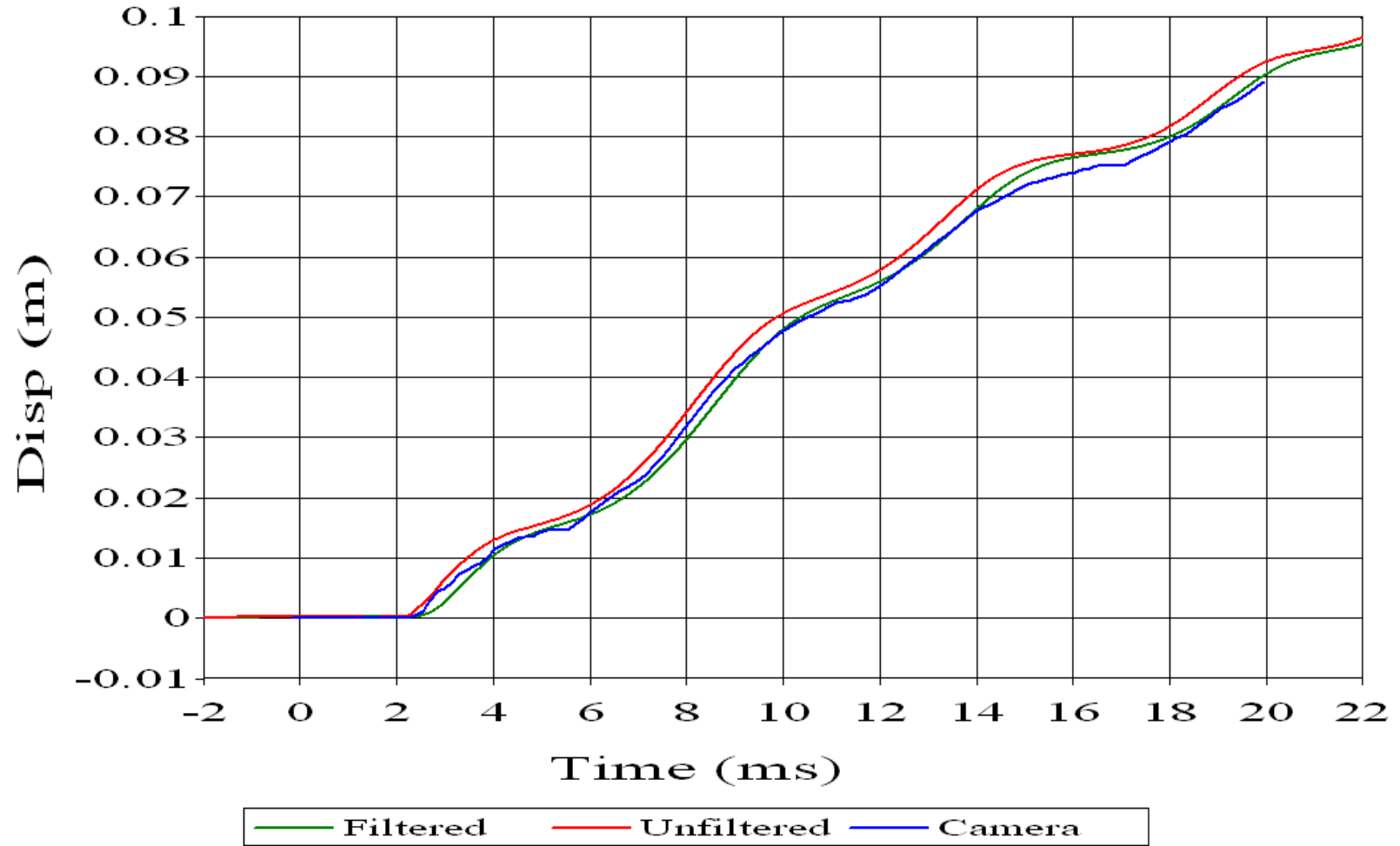
Steel 5 (Right Frame)



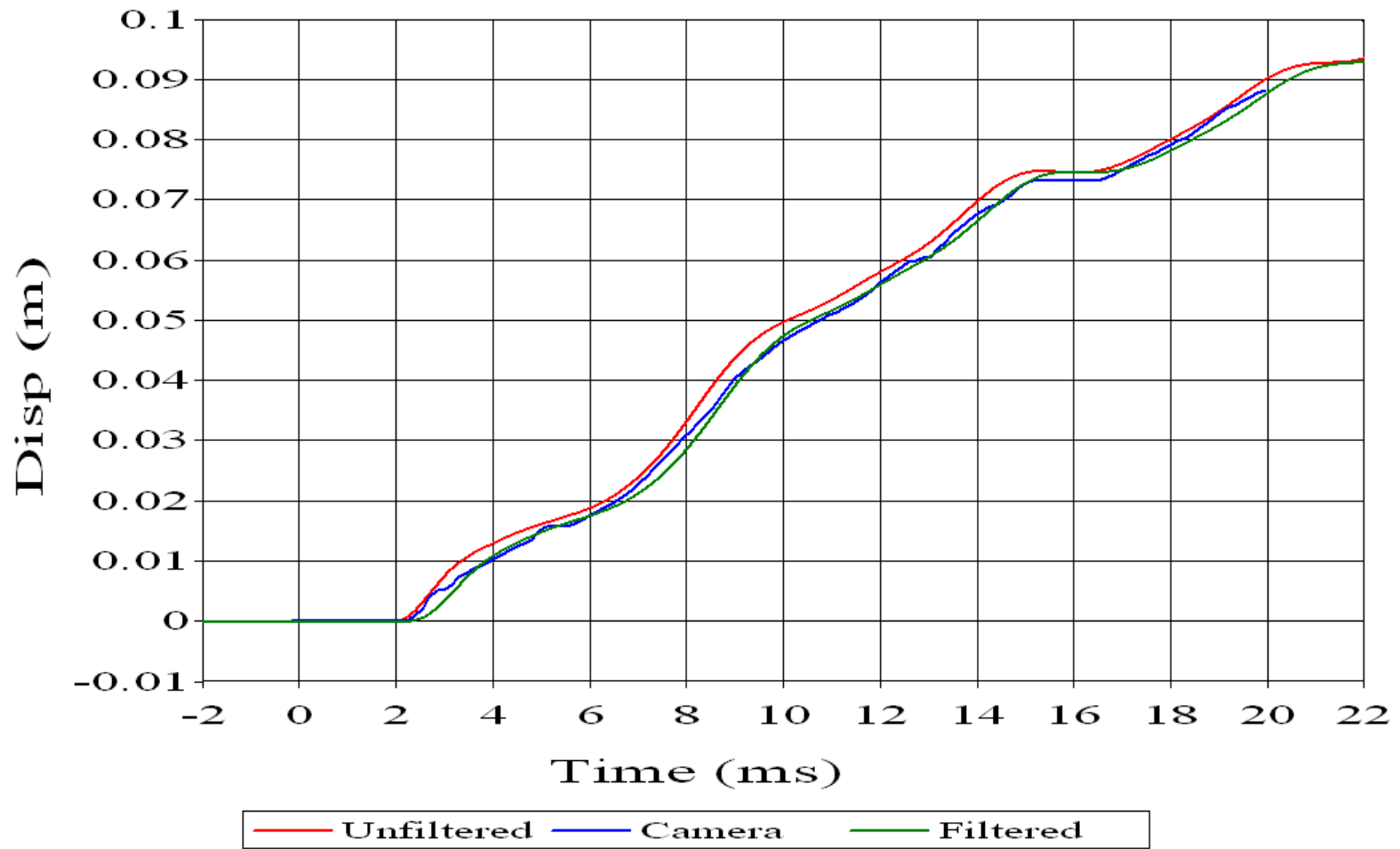
Steel 5 (Corner Frame)



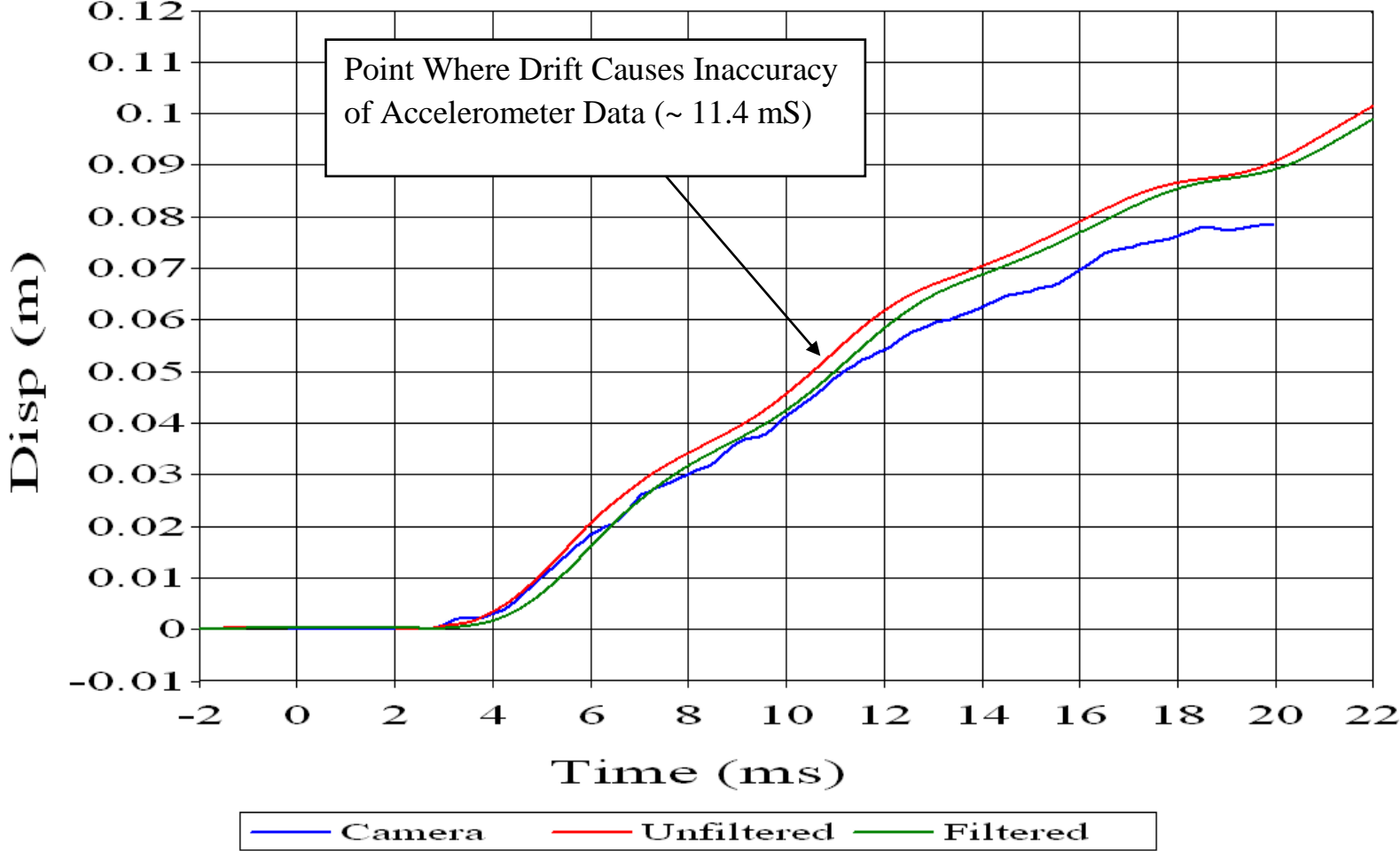
Steel 6 (Left Frame)



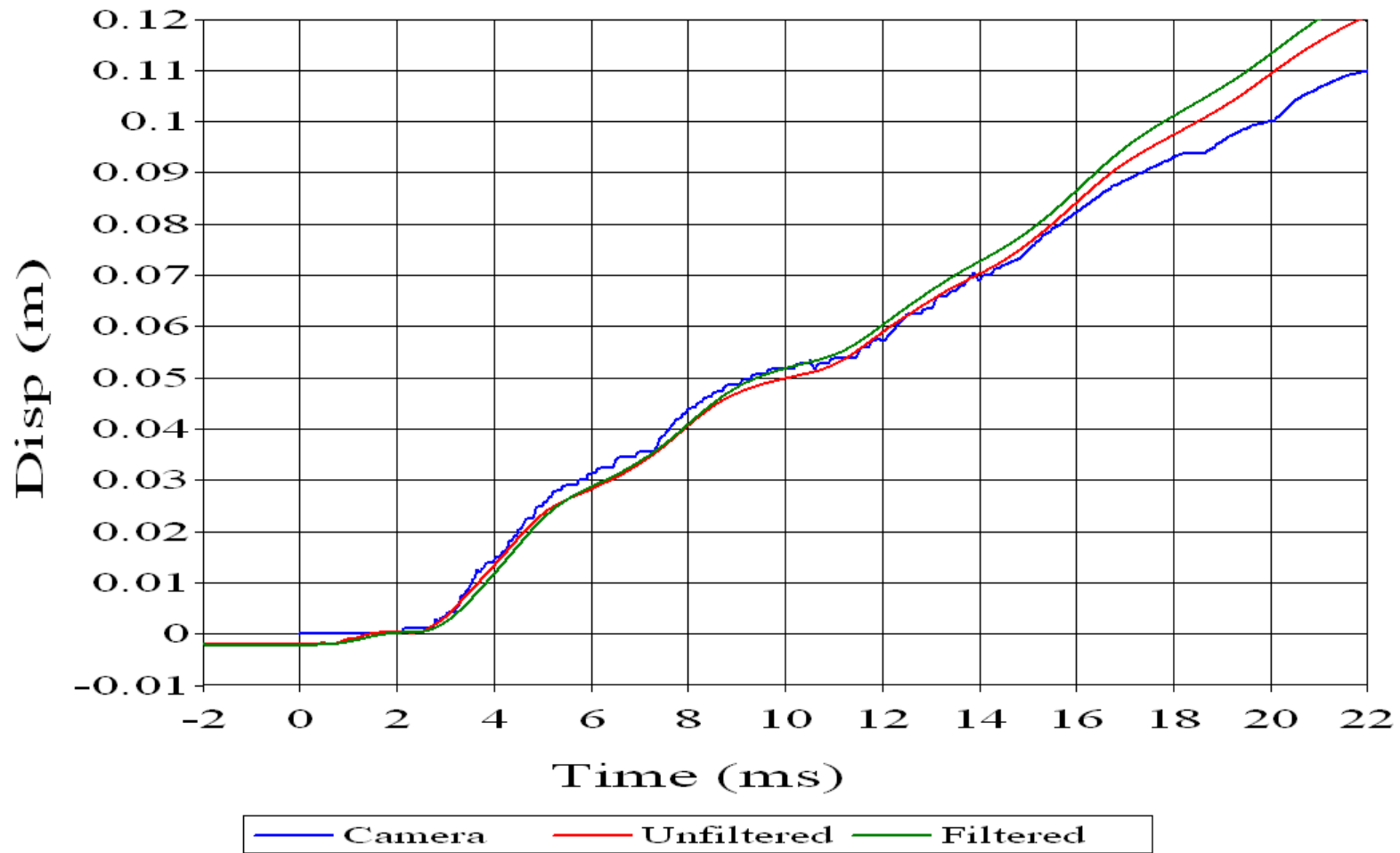
Steel 6 (Right Frame)



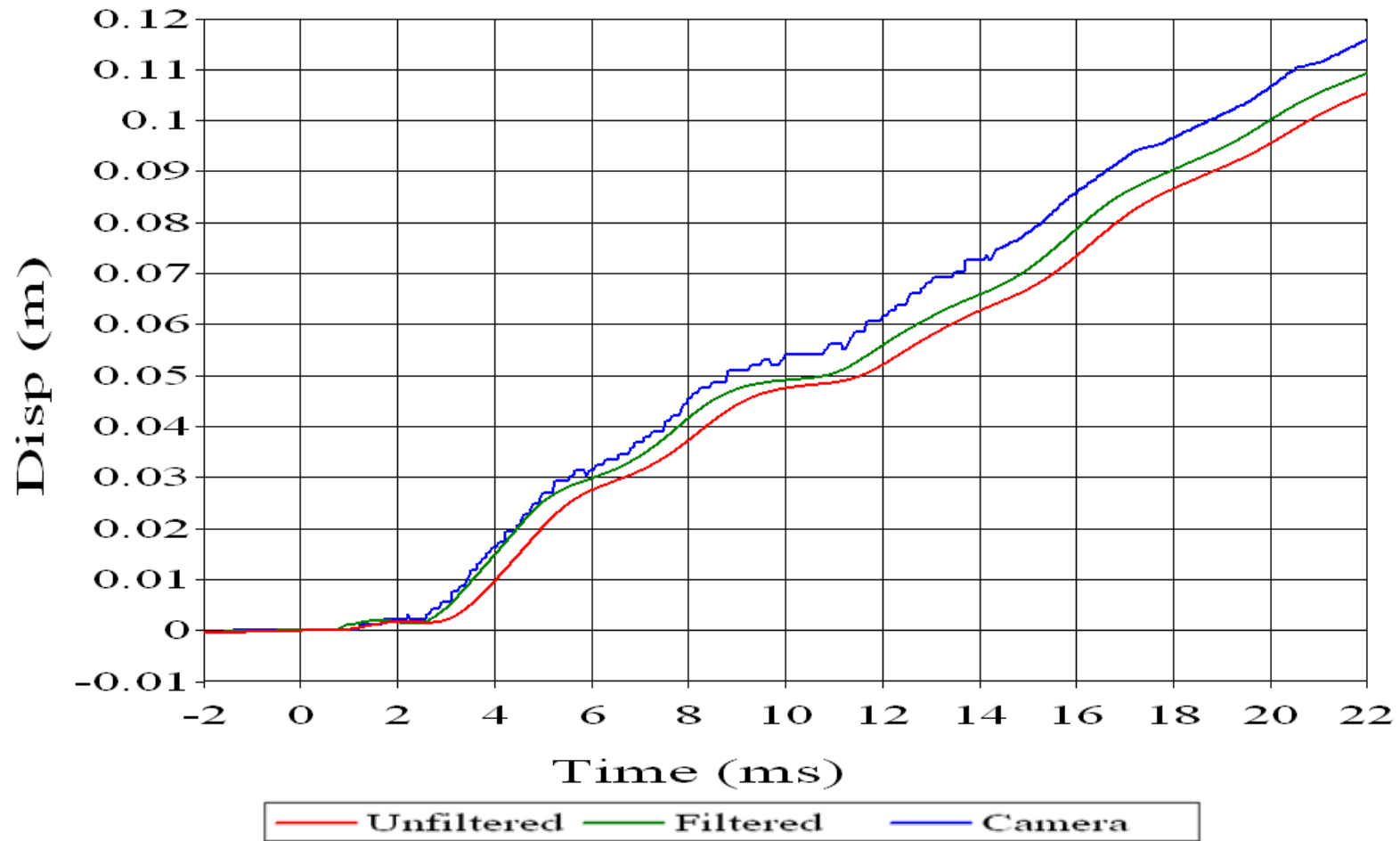
Steel 6 (Corner Frame)



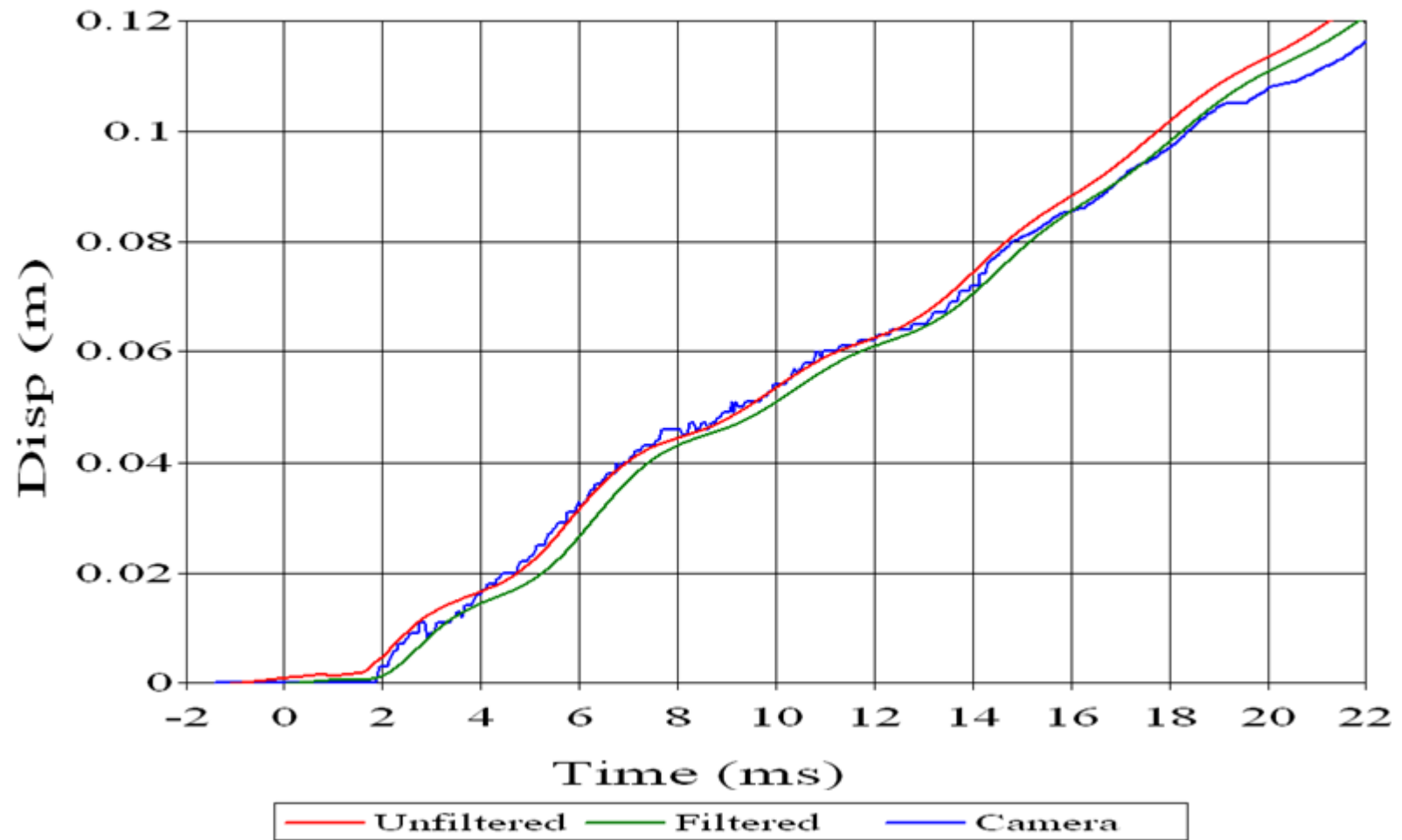
Pocket Plate 1 (Left Frame)



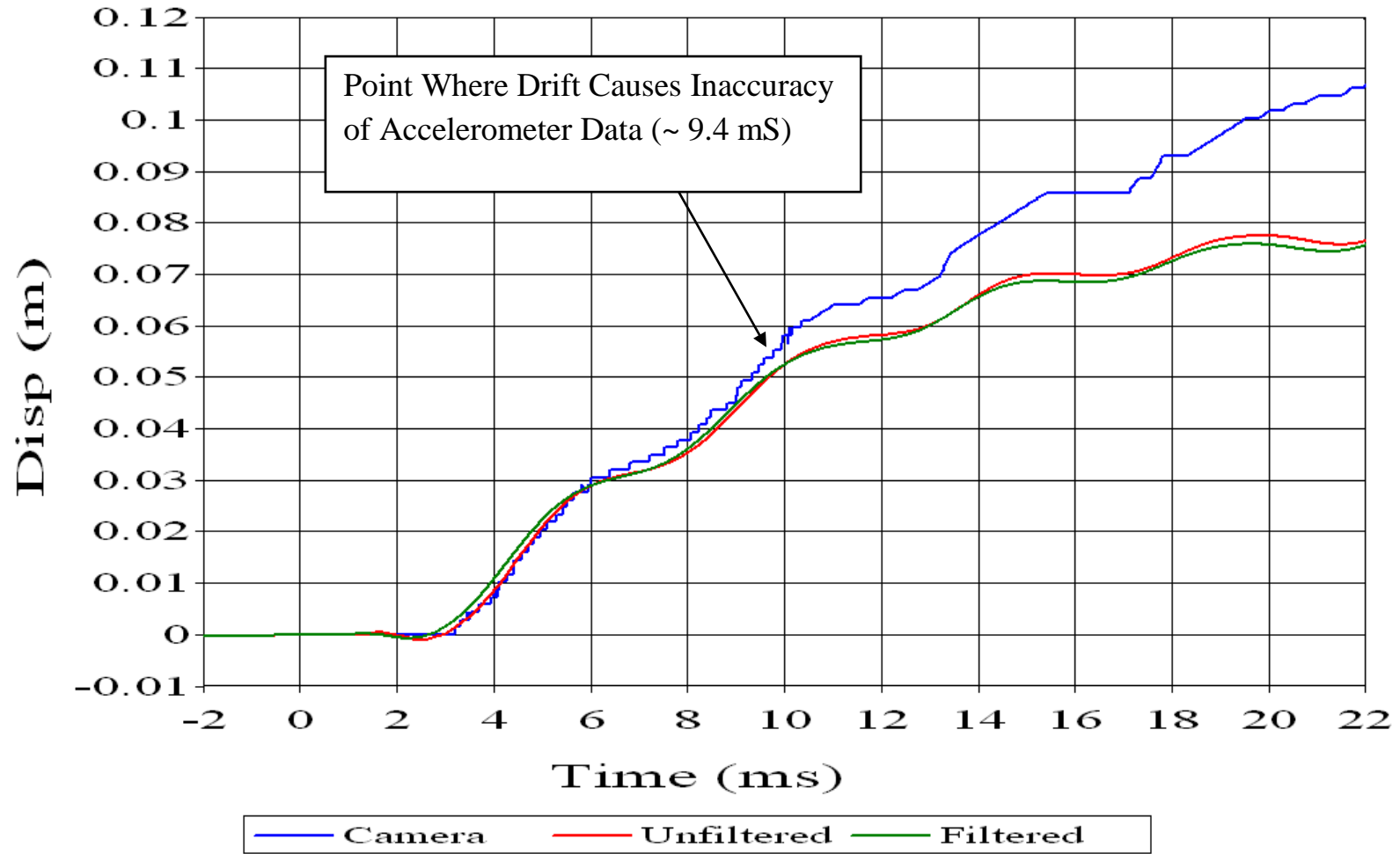
Pocket Plate 1 (Right Frame)



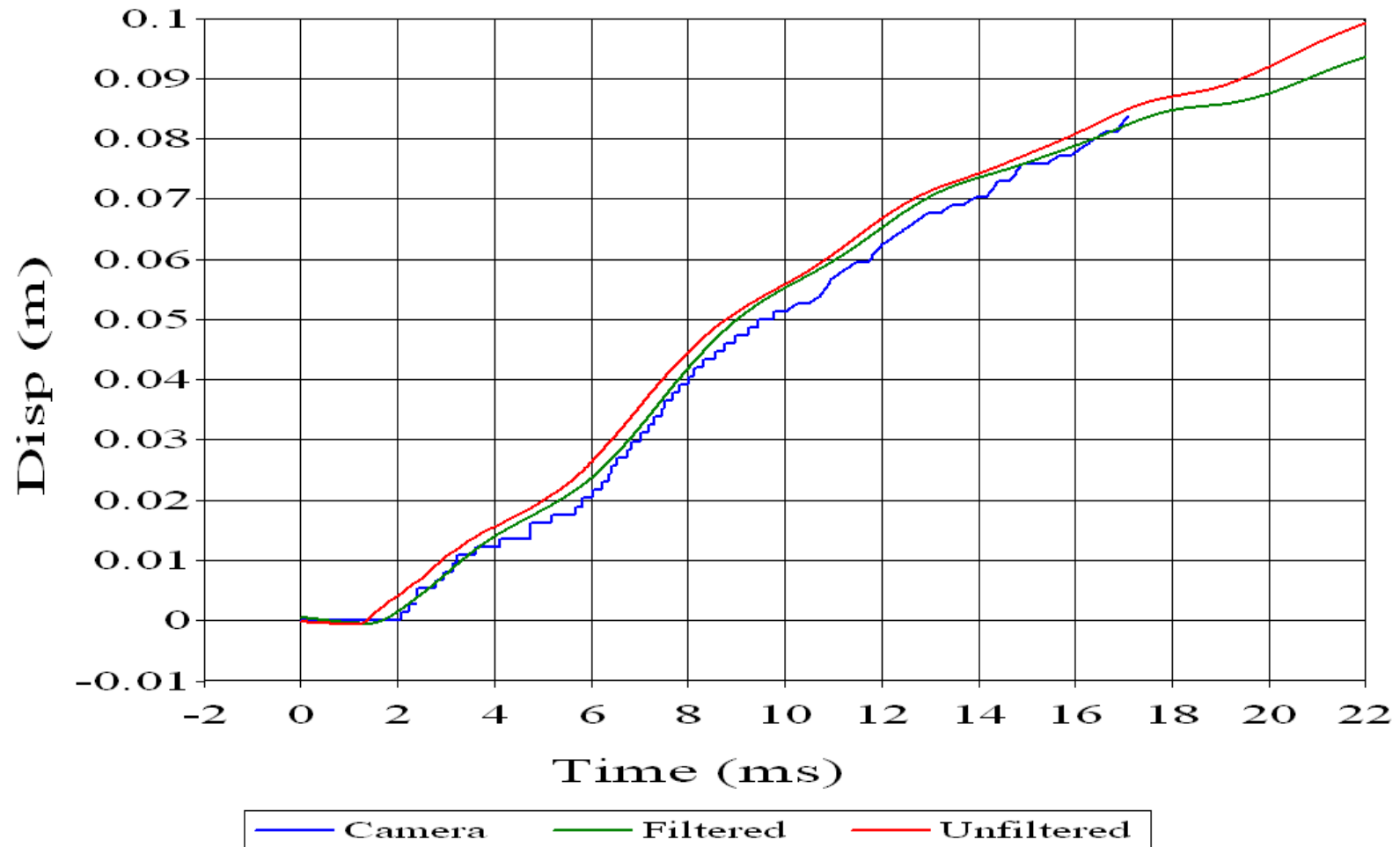
Pocket Plate 1 (Corner Frame)



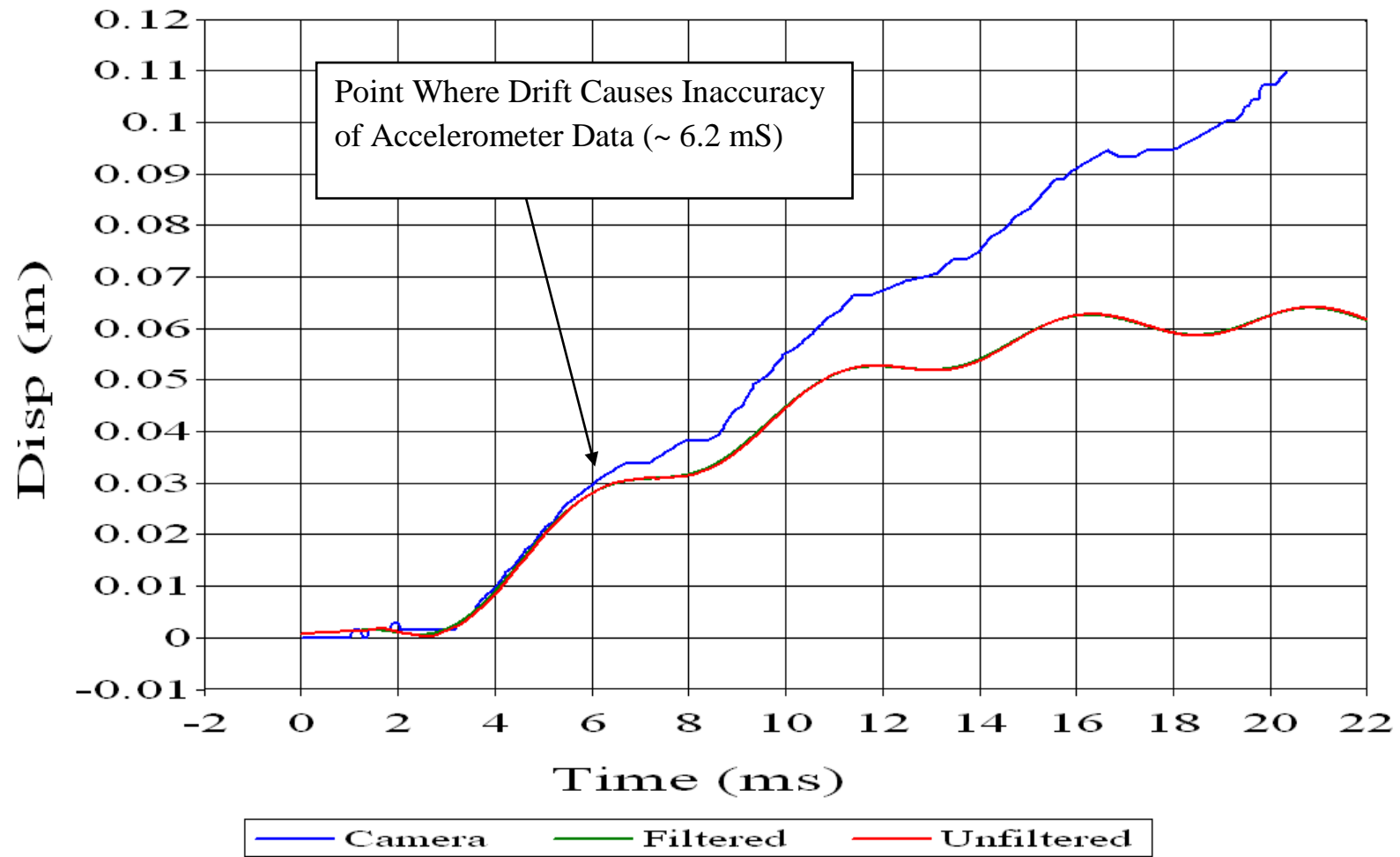
Pocket Plate 2 (Left Frame)



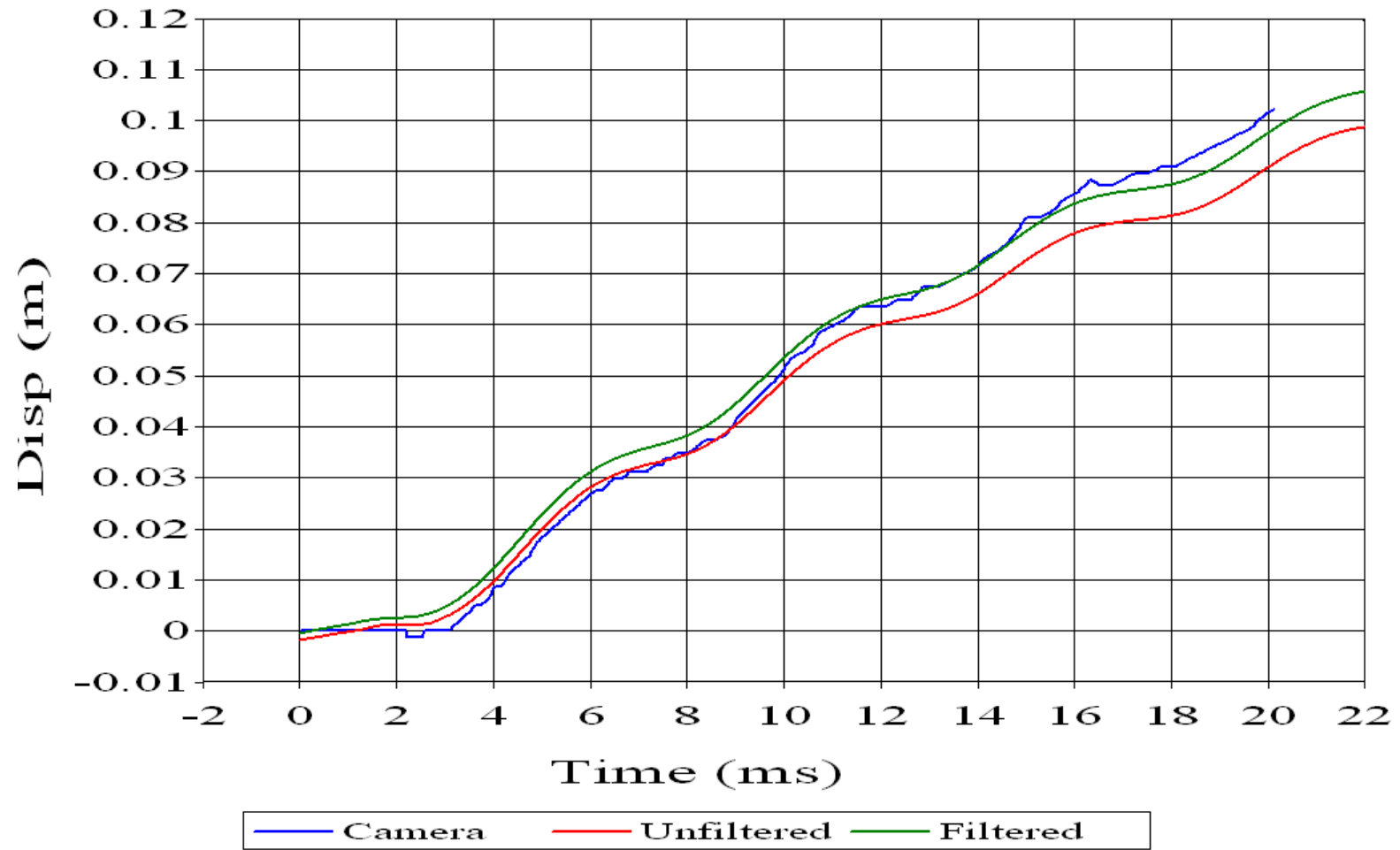
Pocket Plate 2 (Corner Frame)



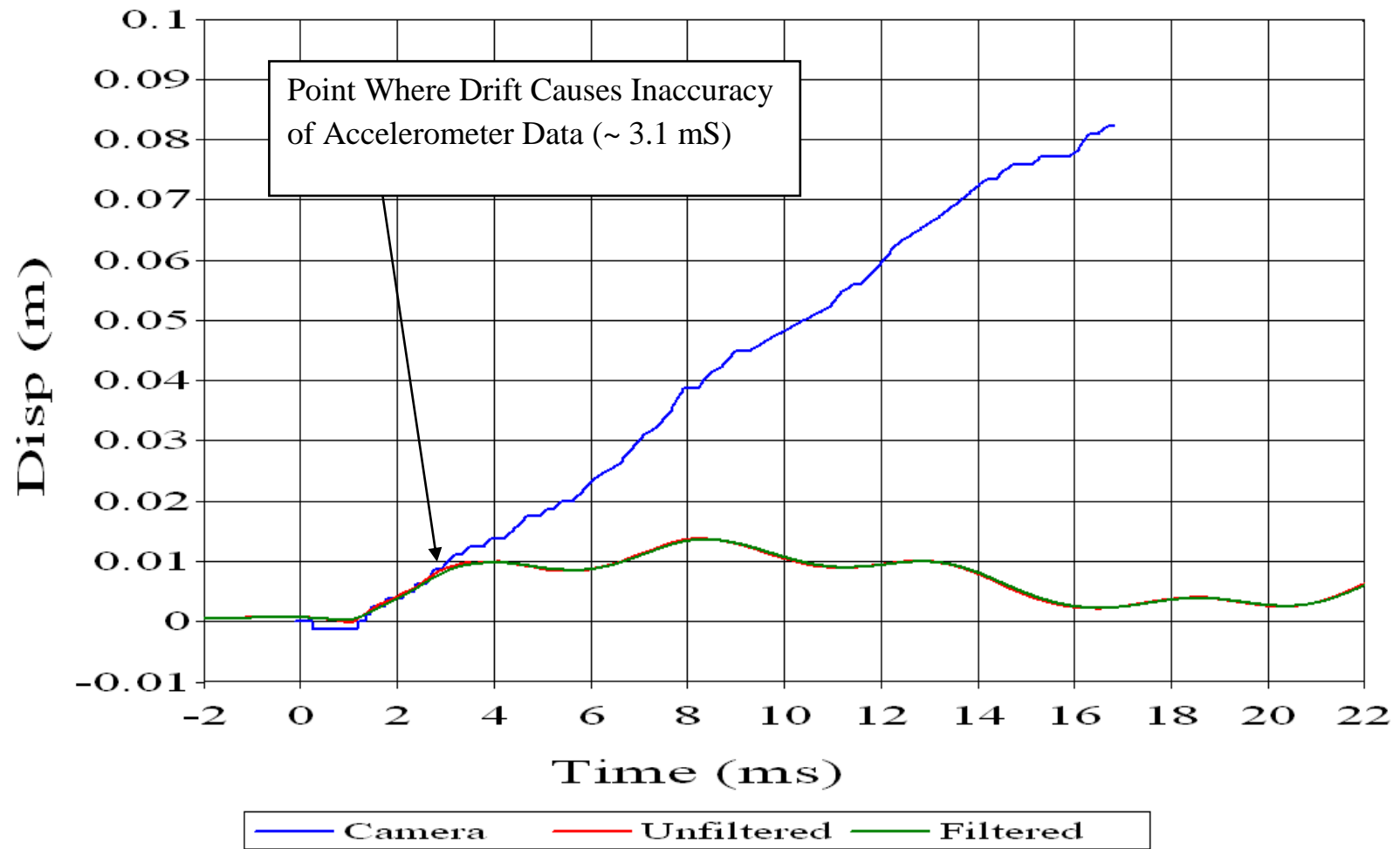
Pocket Plate 3 (Left Frame)



Pocket Plate 3 (Right Frame)



Pocket Plate 3 (Corner Frame)



Bibliography

- [1] Benedetti, Robert. Mitigation of Explosive Blast Effects of Vehicle Floorboard. College Park: University of Maryland, 2008.
- [2] Toon, John. Blast Protection: Crew-Focused Design and Sacrificial “Blast Wedge” Could Improve Survivability in Light Armored Patrol Vehicles. 13 October 2009. 23 March 2010 <<http://gtresearchnews.gatech.edu/blast-wedge/>>.
- [3] Hellman, Christopher. The MRAP: A Case Study in Military Planning (and Congressional Response). 20 July 2007. 23 March 2010 <http://www.arms-controlcenter.org/policy/securityspending/articles/mrap_casestudy/>.
- [4] Atkinson, Rick. About Left of Boom: The Fight Against Roadside Bombs. 30 September 2007. 24 March 2010 <<http://www.washingtonpost.com/wp-dyn/content/graphic/2007/09/28/GR2007092802161.html>>.
- [5] Atkinson, Rick. 'The single most effective weapon against our deployed forces'. 30 September 2007. 24 March 2010 <<http://www.washingtonpost.com/wp-dyn/content/story/2007/09/29/ST2007092900754.html>>.
- [6] Bretall, Damien. Inverse Hybrid Method for Determining Explosive Loading on Plates Due to Buried Mines. College Park: University of Maryland, 2007.
- [7] Blackman, Eric. Helmet Protection against Traumatic Brain Injury: A Physics Perspective. Rochester, NY: University of Rochester, n.d.
- [8] Eiband, Martin A. Human Tolerance to Rapidly Applied Accelerations: A Summary of the Literature. Celeveland, OG: Lewis Research Center, 1959.
- [9] McAndrew, Brendan. Shock Isolation Parameters Based on a Damped Harmonic Oscillator Model for Mine Blast Protected Seating. Aberdeen Proving Ground, MD: Army Research Laboratory, 2007.
- [10] Wenzel, Alex and John Hennessy. "Analysis and Measurements of the Response of Armor Plates to Land Mine Attacks." n.d.
- [11] Schmidt, R M and K A Holsapple. "Theory and Experiments on Cenrifuge Cratering." Journal of Geophysical Research 85.B1 (1980).
- [12] Teledyne Technologies. RP-87 EBW Detonator P/N 167-9643. Teledyne. 28 March 2010 <http://www.teledynersi.com/products/0products_1ebw_page27.asp>.

- [13] Omni Explosives. 28 March 2010 <<http://www.omniexplosives.com>>.
- [14] Teledyne RISI Inc. FS-17 Firing System. 29 March 2010 <http://www.teledynერიsi.com/products/0products_2fs_page49.asp>.
- [15] Genson, Kevin William. Vehicle Shaping for Blast Damage Reduction. College Park: University of Maryland , 2006.
- [16] Fox, D M, et al. "The Response of Small Scale Rigid Targets to Shallow Buried Explosive Detonations." 2010.
- [17] Vision Research. Phantom v12.1. Vision Research. 2 April 2010 <http://www.visionresearch.com/index.cfm?sector=htm/files&page=Phantom_v12>
- [18] Mantz, Paul, et al. UERDTOOLS. Data Analysis Program.
- [19] Tabiei, Ala and Gaurav Nilakantan. Reduction of Acceleration Induced Injuries from Mine Blasts under Infantry Vehicles. Cincinnati, OH: University of Cincinnati, n.d.
- [20] McMaster-Carr. Compression and Die Springs. 6 April 2010 <<http://www.mcmaster.com/#9657k113/=6jryb9>>.
- [21] Line-X. Paxcon. 2010 19 April <http://www.paxcon.com/user_pages/home_0.shtml?page=Home>.
- [22] Isolation Dynamics Corp. SM7 Series. 8 April 2010 <http://www.isolator.com/sm_series_isolators.html>.
- [23] Parametric Technology Corporation. Pro/ENGINEERWildfire 5.0. Program. PTC. 2009.
- [24] ARL. Aircraft Crash Survival Design Guide. Washington DC, 1980.
- [25] PCB Piezotronics. PCB Piezotronics. 2010 15 April <http://www.pcb.com/spec_sheet.asp?model=350C02&item_id=10477>.
- [26] MatWeb. Aluminum 6061-T6. 5 April 2010 <www.matweb.com>.
- [27] MatWeb. AISI 1018 Steel. 8 April 2010 <www.matweb.com>.